



Tomas Bata University in Zlín
Faculty of Applied Informatics

**The Mathematical Modelling of Waste Fats
Treatment into Biogas**

**Matematické modelování zpracování odpadních tuků na
bioplyn**

Doctoral thesis

Author: Ing. Samuel **Emebu**
Degree programme: P3902-Engineering Informatics
Degree course: 3902V037E-Automatic Control and Informatics
Supervisor: doc. Ing. Marek Kubalčík, Ph.D.
Consulting Supervisor: Prof. Ing. Dagmar Janáčková, CSc.

Zlín, 2023

© Samuel Emebu

Published by **Tomas Bata University in Zlín** in the Edition **Doctoral Thesis Summary**.

The publication was issued in the year 2023.

Full text of the doctoral thesis is available in the Library of TBU in Zlín.

ISBN 978-80-.....**

Abstract

The need to supplement or replace fossil energy consumption to enhance energy supply has prompted renewable energy development. Especially from biomass degradation, since it is advantageous for its ability to tackle the challenges of energy security and waste management simultaneously. Specifically, the anaerobic digestion (AD) of biomass (lipid) into biogas has been considered. The work highlighted the current state-of-the-art AD models (single-equation model and multi-step dynamic model) with a specific interest in single-step-degradation model (SSDM) a multi-step dynamic model. The SSDM was modelled in such a way that it could be easily applied to control the pressure, pH, and temperature of the AD. Therefore, in addition to modelling the biochemical stage, other processes such as hydrolysis of lipid, mass transfer, heat transfer, and pH of the process were modelled, together with the necessary microbial activity, physicochemical, and thermodynamic parameters modelled as a function of temperature, as well as pressure. Additionally, the biogas bubble growth and motion dynamics, which enable the estimation of biogas bubble diameter, rising velocity, pressure inside and on the bubble at the gas-liquid interface, were also estimated. Most processes considered in the SSDM were modelled theoretical based on data from literature. However, the hydrolysis process involving the degradation of lipid into LCFA, and glycerol was experimentally modelled as a function of temperature (25 to 50 °C), and the model showed excellent proximity with experimental data, as well as its optimal temperature found to be 45 °C. Having modelled all processes to be considered in the SSDM, the model was simulated in MATLAB for different scenarios, to effectively evaluate its robustness. These scenarios involved evaluating the performance of the SSDM to analyse the effect of pressure (i.e., over-, atmospheric-, and under-pressure) temperature (i.e., 35, 45, and 60 °C), pH on the biogas production, as well as a simplified comparison with the experimental production of biogas at atmospheric pressure. Based on these analyses and comparisons it was found that the developed SSDM was quite adequate to predict the AD of lipid into biogas. Although beyond the scope of this work, it was proposed that further comprehensive comparison or optimisation of the model to real-time experimental data of substrate, microbes, dissolved and evolved biogas species concentrations, as well as water vapour together with biogas water content maybe be necessary to fully validate the model.

Keywords: Anaerobic digestion, single-step-degradation model, lipid hydrolysis, biogas evolution, bubble growth dynamics, water evaporation, pH dynamic

Abstrakt

Potřeba doplnit nebo nahradit spotřebu fosilní energie za účelem zvýšení dodávek energie podnítila rozvoj výroby obnovitelné energie, a to zejména s využitím degradace biomasy. Tento způsob výroby energie je výhodný z hlediska výzev energetické bezpečnosti a nakládání s odpady. Práce se zabývá modelováním anaerobní digesce (AD) biomasy (lipidů) na bioplyn s využitím současných nejmodernější AD modelů (jednorovnicový model a víceukový dynamický model). Zvláštní důraz je kladen na jednostupňový degradační model (SSDM), víceukový dynamický model. SSDM byl modelován takovým způsobem, že jej bylo možné snadno použít pro simulaci řízení tlaku, pH a teploty AD. Proto byly kromě modelování biochemické fáze modelovány další procesy, jako je hydrolýza lipidů, přenos hmoty, přenos tepla a pH procesu, spolu s nezbytnou mikrobiální aktivitou, fyzikálně-chemickými a termodynamickými parametry modelovanými jako funkce teploty a tlaku. Dále byl odhadnut růst a dynamika pohybu bublin bioplynu, která umožňuje odhadnout průměr bublin bioplynu, rychlost stoupání, tlak uvnitř a na bublině na rozhraní plyn-kapalina. Většina procesů uvažovaných v SSDM byla modelována teoreticky na základě dat z literatury. Proces hydrolýzy zahrnující degradaci lipidů na LCFA a glycerol byl modelován experimentálně v závislosti na teplotě (25 až 50 °C) a model vykazoval velmi dobrou shodu s experimentálními daty. Optimální teplota procesu byla experimentálně stanovena jako 45 °C. Po namodelování všech dílčích procesů, které jsou uvažovány v SSDM, byl celkový model simulován v MATLABu pro různé scénáře, aby bylo možné efektivně vyhodnotit jeho robustnost. Tyto scénáře zahrnovaly vyhodnocení efektivity produkce bioplynu s využitím SSDM v závislosti na tlaku (tj. přetlaku, atmosférického a podtlaku), teplotě (tj. 35, 45 a 60 °C). Bylo rovněž provedeno zjednodušené srovnání s experimentální výrobou bioplynu za atmosférického tlaku. Na základě těchto analýz a srovnání bylo zjištěno, že vyvinutý SSDM je zcela adekvátní pro predikci AD lipidů do bioplynu. I když je to nad rámec této práce, model byl navržen tak, aby bylo možno provést další komplexní srovnání nebo optimalizaci modelu na experimentální data substrátu, mikrobů, rozpuštěných a vyvinutých druhů bioplynu, jakož i vodní páry spolu s obsahem vody v bioplynu v reálném čase, což je nutné ke komplexnímu ověření modelu.

Klíčová slova: Anaerobní digesce, model jednostupňové degradace, hydrolýza lipidů, evoluce bioplynu, dynamika růstu bublin, odpařování vody, dynamika pH.

Acknowledgement

My appreciation goes to God for inspiration, perseverance, as well as strength throughout this programme. I also appreciate my supervisors' doc. Ing. Marek Kubalčík, Ph.D., and Prof. Ing. Dagmar Janáčová, CSc., for giving me the opportunity to undertake this thesis, their valuable advice and professional guidance. I also appreciate the immense contribution of doc. Ing. Jiří Pecha, Ph.D., for his theoretical and experimental advice as well as Ing. Lubomír Šánek, Ph.D. and Ing. Jakub Husár for their experimental and miscellaneous contributions. Furthermore, I appreciate the Internal Grant Competition of the Tomas Bata University (UTB) (i.e., CebiaTech/2021/002, CebiaTech/2022/002, and CebiaTech/2023/004), the UTB, and the Faculty of Applied Informatics (FAI) scholarship boards for financial support. Appreciation also goes to the entire Faculty of Applied Informatics for their various administrative as well technical support.

Finally, I appreciate my wife (Mrs. Oluchi Emebu), my mother (Mrs. Martina Emebu), and other family members as well as friends for their prayers, emotional support, and patience during this programme.

Table of contents

1. Introduction.....	9
2. Current state of issues – Research overview.....	11
2.1. Anaerobic hydrolysis of lipid.....	12
3. Aims and objectives.....	14
4. Biogas	15
4.1. Comparative study of biogas with other similar fuel	16
5. Description of anaerobic digestion	18
5.1. Pretreatment of feedstocks	18
5.2. Hydrolysis of feedstocks	19
5.3. Acidogenesis of hydrolysis products	19
5.4. Acetogenesis of products from acidogenesis	20
5.5. Methanogenesis of products from acetogenesis.....	20
6. Model review on anaerobic digestion	21
6.1. Single-based equation model.....	21
6.1.1. Dynamic single-equation model	21
6.1.2. Cumulative single-equation model	21
6.2. Multi-step dynamic model	22
6.2.1. Single-step-degradation model	23
6.2.2. Two-step-degradation model	23
6.2.3. Multi-step-degradation model.....	24
6.3. Theoretical estimation of substrate, microbes, and biogas yield	24
7. Theoretical framework – Model development.....	26
7.1. Material balance of control volume	27
7.1.1. Volumetric balance of control volume.....	27
7.1.2. Mass balance of control volume	27
7.2. Mass balance for liquid phase.....	28
7.2.1. Dynamics of level for liquid phase	29
7.3. Volumetric balance in gas-vapour headspace.....	29
7.4. Liquid phase component balance.....	29
7.4.1. Component balance for hydrolysis of lipid.....	29
7.4.2. Component balance for microbial activities on substrates.....	30
7.4.3. Component balance for substrate	31
7.4.4. Component balance for biogas in liquid phase	32
7.4.5. Component balance of water in liquid phase	33

7.5. Gas headspace component balance	33
7.5.1. Component balance for biogas in gas-headspace.....	33
7.5.2. Component balance of water vapour in gas headspace.....	34
7.5.3. Partial pressure of biogas species, and water vapour in the gas headspace	35
7.6. Computation of water evaporation rate.....	35
7.7. Moisture content in the biogas	36
7.8. Computation of biogas evolution rate.....	37
7.9. Gas bubble growth and motion	39
7.10. Gas bubble size distribution.....	42
7.11. Estimation of biogas outflow rate	42
7.12. Estimation of pH in the bioreactor.....	42
7.13. Energy balance to deduce temperature dynamics	45
7.13.1. Energy balance of bioreactor	46
7.14. Power supplied by mixer or stirrer.....	48
7.15. Material balance on energy jacket	48
7.16. Energy balance for heating jacket.....	48
7.17. Estimation of bioreactor heat transfer with wall temperatures	49
7.17.1. Computation of heat transfer from heating fluid to bioreactor content.....	49
7.17.2. Computation of bioreactor heat transfer coefficient	50
7.17.3. Computation of heating jacket heat transfer coefficient	51
7.17.4. Computation of heat transfer from heating fluid to environment	52
7.18. Experimental analysis of lipid hydrolysis	53
8. Experimental framework – Materials and methods	54
8.1. Collection and storage of sludge sample.....	54
8.2. Determination of TSS, and VSS	54
8.3. Determination of BOD, COD, and TKN	54
8.4. Dispersion of lipid sample in sludge.....	54
8.5. Setup of the anaerobic hydrolysis system	55
8.6. Analysis of hydrolysed lipid	55
8.7. Measurement of produced biogas, and methane content	55
8.8. Modelling lipid hydrolysis kinetics.....	56
8.9. Evaluation of models	56
8.10. Simulation of model.....	56
9. Results and discussion	58
9.1. Hydrolysis kinetics.....	58
9.2. Anaerobic digestion simulation	59

9.2.1. Effect of pressure	59
9.2.2. Effect of pH inhibition	69
9.2.3. Effect of temperature	72
10. Conclusion	80
11. Contribution to science and practice	81
Bibliography	83
Appendix.....	102
List of figures.....	110
List of tables.....	113
List of Abbreviations	114
List of symbols.....	115
List of subscripts	119
List of publications	120
Curriculum vitae	122

1.Introduction

Energy is the currency of all motive physical, chemical, and physiochemical activities within biological, as well as non-biological systems. In the process industry, energy is particularly useful in transforming raw materials to finish products, hence the need to source and store it. Energy can be generated from diverse sources, which can be classified into renewable (e.g., biomass, solar, etc.) and fossil-based energy sources (Petroleum, coal, etc.). Although as of the year 2021, fossil fuel (about 82%) remains the most utilised source of energy worldwide, they are considered unclean energy sources due to their high carbon footprint on global warming [1,2]. However, sequel to the aftermath of the 2022 global energy crisis, which also spilled over to 2023 [3]. There have been accelerated efforts to simultaneously reduce fossil energy consumption, and develop renewable energy resources, as a supplementary energy source to ensure a nation's energy security. Considering that nations are also faced with the challenges of waste generation, treatment, and disposal. It is therefore necessary to consider energy generation from waste [4,5], as a viable means to tackle energy security as well as waste generation. Fundamentally, energy security and waste management are critical global security, economic and environmental reoccurring issues that require persistent solutions. Energy security is a combination of all deliberate actions taken by necessary stakeholders, to ensure that energy sources of a nation are diversified and constantly available to meet energy demand in both normal and critical conditions [6,7]. Apart from tackling the challenges of energy security and waste management, renewable energy from waste also offers the synergy of mitigating climate change and reducing the emission of air pollutants that would have resulted from using fossil energy sources [1,8].

Renewable energy is energy generated from replenishable natural sources, such that the depletion of Earth's resources after energy generation is negligible [9]. Renewable energies are characterised by their wide range of diversity, continuous availability and cause negligible environmental damages [10]. Although in theory, renewable energies are undiminishing, however, to achieve this state in practice certain technical and economic constraints on the operationality of the energy system must be adequately solved [11]. Renewable energy can be deduced from water, wind, solar, biomass and geothermal energy sources [12]. All these sources of renewable energy can be used for electricity generation. However, each of these sources can be used for specific energy needs, for example, geothermal steam, biomass and solar sources can be used directly for heating purposes. Although "biofuels" produced from biomass in addition to heating, can be used to power fuel engines for transportation purposes. In general, renewable energy can be classified based on the magnitude of their emission of greenhouse gas (typically, carbon dioxide). Based on this assertion, renewable energy sources can be scaled as zero (wind, solar, and water), low (geothermal) or neutral (biomass) [13]. Renewable energy sources scaled as zero, releases no emission, scaled as low, release unabsorbable gas emissions and while scaled as neutral, release gas emissions balanced by the amount of carbon dioxide absorbed during the growth of biomaterials. It should however be noted that the environmental impact of each source depends primarily on its overall emissions lifecycle [14,15].

Considering the earlier highlighted challenges of energy security and waste management, and the diverse applicability of energy from biomass, it makes sense to seriously consider this route for renewable energy generation. This assertion is evident in the reported claim that the energy contribution of biomass to the world's renewable energy utilisation constitutes approximately 55%, and over 6% of the global energy supply [16,17]. Conversion of biomass to refined forms, "biofuel" is required for uses in different processes, and this can be achieved using different methods, categorised as, thermal, chemical, and biochemical methods [18]. Thermal conversion method involves the use of heat to transform the biomass through processes such as Gasification or Pyrolysis [19]. Chemical conversion method utilises chemical catalytic transformations of biomass (primarily sugars and sugar alcohols), and it involves processes such as hydrolysis, dehydration, isomerization, aldol condensation, reforming, hydrogenation, and oxidation [20]. Biochemical conversion method utilises microbes in a controlled environment via processes such as

digestion (anaerobic and aerobic), enzymatic or acid hydrolysis, and fermentation [21]. Compared with other methods, the biochemical method is advantageous for reasons such as mild temperature and normal pressure conditions, low equipment cost, low energy, little dependence on chemicals, high specificity of biomass conversion to biofuel and usability of unutilised biomass (digestate) as organic fertilizer [22–24].

The utilisation of biomass for energy in refined forms (such as biogas, biodiesel, and bioethanol) is observably more efficient, convenient, diverse, and environmentally friendly [25–27]. Biofuel can therefore be classified as primary biofuel (wood, used mostly for heating purposes) and secondary biofuel (i.e., biogas, biodiesel, bioethanol etc., used in more diverse applications) [28]. Secondary biofuel can also be classified based on the source of feedstock utilised for its production. First-generation biofuel (sourced from food crops), which involves mainly the production of bioethanol; Second-generation (sourced from non-food crops), and Third-generation biofuels (sourced from microalgae and seaweeds) [28–31]. While Second- and Third-generation biofuels overcome the limitations of food insecurity, Third-generation biofuels additionally overcome the limitation of crop lifecycle. The composition of compounds in the sources or feedstocks of First-to-Third-generation biofuels can be generally categorised to contain mainly or constitutively, Carbohydrate ($C_{n+1}H_{2n}O_n$), Lignin ($(C_9H_{10-11}O_{3-4})_n$), Protein ($(C_4H_{6.2}O_{1.2}N_1P_{0.01}S_{0.01})_n$) and lipid ($(C_{17}H_{35}COO)_3C_3H_5$) [32,33]. However, lipid has more energy density than any of these compounds, hence producing more biofuel [34–39]. Therefore, without consideration of other constraints, feedstock with high lipid content is highly viable for biofuel production.

2. Current state of issues – Research overview

Considering the earlier highlighted advantages of biochemical conversion of biomass to biofuel, in this work the anaerobic digestion of biomass to biogas would be considered. Anaerobic digestion is specifically considered because it can utilise the most variety of organic matter (such as waste material unsuitable to produce other biofuel, typically waste with a high percentage of organic biodegradable matter and high moisture content) [40], hence also suitable for efficient waste management. Its energy yield per square meter of feedstock is higher and more efficient for energy production than other biofuels (i.e., liquid biofuels such as bioethanol, and biodiesel). Although, while the convenience and energy density of liquid biofuels is admirable for some purposes, if energy recovery from biomass is to be maximised, then biogas production is the best choice. Also, for situations where bioethanol and biodiesel production are required, biogas can be produced from their waste products and as such improves the energy yield of the production process [41,42]. Furthermore, considering the earlier highlighted fact that lipid has more energy density than other feedstock, in addition to the fact that lipid-rich waste especially when mixed with a high percentage of organic biodegradable matter as well as high moisture content [40], and unsuitable for biodiesel production due to high content Free fatty acid [43,44] is generated daily in large amounts from food processing companies (edible oil processing plant, dairy plant, slaughterhouses, etc.), cooking waste from hospitality industry (hotels, restaurants, etc.), together with domestic residences [45]. And its disposal can pose serious environmental and ecological issues: Eutrophication due to micro-organisms, phytoplankton, and algae which uses lipid as a food source; Reduction in dissolved oxygen content in aquatic bodies; Rancid odour production; Clogging of drainage systems and water treatment plants etc. [46]. Therefore, based on these highlighted reasons the anaerobic digestion of lipid-rich waste would be prioritized in this work. This consolidation of energy security and waste management through anaerobic digestion is a simple, economical, and popular practice [47–49]. This is indicative of the number of small, medium, and large-scale plants operating around the world. Reports indicate that micro digesters have become an integral part of most rural farming communities in developing countries, where they serve as a fundamental utility for waste treatment and energy generation [50,51]. There is a total of about 50 million micro-scale digesters operating around the globe with 42 million operating in China and 4.9 million in India, however, there are about a total of 700,000 biogas plants installed in the rest of Asia, Africa, and South America [52]. This fact is also indicative of the steady growth in the number of biogas plants in Europe because as of the year 2017, there were 17,783 biogas plants and 540 biomethane plants being operated, which includes biogas plants in countries like Germany (10,971 plants, the highest), Czech Republic (574 plants, 6th position) and Norway (138, 15th position) [53].

Anaerobic digestion on a holistic view is a simple process, however, on an intricate level, it involves four complex biochemical reaction stages: hydrolysis; acidogenesis; acetogenesis; and methanogenesis, to produce biogas. The biogas produced is usually composed of approximately 50 – 75% methane (CH_4), carbon dioxide (CO_2), and impurities such as 0–5% nitrogen, 0–5000 ppm hydrogen sulphide (H_2S), trace amount of hydrogen, carbon monoxide, and moisture [54]. The amount and composition of biogas produced depends on the efficiency of the biochemical and mass transfer processes in AD. These processes are affected by factors such as temperature, partial pressure of biogas species, and pH. And these highlighted factors determine efficiency based on how they influence the degree of stability (i.e., optimal condition) of AD. Therefore, mathematical models that relate these factors to feedstock and intermediates digestion, and production of biogas, are usually required to physically describe these influences, monitor the process (e.g., deduce the rate-limiting step), as well as optimise, and control the stability of AD [55–57]. Note that to ensure a comprehensive description of the AD, these mathematical models should be able to physically interpret the main processes in the AD, i.e., the earlier highlighted biochemical reaction stages, in addition to other processes such as mass and heat transfers, and physicochemical processes (e.g., pH dynamics). Also crucial are auxiliary models to estimate vital parameters (microbial activity parameters, microbe, biogas yields, etc.) needed in the computation of models for the earlier highlighted main processes. Model development for such a comprehensive description of AD would enhance the robustness of the physical

interpretation of the AD process and enable the evaluation of certain phenomena, such as the rate-limiting step of the process. Typically, in analysing the rate-limiting step (i.e., the slowest process) in AD, literature reports have debated that the hydrolysis-, methanogenesis-stage, or mass transfer of biogas could be the rate-limiting step [58–62], therefore adequately modelling these steps is important.

There are numerous mathematical models for AD reported in literature, and they include the popular Anaerobic Digestion Model No. 1 (ADM1) [63], Gaussian, Gompertz, multi-regression, acidogenesis-methanogenesis-two-steps (AM2) models, etc. [64–67]. These models are uniquely different in their overall approach (mechanistic or statistical), initial assumptions, process phenomena, and the biochemical stages considered in their development. In general, AD models can be categorized into single-equation and multi-step dynamic models. The single-equation model could be developed as dynamic- or cumulative single-equation model, which could either be considered as a simple-linear, -nonlinear or multi-regression single-equation model. While the multi-step dynamic model could be modeled as, single-step-degradation model (SSDM), two-step-degradation model (TSDM), and multi-step-degradation model (MSDM) [68]. These classes of models have speciality, advantages and disadvantages as described in literature [68]. In general, most single-equation models are simple, require few numbers and inexpensive experiments to develop. In contrast, multi-step dynamic models are complex, but more accurate, with their complexity as well as accuracy in the order of MSDM > TSDM > SSDM, and require a substantial number of experiment data, as well as procedures, which maybe expensive. In summary, when simplicity, time-, cost-constraint, and not accuracy are prioritised, the single-equation model would be preferred over the multi-step dynamic model [68]. Although, it is worth noting that while the single-equation model is less accurate than its counterpart, resulting data (e.g., biogas production potential, maximum biogas production rate) from its models are useful and suitable for preliminary investigation. Furthermore, while multi-step dynamic models are complex, time-consuming and expensive to develop, they can be consolidated with numerous dynamic models of other main processes (i.e., mass and heat transfers, etc.) and auxiliary models (i.e., models for microbial activity parameters, microbe-, and biogas-yields, etc.). As such resulting in a clearer physical interpretation of the AD process. Therefore, in this work, the multi-step dynamic model would be applied, specifically, the SSDM will be applied because it is simpler and quicker to evaluate unknown parameters, due to its fewer dynamic equations than the other models. The SSDM would be developed with consideration to easily apply it to control the pressure, pH, and temperature of the AD process.

2.1. Anaerobic hydrolysis of lipid

Considering the mathematical modelling of lipid-rich waste into biogas is the focus of this work, summarised literature review to highlight the limitation and progress on this topic is necessary. In general, it is well known that lipid digestion inhibits AD with lag phase occurrence, sludge floatation, and washout [69]. Long-chain fatty acid (LCFA) produced during lipid hydrolysis is the main cause of inhibition due to its toxic effects on microbes responsible for AD [70]. This issue can be resolved in different ways, which include appropriate feeding, mixing, and adjustment of operating conditions [69]. Although a more popular approach reported in literature, is the co-digestion of lipid-rich waste, and thermophilic digestion [71–74], these approaches only limit and do not eliminate the inhibition. Specifically, Cirne et al. [72] reported the inhibitory effect of lipid concentration on hydrolysis and bio-methanation for co-digestion of protein, carbohydrate, and lipid. The methane production profile was used to demonstrate that the higher amounts of lipid the stronger the inhibition in the AD, as observed from resulting lag phases. Angelidaki et al. [71] investigated the inhibitory effect of lipids on thermophilic AD and attempted to utilise bentonite-bound oil to mitigate its inhibition on AD. Hejnfelt and Angelidaki [73] investigated the AD of a mixture of manure and mixed pork waste. The report indicates no difference in methane yield between thermophilic (55°C) and mesophilic (37°C) AD when less amount of lipid-rich waste is digested. However, digestion of a high amount of lipid-rich waste was reported to be possible in mesophilic conditions. Capson-Tojo et al. [74] reported that the Thermophilic digestion of lipids only enhances higher hydrolysis rates, however, its biogas yields were comparable with the Mesophilic digestion of lipids.

The reported effect of temperature on lipid hydrolysis rate highlights the need to quantify the effect of temperature on its kinetics via a mathematical model. Although most literature highlights the kinetic of hydrolysis at constant temperature but has not mathematically quantified its effect. Specifically, Usman et al. [75] compared the kinetics of long-chain fatty acids (LCFAs) degradation in animal and plant lipid-rich wastes, without a kinetic model to quantify their differences. Zeeman and Sanders [76] highlighted two possible approaches to describe the hydrolysis of complex wastewater (composed of protein, carbohydrate, and lipid) in AD. The report suggests that while hydrolysis of particulate polymers can be described by Surface Based Kinetics, the first-order kinetic model was proposed to be more practicable for AD. This fact is collaborated by the application of the first-order kinetic model in the simulation of lipid-rich waste AD via the anaerobic digestion model n°1 (ADM1) [77]. Given these facts, it is proposed in this work to develop a kinetics model to describe the hydrolysis of lipids during AD at different temperatures, in addition to modelling the AD of lipids to biogas via the SSDM. Specifically, in addition to the SSDM, it is intended in this work to experimentally develop a first-order kinetic model for lipid hydrolysis at different temperatures (25 – 50°C), as well as an experimental investigation of biogas production for the overall AD at 35°C.

3.Aims and objectives

Therefore, this work aims to theoretically model a single-step-degradation model (SSDM) to describe the anaerobic digestion of lipid-rich waste into biogas. In addition to experimentally investigate as well as model the kinetic of lipid hydrolysis into LCFA, and glycerol with incorporation of the effect of temperature. Further with the application of the lipid hydrolysis kinetic into the SSDM. Therefore, the scope of the work entails the following objectives:

1. Source for, prepare, and characterise suitable industrial anaerobic sludge.
2. Propose a suitable experimental setup for anaerobic digestion experiments.
3. Homogenise stabilise lipid in the aqueous sludge sample.
4. Develop methodologies to determine to describe lipid degradation qualitatively and quantitatively in AD.
5. Investigate and develop a model to describe lipid hydrolysis kinetics in AD at different temperatures.
6. Curve-fit model or source for reported models to describe essential physiochemical (e.g., density), thermodynamic (e.g., specific heat capacity), and biochemical (e.g., microbe specific growth rate) parameters as a function of temperature, and/or pressure.
7. Develop a unique SSDM to describe lipid anaerobic digestion into biogas.
8. Validate the developed models for lipid hydrolysis kinetics as well as the SSDM via comparison with experimental results using adequate statistical tools when applicable.

4. Biogas

Biogas is the gaseous form of biofuel. In general, biofuel can exist in all three states of matter, i.e., solid, liquid or gas, depending on the production process. Fuel derived from recent organic matter (i.e., biomass) rather than fossil matter is termed biofuel. This includes ethanol from plant matter (typically containing carbohydrates), biodiesel from plant or animal lipids, as well as biogas from any biomass [29]. The biogas's unique characteristic makes it the most energy-efficient and environmentally reliable technology for renewable energy production [78]. Biogas is about five times less dense than air, odourless or may have an egglike smell (depending on the hydrogen sulfide content), colourless, has an ignition temperature within 650 – 750 °C, a flame temperature of 870 °C and burns with clear blue flame like that of natural gas. It has a calorific value of 20 MJ.m⁻³ and burns with an efficiency of about 60% in conventional biogas burner, for a methane content of more than 45% [79].

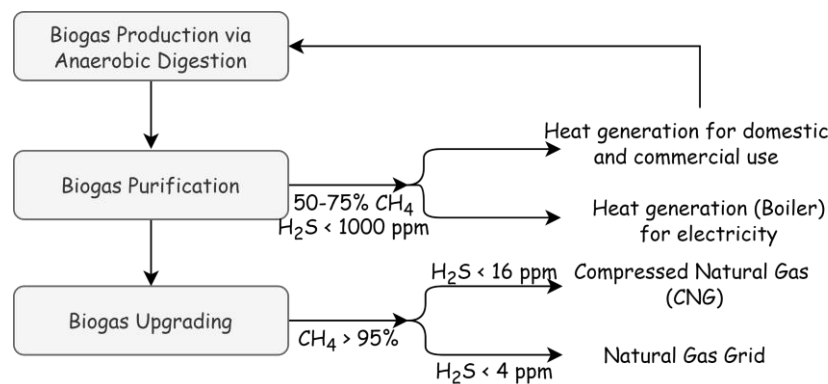


Figure 4.1. Summary of biogas utilisation with treatment level

Biogas technology is an established green system with set objectives to achieve cost-effective energy, and organic soil nutrients (digestate). Raw biogas is composed of methane (CH₄), carbon dioxide (CO₂), and components such as 0 – 5% nitrogen (N₂), 0 – 5000 ppm hydrogen sulfide (H₂S), trace concentrations of hydrogen (H₂), carbon monoxide (CO) and saturated moisture (H₂O) [54]. The presence of components other than methane (with the highest caloric value) in the biogas, suggests the need to purify the biogas to improve its calorific value. This is achieved through the removal or transformation of CO₂, via a process called biogas upgrading and purification from impurities such as H₂S, H₂O etc. This is because CO₂ is an inert gas, as such reduced its caloric value.

Table 4.1. Biogas utilisation and required composition [80]

Application	CO ₂	H ₂ O	H ₂ S
Gas Engines	–	-	<1000 ppm
Kitchen stove	–	-	+
Natural gas grid	*	+	+
Vehicle fuel	*	+	+

+ Allowable, – Not allowed and * Negligible.

Biogas upgrading is particularly necessary when it is required for use as transportation fuel or added to natural gas grids [81]. The energy value of pure methane is about 35 MJ.m⁻³ while the energy value of biogas can vary between 16 – 30 MJ.m⁻³, depending on whether it has been purified or upgraded.

A summary of biogas usage based on its treatment is illustrated in Figure (4.1) and Table (4.1). A summary of the thermodynamic properties of biogas is also given in Table (4.2). Typically, biogas containing 60% methane has an energy content of approximately 22 MJ.m⁻³.

Table 4.2. Thermophysical properties of biogas [82]

Property	Composition				Biogas 60% CH ₄ & 40% CO ₂
	CH ₄	CO ₂	H ₂	H ₂ S	
Theoretical content, %	50 – 75	25 – 50%	<1	<3	100
Calorific value, MJ.m ⁻³	37.7	–	10.8	22.8	20
Critical density, kg.m ⁻³	162	468	31	349	320
Critical pressure, Mpa	4.6	7.3	1.3	8.9	7.3 – 8.9
Critical temperature, °C	-82.5	-31.0	-	100.0	-82.5
Density, kg.m ⁻³	0.72	1.98	0.09	1.54	1.2
Flash point, °C	650-750	-	530 – 590	290 – 487	650-750
Lower explosive limit, %	5-15	-	4 – 74	4 – 42	6 – 12

4.1. Comparative study of biogas with other similar fuel

Biogas is usually compared to petrol and diesel, especially regarding the possibility of system enlargement for fuel as well as chemical fertiliser, because anaerobic digestion also produces valuable organic fertiliser. Typical comparisons indicate that about 1.3 – 1.9 m³ of biogas (i.e., 55% CH₄ and 45% CO₂ content) is equivalent to one litre of gasoline, while 1.5 – 2.1 m³ of biogas is equivalent to one litre of diesel fuel [83]. Biogas is also popularly compared to natural gas in terms of environmental performance.

The usage of biogas can be categorised into two basic purposes. It can be used directly for heating or indirectly in combustion engines for electricity generation or motive engines just like natural gas. Natural gas and biogas are similar, with both composed of methane, however, natural gas contains more methane and can be processed into compressed natural gas (CNG) as well as liquefied natural gas (LNG).

Table 4.3. Comparative Compositions of Natural Gas and Biogas [84]

Composition	Natural Gas (%)	Biogas (%)
Methane (CH ₄)	95	50 – 75
Ethane (C ₂ H ₆)	5	–
Propane (C ₃ H ₈)	+	–
Butane (C ₄ H ₁₀)	+	–
Carbon dioxides (CO ₂)	+	30 – 40
Hydrogen sulfide (H ₂ S)	–	0.3 – 3.0
Ammonia (NH ₃)	–	0.0 – 1.0
Moisture (H ₂ O)	–	0.0 – 10
Nitrogen (N ₂)	+	0.0 – 5.0
Oxygen (O ₂)	–	0.0 – 2.0
Hydrogen (H ₂)	–	0.0 – 1.0

+ & –, indicate the minute presence and absence of the components respectively.

Natural gas is created via underground decomposition of biomass, buried over millions of years (unlike biogas which takes about a week), and it is the cleanest of all fossil fuels [85]. Therefore, biogas can be used as a substitute for natural gas. However, there are a few differences between the characteristics of biogas and natural gas. Table (4.3) shows similarities as well as differences in the compositions of natural gas and biogas, and it can be observed that the higher content of CO₂ in biogas is why it has a much lower energy density than natural gas [84].

Biogas, like natural gas, has a low volumetric energy density compared to liquid biofuels such as ethanol and biodiesel. The comparison of biogas energy density with other biofuels is shown in Table (4.4). However as stated earlier, it should be noted that biogas can be upgraded and purified to a state equivalent to natural gas and made available for supplied in pipeline injection and even compressed to CNG or LNG for use as a transportation fuel.

Table 4.4. Energy density of biofuels [86]

Biofuel	Energy density, MJ.m ⁻³
Biogas (60% CH ₄)	22.4000
Purified biogas (98% CH ₄)	36.5000
Pressurised biogas (207 bar, 98% CH ₄)	7302.80
Ethanol	21198.7
Biodiesel	30528.1

5. Description of anaerobic digestion

Anaerobic digestion is a simple process, yet involves complex biochemical reactions made possible by a group of microbes that works both independently and collectively to metabolise feedstocks to a mixture of gases (mostly CH_4 & CO_2) in the absence of oxygen [80]. The microbes in anaerobic digestion are known to be sensitive to variations in process parameters, such as temperature, partial pressure, hydrogen, pH, substrate types, inoculum types, organic loading ratio, ammonia, volatile fatty acid, nutrients and trace elements, hydraulic retention time (HRT) or solids retention time (SRT), stirring, total solid (TS), and reactor configuration. Therefore, it is important to understand how these factors affect the process, and such details have been elaborated in reports [80,87–98]. Therefore, anaerobic digestion needs to be monitored, optimised, and controlled properly (e.g., via mathematical models) to reduce or prevent process instabilities. To do this, it is important to understand the various stages involved in AD. These stages can be divided into two categories: Extracellular steps (pretreatment and hydrolysis processes) and Intracellular steps (acidogenesis, acetogenesis and methanogenesis) [99], as illustrated in Figure (5.1). Note that for consistency and clarity, the reaction schemes in each stage shall be illustrated with lipids.

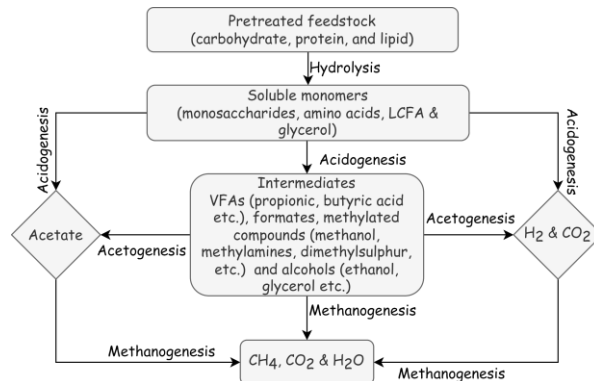


Figure 5.1. Illustrative scheme of anaerobic digestion stages [68].

*LCFA – long chain fatty acids, and VFA – volatile fatty acids

5.1. Pretreatment of feedstocks

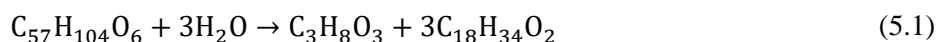
Although AD can utilise most varieties of feedstock, however, to enhance the utilisation of macronutrients, pretreatment of the feedstock may be necessary. Pretreatment includes several steps such as lysis (rupture of cell membrane via microbial, or osmotic mechanisms), nonenzymatic decay, phase separation, and physical breakdown [80]. Pretreatment can be independent or combined mechanical, chemical, thermal, and biological processes [100]. The necessity of pretreatment arises from the difficulty to utilise certain feedstocks due to: The presence of chemicals that inhibit the growth and activity of the microorganisms; Poor accessibility of their molecular structure by microbes and their enzymes (especially for feedstocks with high crystalline structure or low surface area); Poor physicochemical characteristics resulting to issues of floating, foaming or clumping, block impellers and pipes, etc [101]. To buttress the necessity of pretreatment, feedstock based on food waste, containing high levels of biodegradable matter, such as protein, carbohydrates, and lipids, may still require pretreatment. For example, AD of lipid-rich waste, without pretreatment (such as thermal pretreatment) can cause low digestion efficiency and severe inhibition, because of slow degradation rate as well as accumulation of long-chain fatty acid [102,103]. Typically, thermal pretreatment can facilitate the elimination of pathogens in feedstocks and ensure appropriate microbes' quality compatible with AD [104] (These, pathogens may affect the process

negatively, and usually cause heterogeneous results in disturbance and yield for the same feedstock, microbe culture and process conditions). On the other hand, thermal pretreatment should be carefully implemented, as it can negatively affect and inactivate feedstock's pre-existing microbial culture vital for efficient AD [105].

5.2. Hydrolysis of feedstocks

Proceeding the pretreated feedstock is the hydrolysis of macronutrients (carbohydrates, proteins, and lipids), however, the pretreatment process can be intertwined with hydrolysis. Hydrolysis facilitates the degradation of macronutrients to their respective monomers or substrate (fatty acid-and-glycerol, glucose, amino acids). Hydrolysis has been proposed as the rate-limiting step for anaerobic digestion [60–62], therefore it is necessary to ensure it is comprehensively analysed as well as implemented. It is usually the reason why anaerobic digestion may experience a long residence time if not effectively executed [80]. The hydrolysis rate depends on the macronutrients type (typically, lipids < proteins < carbohydrates [106,107]), substrate concentration, particle size, pH (optimum, 5 – 7), and temperature (optimum, 30 – 50 °C) [62,108,109].

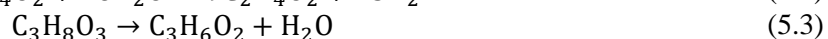
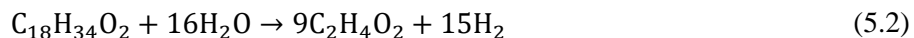
Hydrolytic/acidogenic bacteria are responsible for the hydrolysis of macronutrients (F) into substrates (S) via the production of extracellular enzymes such as cellobiase (carbohydrates (F) into glucose (S)), proteases (protein (F) into amino acid (S)) and lipase (lipids (F) into glycerol and fatty acids (S)) [109–111].



Equation (5.1) is a typical illustration of lipid hydrolysis (i.e., triglyceride with three (5) identical LCFA) into glycerol and LCFA. Note that other glycerides in the lipid – diglyceride and monoglyceride also undergo hydrolysis.

5.3. Acidogenesis of hydrolysis products

Acidogenesis involves the fermentation of simple sugar (e.g., glucose) and amino acids, as well as the anaerobic oxidation of alcohols (e.g., glycerol) together with LCFA (e.g., oleic acid) by acid-forming bacteria (acidogenes) [112,113]. In addition to the formation of side (carbon dioxide, water, hydrogen, acetic acid, etc.) and intermediary (propionic, butyric, valeric acid etc., known as volatile fatty acid, VFAs) products. Acidogenes prefer the degradation substrates to acetic acid since this pathway results in the highest energy yield for their rapid growth (with a minimum doubling time of about 30 minutes) and they can tolerate a pH within the range of about 5.0 – 6.0 [109,114–116]. The rapidness of acidogenesis can result in a large formation of carbon dioxide as well as hydrogen gas, and much more hydrogen gas can be formed, especially for feedstock with high carbohydrate content. The generated hydrogen gas can be directly extracted in this stage [117–119]. Although acidogenesis is fast, the sudden formation of its acidic products (resulting in decreasing pH) can inhibit the entire AD especially when these products are not quickly metabolised by acetogenes in the next or concurrent acetogenesis stage [120,121].

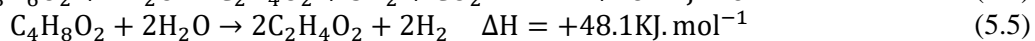
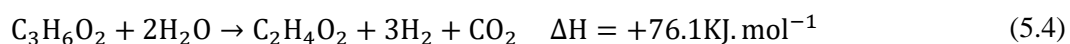


Equations (5.2) and (5.3), respectively illustrate the acidogenesis of fatty LCFA (oleic fatty acid) and glycerol without consideration of the biochemical activities of microbes. A certain amount of these components is used for the formation of new microbial cells ($C_5H_7NO_2$), energy for their growth and maintenance. Although the degradation of LCFA is illustrated in this stage, it is however an oxidation reaction with an external electron acceptor [122,123] and should be more appropriately categorised in the

acetogenesis stage. Furthermore, it is assumed that glycerol molecules are completely converted to propionic acid rather than directly to acetic acid, Equation (5.3) [124].

5.4. Acetogenesis of products from acidogenesis

Acetogenesis is an intertwined or a subsidiary of acidogenesis, involving the anaerobic oxidation of VFAs (Propionic, butyric, valeric acid etc.) and alcohols (glycerol, ethanol, etc.) from acidogenesis into acetic acid, hydrogen, and carbon dioxide by acetogens [125]. Acetogenesis may inhibit the preceding methanogenesis stage if the produced hydrogen is not quickly metabolised by methanogenic bacteria. This is because high partial pressure of hydrogen ($\geq 1.01 \times 10^{-6}$ bars) is thermodynamically unfavourable to acetogenesis, thus resulting in VFA accumulation and changes in VFA distribution [126]. The growth of acetogens is slow (with a minimum doubling time of 1.5 to 4 days), even under optimum conditions (low dissolved hydrogen concentration, pH 6.0 – 6.2, etc.,) [116,120,127].

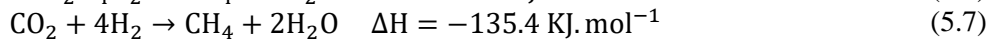


Equations (5.4) and (5.5), illustrate the acetogenesis of propionic, and butyric acid into acetic acid, carbon dioxide, as well as hydrogen, without consideration of new microbial cells ($\text{C}_5\text{H}_7\text{NO}_2$) formation, energy for their growth and maintenance.

5.5. Methanogenesis of products from acetogenesis

Methanogenesis involves the formation of methane from acetic acid (facilitated by the slow-growing acetoclastic methanogens with a minimum doubling time of about 2 – 3 days, due to low energy yield of the reaction pathway). It also utilises hydrogen and carbon dioxide (through the fast-growing hydrogenotrophic methanogens, with a minimum doubling time of about 6 hours) [120,128,129]. Acetoclastic methanogens are particularly sensitive to parameters such as pH, nutrient, and trace element concentrations. The methane produced by this type of methanogen accounts for about 70% of the total methane produced, and typical examples of these microbes are the Methanosarcina, Methanosaeta species etc. [130]. In general, methanogens are the “autopilot” of the anaerobic digestion process, because they help control the amount of VFAs and carbon dioxide (i.e., alkalinity) [131,132] and operate at an optimal pH close to neutral region ($\sim 7.0 - 7.2$) [116].

The methane content of biogas depends on the composition of macronutrients, particularly on the oxidation state of the organic carbon present in the substrate [133]. Equations (5.6) and (5.7), illustrate methanogenesis from Acetoclastic and Hydrogenotrophic methanogens respectively, without considering new microbial cells ($\text{C}_5\text{H}_7\text{NO}_2$) formation, energy for their growth as well as maintenance.



The methanogenesis step is as important as the hydrolysis step because it is arguably considered the rate-limiting step in anaerobic digestion. Methanogenesis has been reported to be rate-limiting, especially at conditions of higher temperature, and when the feedstock is mainly soluble, as solubility enhances the rate of hydrolysis [62,120].

6. Model review on anaerobic digestion

Popular models for AD highlighted in literature can be grouped into single-equation models and multi-step dynamic models as proposed by Emebu et al. [68]. The multi-step dynamic model as illustrated in Figure (6.2), shall be of focus. The single-equation model could be developed as a dynamic- or cumulative single-equation model, which could either be considered as a simple-linear, simple-nonlinear or multi-regression single-equation model. While the multi-step dynamic model could be modelled as, a single-step-degradation model (SSDM), two-step-degradation model (TSDM), and multi-step-degradation model (MSDM) [68].

6.1. Single-based equation model

Single-based equation models consider a holistic description of the anaerobic digestion of feedstocks with one equation without the various biochemical, mass transfer, and physicochemical processes, and their interconnections via equations.

6.1.1. Dynamic single-equation model

Dynamic single-equation models, Table (6.1), are developed to predict the biogas production rate ($\text{mg.g}^{-1}.\text{time}^{-1}$) from a given feedstock. They are generic analytical expressions not based on AD concepts, but on data trends. Therefore, their constants do not have biochemical meaning to AD. These models may be useful for simple process control of AD [134,135].

Table 6.1. Popularly reported dynamic single-equation model

Model	Expression	
Linear model [136]	$y = a + bt$	(6.1)
Exponential model [137]	$y = a + b\exp(ct)$	(6.2)
Gaussian model [138]	$y = a \cdot \exp(-0.5((t - t_0)/b^*)^2)$	(6.3)
Multi regression model [139]	$f(x) = \beta_0 + \sum_{i=1}^n \beta_i x_i + \sum_{i=1}^n \beta_{ii} x_i^2 + \sum_{i=1}^n \sum_{j=1}^n \beta_{ij} x_i x_j$	(6.4)
Polynomial model [140]	$f(x) = \beta_0 + \sum_{j=1}^n \beta_j x^j$	(6.5)

Where y ($\text{mg.g}^{-1}.\text{time}^{-1}$) is the biogas production rate over digestion time, t with constants, a ($\text{mg.g}^{-1}.\text{time}^{-1}$), a^* ($\text{mg.g}^{-1}.\text{time}^{-1}$), b ($\text{mg.g}^{-1}.\text{time}^{-2}$), b^* (time^{-1}), c (time^{-1}) and t_0 is the time when the maximal biogas production rate occurs. While for the multi-regression model $f(x)$ is the response i.e., biogas yield, x_i and x_j represent the process factors (x) (pH, concentration of substrate, temperature, etc.), β_0 is the model constant, β_i , a linear term, β_{ii} , quadratic term, β_{ij} , interactive term coefficient, and n , the number of process factors. However, for the polynomial model n and $j=1, 2, \dots, n$ are the order and order sequence of the polynomial model. Note that multi-regression and polynomial models can also be developed as cumulative single-equation models.

6.1.2. Cumulative single-equation model

Cumulative single-equation models reported in literature are mostly non-linear, Table (6.2). They are developed based on the prevailing assumption of the rate-limiting step (e.g., microbial activity, hydrolysis rate, or biogas evolution rate) in the AD. Therefore, they can be called, specific rate-limiting models, and they can be used to determine useful parameters (biogas production potential, maximum biogas production rate, biogas production delay phase, etc.) in the AD [141,142].

Table 6.2. Popularly reported cumulative single-equation model

Model	Expression	
Thermogravimetry model (TGM) [143]	$\chi^{1/\sigma} = kt$	(6.6)
First-order model [144]	$y = A\{1 - \exp(-kt)\}$	(6.7)
Gompertz model (GM) [145]	$y = A\exp(-\exp(b - ct))$	(6.8a)
Modified GM [146]	$y = A\exp\{-\exp([R_m e(\lambda - t)/A] + 1)\}$	(6.8b)
Schnute model (SM) [147]	$y = y_1^\beta + (y_2^\beta - y_1^\beta) \{ [1 - \exp(-\alpha(t - t_1))] / [1 - \exp(-\alpha(t_2 - t_1))] \}^{1/\beta}$	(6.9a)
Modified SM [148]	$y = R_m(1 - \beta) / \alpha \{ (1 - \beta \exp(\alpha\lambda + 1 - \beta - \alpha t)) / (1 - \beta) \}^{1/\beta}$	(6.9b)
Richard model (RM) [149]	$y = a\{1 + \delta \exp[k(\tau - t)]\}^{-1/\delta}$	(6.10a)
Modified RM [150]	$y = A[1 + \delta \exp(1 + \delta) \cdot \exp\{(R_{\max}(1 + \delta)/A)(1 + 1/\delta)(\lambda - t)\}^{-1/\delta}]^{-1/\delta}$	(6.10b)
Logistic model (LM) [149]	$y = a / \{1 + \exp(b - ct)\}$	(6.11a)
Modified LM [149,150]	$y = A / [1 + \exp\{(4R_{\max}(\lambda - t)/A) + 2\}]$	(6.11b)
Transference model (TM) [151]	$y = a\{1 - \exp(b - ct)\}$	(6.12a)
Modified TM [152]	$y = A\{1 - \exp(-R_{\max}(t - \lambda)/A)\}$	(6.12b)
Cone model [153]	$y = A / (1 + (k_{\text{hyd}}t)^{-\sigma})$	(6.13)
Fitzhugh model [154]	$y = A(1 - \exp(-kt)^\sigma)$	(6.14)

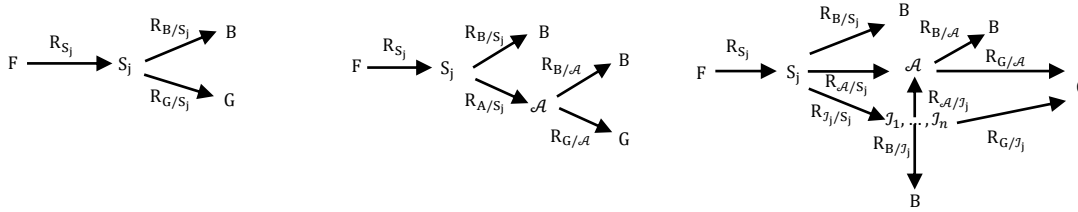
In the Thermogravimetry model, $\chi = V_t/V_\infty$, V_t is the volume of biogas generated over a time, t , V_t is the volume of biogas produced over time, V_∞ the total volume of biogas produced, k are rate constants (time^{-1}) and σ describes the processes of nucleation, with the value range, 2 – 4 most applicable. While for the other models k_{hyd} , α , a , b , c & k are rate constants (time^{-1}), λ is the lag time, σ , β & δ are dimensionless shape factors, A is the biogas production potential ($\text{mg} \cdot \text{g}^{-1}$), R_{\max} is the maximal biogas production rate ($\text{mg} \cdot \text{g}^{-1} \cdot \text{time}^{-1}$), $e = \exp(1)$ and y_1 and y_2 are biogas produced at the time t_1 and t_2 respectively.

6.2. Multi-step dynamic model

The Multi-step dynamic model in addition to the biochemical steps can accounts for a broad range of process phenomena involved in AD, using more than one sequentially interconnected dynamic equation (such as dynamics of microbial growth, feedstock hydrolysis, resulting substrate utilisation, biogas formation, biogas evolution, and heat transfer). The term “Multi-step” implies the biochemical stages in AD, and “dynamic” implies the description of the stages using a time-dependent differential equation. Based on the substrate degradation level considered, as illustrated in [Figure \(6.1\)](#), this model can be: **Single-step-degradation model (SSDM)** considers the direct degradation of substrates (S_j , amino acids, sugars,

LCFA & glycerol, etc. obtained from their respective feedstocks (F) of proteins, carbohydrates, lipids, etc.) into biogas (G); **Two-step-degradation model (TSDM)**, considers the Acidogenesis of substrates into acetic acid (\mathcal{A}) and Methanogenesis of acetic acid into biogas and; **Multi-step-degradation model (MSDM)** considers all substrate degradation levels, i.e. Acidogenesis of a substrate to acetic acid and intermediates (J_j , volatile fatty acids, alcohols, etc.), Acetogenesis of intermediates, as well as Methanogenesis of products from Acidogenesis, including Acetogenesis into biogas. Note that in these models it is also essential to consider the utilisation of some portion of feedstock, substrates, and intermediates into biomass (B). The Multi-step dynamic model is popularly reported in literature, and the popular Anaerobic digestion model no.1 (**ADM1**) is an example of this model [155,156].

In Equation (6.15) – (6.20), $R_j = R_{S_j}, R_{B/S_j}, R_{G_j/S_j}$, represent the reactive terms in the degradation process. Typically, for illustrative purposes, the reactive terms starting with B (e.g., R_{B/S_j}) represent the consumption rate of a given reaction component (e.g., substrate, S_j) into microbial biomass, B. Where $j = 1, 2, \dots, n$ indicate the number of species being considered, i.e. various substrates, S_j (e.g. LCFA and glycerol from lipid feedstock, with input composition, S_{i-j}), intermediates, J_j (VFAs, alcohol, etc., with input composition, J_{i-j}) and biogas constituents, G_j (e.g. $\text{CH}_4, \text{CO}_2, \text{H}_2$, etc.) in the process. \mathcal{D} is the bioreactor dilution rate (i.e., the inlet volumetric feed rate to liquid volume ratio).



a. Single-Step Degradation b. Two-Step-Degradation c. Multi-Step Degradation

Figure 6.1. Illustration of degradation level considered in the multi-step dynamic models

6.2.1. Single-step-degradation model

The SSDM is a simple model of biogas yield from the substrate, S_j , as illustrated by Equation (6.15), a generic expression, and the SSDM has been reported in literature [57].

$$dS_j/dt = \mathcal{D}(S_{i-j} - S_j) + R_{S_j} - R_{B/S_j} - \sum_{j=1}^n R_{G_j/S_j} \quad (6.15)$$

6.2.2. Two-step-degradation model

The TSDM also referred to as the AM2 model (Acidogenesis methanogenesis, two-step model) is popularly reported in literature [66,67,157], and it models the yield of biogas from acetic acid, \mathcal{A} , formed from substrates, S_j , Equation (6.16) – (6.17).

$$dS_j/dt = \mathcal{D}(S_{i-j} - S_j) + R_{S_j} - R_{B/S_j} - R_{\mathcal{A}/S_j} \quad (6.16)$$

$$d\mathcal{A}/dt = \mathcal{D}(\mathcal{A}_i - \mathcal{A}) + R_{\mathcal{A}/S_j} - R_{B/A} - \sum_{j=1}^n R_{G_j/\mathcal{A}} \quad (6.17)$$

6.2.3. Multi-step-degradation model

The MSDM is popularly reported in literature [63,158,159], and the ADM1 is an example of this model. It also models the yield of biogas from acetic acid, \mathcal{A} , formed from intermediates, J_j (VFAs, alcohols etc) generated from substrates, S_j degradation, Equation (6.18) – (6.20).

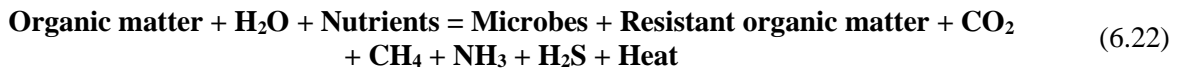
$$dS_j/dt = \mathcal{D}(S_{i-j} - S_j) + R_{S_j} - R_{B/S_j} - R_{\mathcal{A}/S_j} - \sum_{j=1}^n R_{J_j/S_j} \quad (6.18)$$

$$dJ_j/dt = \mathcal{D}(J_{i-j} - J_j) + R_{J_j/S_j} - R_{B/J_j} - R_{\mathcal{A}/J_j} - \sum_{j=1}^n R_{G_j/J_j} \quad (6.19)$$

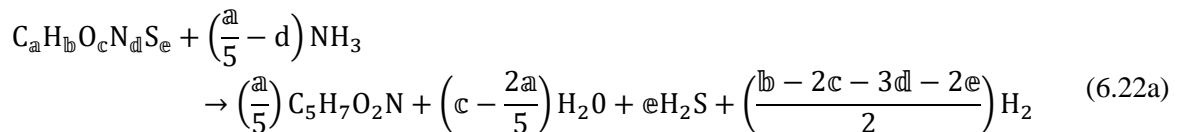
$$d\mathcal{A}/dt = \mathcal{D}(\mathcal{A}_i - \mathcal{A}) + R_{\mathcal{A}/S_j} + R_{\mathcal{A}/J_j} - R_{B/\mathcal{A}} - \sum_{j=1}^n R_{G_j/\mathcal{A}} \quad (6.20)$$

6.3. Theoretical estimation of substrate, microbes, and biogas yield

Theoretical computation of microbes and biogas yield from substrate gives an idea of their maximum possible value in the AD. This estimation assumes the complete conversion of the substrate into CO_2 , CH_4 , NH_3 , etc. This estimation makes it possible to compare the theoretical and the experimental yields (by bottle assays) [61]. It can also be used to estimate reaction terms in dynamic models, as support or in the absence of experimental data. The generic expressional statement for the transformation of organic matter in AD is given by Equation (6.22) [160]. Typical illustrations of the estimated essential theoretical yield of substrate, microbes and biogas from lipid is given in Table (6.3).



According to Equation (6.22), not all organic matter is biodegradable, due to the presence of non-degradable components, inhibitory substances, operating conditions, etc. **Filer et al.** [98] reported that 10% of the substrate in AD is converted into microbes and transformed into heat. A typical illustration by following the VD1 4630 guideline for digestion of cellulose via the Biochemical Methane Potential (BMP) test, produces biogas with a yield of at least 80 – 85% of its theoretical maximum. The microbe yield, Y_{B_j/S_j} (kg.kg^{-1}), from a generic substrate, $S_j = C_a H_b O_c N_d S_e$ can be deduced from Equation (6.22a), via Equation (6.22b) on the basis that the chemical composition of microbes consists of 92% $C_5 H_7 O_2 N$ on total dry weight [161]. Usually, microbes undergo different growth stages, i.e., **lag**, **acceleration**, constant and **decay** phases, Figure (6.2) [162]. Note that the yield, $Y_{G_{Dj^*}/S_j}$ (kg.kg^{-1}), of some produced biogas components such as ammonia, hydrogen sulphide, and hydrogen can also be estimated, Equation (6.22c). Depending on the sign of the stoichiometric coefficient, n_{j^*} of NH_3 , H_2O and H_2 , they might become present as a product or reactant (if its coefficient is less than zero, e.g., NH_3 become a product, for $(a/5-d) < 0$, H_2 becomes reactant for $(b - 2c - 3d - 2e) < 0$) and even absent if its coefficient is zero. Note that the yield of ammonia for microbes' formation, $Y_{G_{Dj^*}/B_j}$ (kg.kg^{-1}), can also be estimated.

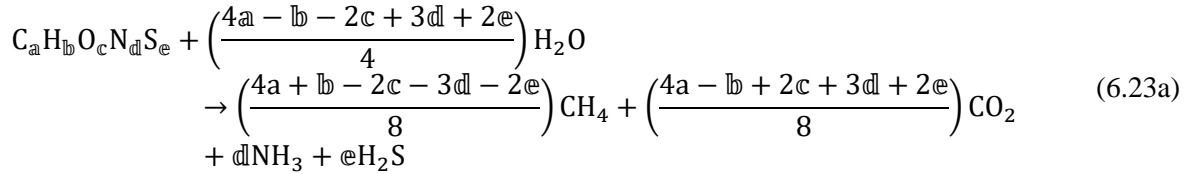


$$Y_{B_j/S_j} = \frac{(113a/5)}{0.92(12a + b + 16c + 14d + 32e)} \quad (6.22b)$$

$$Y_{G_{Dj^*}/S_j} = \frac{M_{j^*} n_{j^*}}{(12a + b + 16c + 14d + 32e)} \quad (6.22c)$$

$$Y_{G_{Dj^*}/B_j} = \frac{0.92M_{j^*}n_{j^*}}{(113a/5)} \quad (6.22d)$$

The theoretical biogas (CH₄ and CO₂) yield, $Y_{G_{Dj^*}/S_j}$, can be estimated via diverse approaches. The modified **Buswell & Neave** [163] stoichiometric balance is a typical example, based on the generic substrate, $S_j = C_aH_bO_cN_dS_e$ [164] as given by [Equations \(6.23a\) and \(6.23b\)](#) (kg.kg⁻¹) or [\(6.23c\)](#) (m³.kg⁻¹). Where M_{j^*} and n_{j^*} are the molar mass and stoichiometric ratio of specific biogas species, j^* .



$$Y_{G_{Dj^*}/S_j} = \frac{M_{j^*}n_{j^*}}{(12a + b + 16c + 14d + 32e)} \quad (6.23b)$$

$$Y_{G_{Dj^*}/S_j} = \frac{23.415n_{j^*}}{(12a + b + 16c + 14d + 32e)} \quad (6.23c)$$

Table 6.3. Theoretical yield estimate of the substrate from feedstock, biogas and microbes from the substrate, ammonia from microbes for lipid (triglyceride with oleic acid)

Yield (Kg.kg ⁻¹)	S _j =LCFA, C ₁₈ H ₃₄ O ₂	S _j =Glycerol, C ₃ H ₈ O ₃
Feed, Y _{S_j/F}	0.9570	0.1041
Microbes, Y _{B_j/S_j}	1.5680	0.8010
NH ₃ from microbes, Y _{G_DNH₃*/B_j}	0.1384	0.1383
CH ₄ , Y _{G_DCH₄/S_j}	0.7234	0.3043
CO ₂ , Y _{G_DCO₂/S_j}	0.8191	0.5978
H ₂ , Y _{G_DH₂/S_j}	0.1064	0.0071

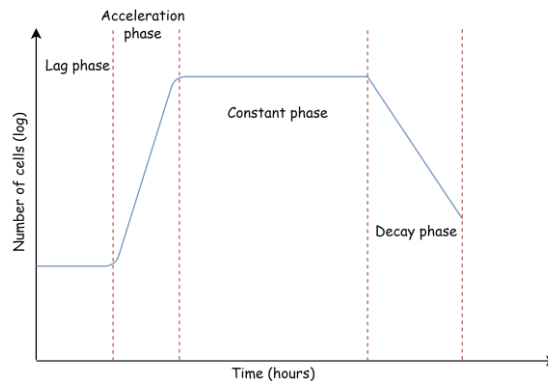


Figure 6.2. Typical growth curve of biomass in a biochemical process

7. Theoretical framework – Model development

Considering multi-step dynamic models are advantageous for their ability to develop them according to specific scope of processes (i.e., biochemical, mass- and heat-transfer process, etc.) to investigate in AD. Specifically, the SSDM will be developed, because it is simpler and quicker to evaluate its parameters, in addition to the fact that it can easily be applied to control the pressure, pH, and temperature of the AD.

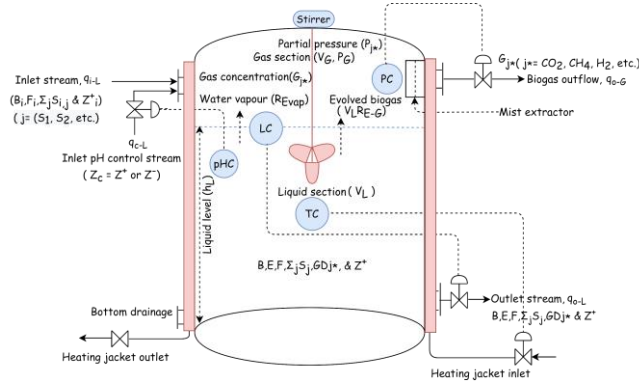


Figure 7.1. Description of anaerobic digestion in a continuous stirred tank reactor (CSTR) type bioreactor with material and heat transfer.

Considered the CSTR bioreactor, [Figure \(6.1\)](#), with inlet streams into the bioreactor ($\sim 35^{\circ}\text{C}$). The inlet stream constitutes of microbes, B_i , lipid feedstock, F_i , and possibly some substrate, S_i , hydrolysed from the lipid as well as a possibility of some dissolved gases, G_{D_i} . Depending on the hydraulic retention time (HRT) and stage of the biochemical reaction, the level, temperature, as well as pH of the bioreactor are controlled to an acceptable set point via the level (LC), temperature (TC), and pH (pHC) controllers. The PC ensures the pressure of the bioreactor is maintained at a specific pressure (e.g., atmospheric pressure), through immediate release (via q_{0-G}) of accumulated biogas produced. This pressure control ensures adequate evolution of biogas ($V_L R_{E-G}$) from biogases formed in the liquid sludge (G_D). The temperature control is executed with hot water (HW) fed through the heating jacket (HJ). Adequate temperature and stirring ensure the homogeneity of the system. While stirring ensures uniformity in temperature, substrate solubility and enhanced contact of microbes with substrates; increasing temperature further improves the efficiency of mass transfer in the reactor volume (V_L). The temperature change in the bioreactor is affected by the temperature of the inlet stream, and that of the surroundings. Heat is usually lost to the surrounding from the bioreactor, and heat loss is via convection and radiation to the surroundings. The other components of the bioreactor are the bottom drainage, which serves for maintenance purposes and handles emergence overflow, also is the mist extractor which adsorbs moisture from the discharge outlet gas stream (q_{0-G}). A typical laboratory-scaled semi-batch bioreactor utilised in this work is illustrated in [Figure \(6.2\)](#).

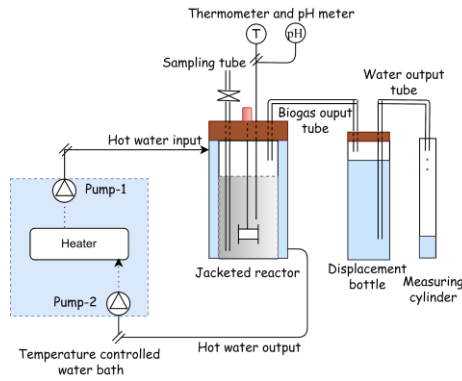


Figure 7.2. Schematics of semi-batch anaerobic digestion bioreactor at atmospheric condition

7.1. Material balance of control volume

In modelling the material flow of streams in and out of the bioreactor, it is assumed, that the flow profile is approximately laminar and that the stream distribution during changes in the level of bioreactor content is uniform. This implies that the streams can be thought to be a uniform flowing and growing layer, whose fluid properties are approximately the same at any time and spatial coordinate in the bioreactor. This assumption is reasonably valid for a stirred system. However, HW flows turbulently (i.e., $Re > 2100$) through the HJ in a steady state, and as such the rate of inflow, q_{i-hw} same as outflow, q_{o-hw} (i.e., $q_{i-hw} = q_{o-hw} = q_{hw}$).

7.1.1. Volumetric balance of control volume

The volume of the bioreactor, $V_R = \pi r_{Ri}^2 h_R$ (a constant control volume, m^3), can be divided into two dynamic sections: The liquid volume, $V_L(t) = \pi r_{Ri}^2 h_L(t)$; and the gas volume, $V_G(t)$.

$$V = V_L(t) + V_G(t) \quad (7.1a)$$

$$\pi r_{Ri}^2 h_R = \pi r_{Ri}^2 h_L(t) + V_G(t) \quad (7.1b)$$

Differentiating Equation (7.1b) yields Equation (7.1c), since V_R is constant therefore $dV/dt = 0$

$$0 = \pi r_{Ri}^2 \frac{dh_L}{dt} + \frac{dV_G}{dt} \quad (7.1c)$$

Also, the differential equation for liquid is given by Equation (7.1d) and that of the gaseous section by Equation (7.1e), where h_R , h_L and r_{Ri} are the height of the reactor, level of the liquid and inner radius of the bioreactor in meters (m).

$$\frac{dV_L}{dt} = \pi r_{Ri}^2 \frac{dh_L}{dt} \quad (7.1d)$$

$$\frac{dV_G}{dt} = -\pi r_{Ri}^2 \frac{dh_L}{dt} \quad (7.1e)$$

7.1.2. Mass balance of control volume

The entire mass balance of the control volume can be deduced from the immediate expressional statement, Equation (7.2a).

$$\text{Rate of mass input} = \text{Rate of accumulated mass} + \text{Rate of mass output} \quad (7.2a)$$

$$\begin{aligned} \dot{m}_{i-L} + \dot{m}_{c-L} &= \frac{dm}{dt} + (\dot{m}_{o-L} + \dot{m}_{o-G} + \dot{m}_{o-w_v} + \dot{m}_{o-Gw}) \\ \frac{dm}{dt} &= (\dot{m}_{i-L} + \dot{m}_{c-L}) - (\dot{m}_{o-L} + \dot{m}_{o-G} + \dot{m}_{o-w_v} + \dot{m}_{o-Gw}) \end{aligned} \quad (7.2b)$$

Applying the necessary mathematical expression to Equation (7.2a) (i.e., rate of mass input ($\dot{m}_{i-L} + \dot{m}_{c-L}$), accumulated mass (dm/dt), and mass output ($\dot{m}_{o-L} + \dot{m}_{o-G} + \dot{m}_{o-w_v}$) yields Equation (7.2b). Where \dot{m}_{i-L} , \dot{m}_{c-L} , \dot{m}_{o-L} , \dot{m}_{o-G} , \dot{m}_{o-w_v} and \dot{m}_{o-Gw} are respectively, the mass inflow rate, inflow rate of pH controller, outflow rate of liquid, outflow rate of biogas, outflow of water vapour, and outflow of biogas water content from the bioreactor, expressed in $\text{kg}\cdot\text{s}^{-1}$. Rearranging Equation (7.2b) to (7.2c), and expressing the accumulation term, dm/dt in terms of individual liquid, gas, and vapour phases ($dm_L/dt + dm_G/dt + dm_{w_v}/dt$), Equation (7.2d). Noting that the masses of the various phases can be expressed in terms of their density or concentration, i.e., $m_L = V_L\rho_L$; $m_G = V_GG$; $m_{w_v} = V_Gw_v$; $\dot{m}_{i-L} = q_{i-L}\rho_{i-L}$; $\dot{m}_{c-L} = q_{c-L}\rho_{c-L}$; $\dot{m}_{o-L} = q_{o-L}\rho_{o-L}$; $\dot{m}_{o-G} = q_{o-G}G$; $\dot{m}_{o-w_v} = q_{o-G}w_v$ and $\dot{m}_{o-Gw} = q_{o-GG}W_{H_2O}$. Note that q_{o-G} , which includes gases and water vapour flowing out of the bioreactor gaseous outlet, is different from, q_{o-GG} , the flowrate of biogas or gaseous component only.

$$\frac{dm}{dt} = q_{i-L}\rho_{i-L} + q_{c-L}\rho_{c-L} - q_{o-L}\rho_{o-L} - q_{o-G}G - q_{o-G}w_v - q_{o-GG}W_{H_2O} \quad (7.2c)$$

$$\frac{dm}{dt} = \frac{dm_L}{dt} + \frac{dm_G}{dt} + \frac{dm_{w_v}}{dt} = \frac{d(V_L\rho_L)}{dt} + \frac{d(V_GG)}{dt} + \frac{d(V_Gw_v)}{dt} \quad (7.2d)$$

Substituting Equation (7.2d) into (7.2b) and (7.2c), as well as rearranging yields Equation (7.2e) and (7.2f). Noting that for: liquid, $\rho_{i-L} \cong \rho_{c-L} \cong \rho_{o-L} \cong \rho_L$, and $d(V_L\rho_L)/dt = \rho_L dV_L/dt$; gases, $d(V_GG)/dt = V_G dG/dt + G dV_G/dt$, as well as water vapour, $d(V_Gw_v)/dt = V_G dw_v/dt + w_v dV_G/dt$. Note that it is assumed of water accompanying the outflow of water that makes the biogas water content, \dot{m}_{o-Gw} , is not cumulative on the headspace, but instantaneously from the liquid phase to the biogas outlet.

$$\begin{aligned} \rho_L \frac{dV_L}{dt} + \left(V_G \frac{dG}{dt} + G \frac{dV_G}{dt} \right) + \left(V_G \frac{dw_v}{dt} + w_v \frac{dV_G}{dt} \right) \\ = \dot{m}_{i-L} + \dot{m}_{c-L} - \dot{m}_{o-L} - \dot{m}_{o-G} - \dot{m}_{o-w_v} - \dot{m}_{o-Gw} \end{aligned} \quad (7.2e)$$

$$\begin{aligned} \rho_L \frac{dV_L}{dt} + V_G \left(\frac{dG}{dt} + \frac{dw_v}{dt} \right) + (G + w_v) \frac{dV_G}{dt} \\ = q_{i-L}\rho_{i-L} + q_{c-L}\rho_{c-L} - q_{o-L}\rho_{o-L} - q_{o-G}G - q_{o-G}w_v - q_{o-GG}W_{H_2O} \\ \rho_L \frac{dV_L}{dt} + V_G \left(\frac{dG}{dt} + \frac{dw_v}{dt} \right) + (G + w_v) \frac{dV_G}{dt} \\ = (q_{i-L} + q_{c-L} - q_{o-L})\rho_L - q_{o-G}(G + w_v) - q_{o-GG}W_{H_2O} \end{aligned} \quad (7.2f)$$

7.2. Mass balance for liquid phase

The liquid mass balance of the control volume can be deduced from Equation (7.3a) – (7.3b).

$$\text{Liquid input rate} = \text{Liquid accumulation rate} + \text{Liquid output rate} + \text{Biogas evolution rate} + \text{Water vapour evaporation rate} \quad (7.3a)$$

$$\begin{aligned}\dot{m}_{i-L} + \dot{m}_{c-L} &= \frac{dm_L}{dt} + \dot{m}_{o-L} + V_L R_{E-G} + R_{Evap} + q_{o-GG} W_{H_2O} \\ \frac{dm_L}{dt} &= (\dot{m}_{i-L} + \dot{m}_{c-L}) - (\dot{m}_{o-L} + \dot{m}_{o-G} + \dot{m}_{o-w_v} + \dot{m}_{o-Gw})\end{aligned}\quad (7.3b)$$

Applying the necessary mathematical expressions earlier highlighted, yields the dynamics for liquid volume Equation (7.3c), and (7.3d).

$$\rho_L \frac{dV_L}{dt} = (q_{i-L} + q_{c-L} - q_{o-L}) \rho_L - (V_L R_{E-G} + R_{Evap} + q_{o-GG} W_{H_2O}) \quad (7.3c)$$

$$\frac{dV_L}{dt} = q_{i-L} + q_{c-L} - q_{o-L} - (V_L R_{E-G} + R_{Evap} + q_{o-GG} W_{H_2O}) / \rho_L \quad (7.3d)$$

The changes in liquid volume, in addition to the flowrate of input and output in the CSTR, are also affected by evaporation of water, R_{Evap} ($\text{kg}\cdot\text{s}^{-1}$), evolution of gases, $R_{E-G} = \sum_{j_*} R_{E-Gj_*}$ ($\text{kg}\cdot\text{m}^{-3}\cdot\text{s}^{-1}$), and inherent moisture accompanying biogas output from the bioreactor, W_{H_2O} ($\text{kg H}_2\text{O}$ per m^3 biogas or gaseous species), from the liquid phase. Where $j_* = \text{CH}_4, \text{CO}_2$ and H_2 i.e., the various biogas species.

7.2.1. Dynamics of level for liquid phase

The dynamics of liquid level can be deduced by combining Equation (7.1d) and (7.3d) to yield Equation (7.3e).

$$\frac{dh_L}{dt} = \frac{q_{i-L} + q_{c-L} - q_{o-L} - (V_L R_{E-G} + R_{Evap} + q_{o-GG} W_{H_2O}) / \rho_L}{r_{Ri}^2} \quad (7.3e)$$

7.3. Volumetric balance in gas-vapour headspace

Consequent to the derivation of Equation (7.3d) and (7.3e), the gas-vapour headspace volumetric balance can be deduced by combining Equation (7.3e) and (7.1e) to yield Equation (7.3f).

$$\frac{dV_G}{dt} = q_{o-L} - q_{i-L} + q_{c-L} + (V_L R_{E-G} + R_{Evap} + q_{o-GG} W_{H_2O}) / \rho_L \quad (7.3f)$$

7.4. Liquid phase component balance

The components balance for the various substance present in the liquid phases are considered in the following sections.

7.4.1. Component balance for hydrolysis of lipid

The hydrolysis reaction of lipid feedstock with concentration, F_i ($\text{kg}\cdot\text{m}^{-3}$) to primarily long-chain-fatty-acid (LCFA—oleic acid, $\text{C}_{18}\text{H}_{34}\text{O}_2$ as basis) substrate, S_1 and secondarily glycerol ($\text{C}_3\text{H}_8\text{O}_3$) substrate, S_2 . The lipid balance in the liquid phase can be deduced from Equation (7.4a) – (7.4b). Noting that $R_F = K_{lipid} F$ represents the hydrolysis reaction rate term catalysed by enzymes from microbes, where K_{lipid} (s^{-1}) is the hydrolysis rate constant.

$$\begin{aligned}\text{Feedstock input rate} &= \text{Feedstock accumulation rate} + \text{Feedstock output rate} \\ &+ \text{Feedstock hydrolysis rate}\end{aligned}\quad (7.4a)$$

$$\dot{m}_{i-F} = \frac{dm_F}{dt} + \dot{m}_{o-F} + V_L R_F \quad (7.4b)$$

Applying the equivalent mathematical expression to Equation (7.4b) yields Equation (7.4c).

$$q_{i-L}F_i = \frac{d(V_L F)}{dt} + q_{o-L}F + V_L R_F \quad (7.4c)$$

Expanding the expression $d(V_L F)/dt$, Equation (7.4d) and substituting in Equation (7.3d) yield Equation (7.4e).

$$\frac{d(V_L F)}{dt} = V_L \frac{dF}{dt} + F \frac{dV_L}{dt} \quad (7.4d)$$

$$\frac{d(V_L F)}{dt} = V_L \frac{dF}{dt} + F[q_{i-L} + q_{c-L} - q_{o-L} - (V_L R_{E-G} + R_{Evap} + q_{o-GG} W_{H_2O})/\rho_L] \quad (7.4e)$$

Substituting Equation (7.4e) into (7.4c), and rearranging yields Equation (7.4f). Noting that $R_F = K_{lipid}F$ represents the hydrolysis reaction rate term catalysed by enzymes from microbes, where $K_{lipid}(s^{-1})$ is the hydrolysis rate constant.

$$\begin{aligned} q_{i-L}F_i &= V_L \frac{dF}{dt} + F[q_{i-L} + q_{c-L} - q_{o-L} - (V_L R_{E-G} + R_{Evap} + q_{o-GG} W_{H_2O})/\rho_L] + q_{o-L}F \\ &\quad + V_L (K_{lipid}F) \\ \frac{dF}{dt} &= \frac{q_{i-L}}{V_L} (F_i - F) - \frac{q_{c-L}}{V_L} F + \frac{F}{\rho_L} \left(R_{E-G} + \frac{R_{Evap}}{V_L} + q_{o-GG} W_{H_2O} \right) - K_{lipid}F \end{aligned} \quad (7.4f)$$

7.4.2. Component balance for microbial activities on substrates

Having hydrolysed the feedstock to substrates (by enzymes or extracellular microbes, whose balance does not necessarily have to be accounted for). The subsequent utilisation of substrates is made possible by intracellular microbes. The growth dynamics for these intracellular microbes' concentration, B_j , ($kg.m^{-3}$) in the control volume can be deduced from Equation (7.5a) – (7.5b) by following similar derivation steps for lipid hydrolysis, and rearranging. Noting that $R_{Bg} = \mu_j B_j$ and $R_{Bd} = K_{d-j} B_j$ respectively represents the kinetic for microbial growth rate and death rate, as well as $j = 1$ for LCFA microbes and $j = 2$ for glycerol microbes.

$$\begin{aligned} \text{Microbes input rate} + \text{Microbes growth rate} &= \text{Microbes accumulation rate} \\ &+ \text{Microbes output rate} + \text{Microbes death rate} \end{aligned} \quad (7.5a)$$

$$\frac{dB_j}{dt} = \frac{q_{i-L}}{V_L} (B_{i-j} - B_j) - \frac{q_{c-L}}{V_L} B_j + \frac{B_j}{\rho_L} \left(R_{E-G} + \frac{R_{Evap}}{V_L} + q_{o-GG} W_{H_2O} \right) + (\mu_j - K_{d-j}) B_j \quad (7.5b)$$

Note that as obtainable from a realistic perspective, Equation (7.5b) has been developed in a multiplicity of microbes (B_j) responsible for the different substrates present in the system, such that their difference is only in the value of specific growth rate, μ_j (s^{-1}), and the death rate K_{d-j} (s^{-1}) as popularly reported in literature[158]. Alternatively, various microbes responsible for the different substrates can expressed as an average single microbe (B) responsible for all substrates, such that the average specific growth rate, $\mu_j = f(\mu_1, \mu_2, \dots, \mu_j)$, and average death rate, $K_{d-j} = f(K_{d-1}, K_{d-2}, \dots, K_{d-j})$, Equation (7.5c). A typical example is the **Yoon et al.** [167]

proposition for the utilisation of two mixed substrates by one microbe, where $\mu = \mu_1 + \mu_2$, as such $K_d = K_{d-1} + K_{d-2}$.

$$\frac{dB}{dt} = \frac{q_{i-L}}{V_L} (B_i - B) - \frac{q_{c-L}}{V_L} B_j + \frac{B}{\rho_L} \left(R_{E-G} + \frac{R_{Evap}}{V_L} + q_{o-GG} W_{H_2O} \right) + (\mu - K_d) B \quad (7.5c)$$

Specific growth and death rate

The specific microbe growth rate, μ (s^{-1}) can be deduced via the popular Monod model, Equation (7.5d). Where \mathcal{K}_s is half-saturation coefficient, and μ_{max} the maximum specific microbe growth rate.

$$\mu_j = \mu_{max-j} \frac{S_j}{\mathcal{K}_{s-j} + S_j} \quad (7.5d)$$

$$\mu_{max-j} = \{ \mathcal{B}_{1-j} (T - T_{min-j}) \}^2 \{ 1 - \exp[\mathcal{B}_{2-j} (T - T_{max-j})] \}^2 \quad (7.5e)$$

The maximum specific microbe growth rate can be deduced via the Ratkowsky model, Equation (7.5e), $\mathcal{B}_1(K^{-1} \cdot s^{-1/2})$ and $\mathcal{B}_2(K^{-1})$ are constants, while $T_{min}(K)$ and $T_{max}(K)$ are the minimum and maximum temperatures (K) at which the reaction rate is zero [168]. Furthermore, the microbe death rate, K_d , can be estimated to be about 5% of the maximum microbial specific growth rate μ_{max} . It is also common to ignore decay in methanogen growth, due to its low decay coefficient (about 1% of $\mu_{max,m}$) [128].

7.4.3. Component balance for substrate

The general dynamics for substrate in the control volume can be deduced from Equation (7.6a) – (7.6b) and applying the equivalent mathematical expression by following similar derivation steps highlighted previously as well as rearranging. Noting that $R_{S_j} = Y_{S_j/F} K_{lipid} F$ and $R_{B_j/S_j} = \mu_j B_j / Y_{B_j/S_j}$ respectively represents the substrate formation (from hydrolysis of feedstock) and consumption (to biogas and microbe growth) rate. $Y_{S_j/F}$ is the stoichiometric(theoretical) or experimental equivalent of substrate to feedstock and Y_{B_j/S_j} is the microbe yield from the substrate. The input substrate (S_{i-j}) is the free fatty acids (FFA) or free glycerol in the lipid already hydrolysed naturally before the hydrolysis stage.

$$\text{Substrate input rate} + \text{Substrate formation rate} = \text{Substrate accumulation rate} + \text{Substrate output rate} + \text{Substrate consumption rate} \quad (7.6a)$$

$$\frac{dS_j}{dt} = \frac{q_{i-L}}{V_L} (S_{i-j} - S_j) - \frac{q_{c-L}}{V_L} S_j + \frac{S_j}{\rho_L} \left(R_{E-G} + \frac{R_{Evap}}{V_L} + q_{o-GG} W_{H_2O} \right) + Y_{S_j/F} K_{lipid} F - \frac{\mu_j B_j}{Y_{B_j/S_j}} \quad (7.6b)$$

Therefore, the component balance for LCFA and glycerol can be deduced from Equation (7.6b) by applying $j = 1$ for LCFA and $j = 2$ for glycerol substrates to yield Equation (7.6g) – (7.6h). Furthermore, applying the Yoon et al. [167] proposition for the utilisation of two mixed substrates by one microbe (B). Where $Y_{S_1/F}$, $Y_{S_2/F}$, Y_{B/S_1} and Y_{B/S_2} are as given in Table (7.3).

$$\frac{dS_j}{dt} = \frac{q_{i-L}}{V_L} (S_{i-j} - S_j) - \frac{q_{c-L}}{V_L} S_j + \frac{S_j}{\rho_L} \left(R_{E-G} + \frac{R_{Evap}}{V_L} + q_{o-GG} W_{H_2O} \right) + Y_{S_j/F} K_{lipid} F - \frac{\mu_j B}{Y_{B_j/S_j}} \quad (7.6c)$$

7.4.4. Component balance for biogas in liquid phase

It is assumed that the biogas produced are initially encapsulated in the liquid phase, before being released to the gas-headspace. The dynamics of the various biogas species in the liquid phase (i.e., assumably dissolved gases, G_{Dj_*}) with concentration ($\text{kg}\cdot\text{m}^{-3}$) can be deduced from Equation (7.7a) – (7.7b) by following similar derivation steps highlighted previously as well as rearranging. Also, it is assumed that no liquid-phase biogas is present in the input stream. The formation rate of each biogas species, $R_{G_{Dj_*}}$ is given by Equation (7.7c) – (7.7d), and R_{E-j_*} is the evolution rate of each biogas species, given by Equation (7.14a).

$$\text{Liquid biogas input rate} + \text{Biogas formation rate} = \text{Liquid biogas accumulation rate} + \text{Liquid biogas output rate} + \text{Biogas evolution rate from liquid phase} \quad (7.7a)$$

$$\frac{dG_{Dj_*}}{dt} = -\frac{q_{i-L}}{V_L} G_{Dj_*} - \frac{q_{c-L}}{V_L} G_{Dj_*} + \frac{G_{Dj_*}}{\rho_L} \left(R_{E-G} + \frac{R_{Evap}}{V_L} + q_{o-GG} W_{H_2O} \right) + R_{G_{Dj_*}} - R_{E-j_*} \quad (7.7b)$$

$$R_{G_{Dj_*}} = \sum_{j=1}^J (Y_{G_{Dj_*}/S_j} \hat{i}_{i-j_*}) \left(\frac{\mu_j B_j}{Y_{B_j/S_j}} \Phi_v \right) \quad (7.7c)$$

Where, $j_* = \text{CH}_4, \text{CO}_2, \text{H}_2$, etc., and $j = 1, 2, \dots$, etc., indicates the number of substrates species being considered, S_j (i.e., LCFA, S_1 and glycerol, S_2 substrates), B_j (i.e., microbes for utilisation of LCFA, B_1 and glycerol, B_2 substrates [167]), Y_{G_D/S_j} (i.e. total biogas yield from substrates species of LCFA, S_1 and glycerol, S_2 , typically Y_{G_D/S_1} and Y_{G_D/S_2}), $Y_{G_{D-j_*}/S_j}$ (i.e. biogas species, $\text{CH}_4, \text{CO}_2, \text{H}_2$, etc., yield from substrates species of LCFA, S_1 and glycerol, S_2 , typically $Y_{G_{DCH_4}/S_1}, Y_{G_{DCH_4}/S_2}$, etc.) and \hat{i}_{i-j_*} (i.e. inhibition of various biogas species, $\text{CH}_4, \text{CO}_2, \text{H}_2$, etc., typically $\hat{i}_{i-\text{CH}_4}, \hat{i}_{i-\text{H}_2}$, etc.). The inhibition, \hat{i}_{i-j_*} , in this study is assumed to be predominantly influenced by pH, i.e., \hat{i}_{pH-j_*} , hence Equation (7.7e) [169] was applied with pH_{ul-j_*} and pH_{ll-j_*} being the upper and lower pH limits at which biogas species are inhibited.

. Applying the earlier assumption for a single microbe competing for LCFA, S_1 and glycerol, S_2 substrates, Equation (7.7c) can be typically expressed as given by Equation (7.7d).

$$R_{G_{Dj_*}} = (Y_{G_{Dj_*}/S_1} \hat{i}_{pH-j_*}) \left(\frac{\mu_1 B}{Y_{B/S_1}} \Phi_v \right) + (Y_{G_{Dj_*}/S_2} \hat{i}_{pH-j_*}) \left(\frac{\mu_2 B}{Y_{B/S_2}} \Phi_v \right) \quad (7.7d)$$

$$\hat{i}_{pH-j_*} = \frac{1 + 2(10^{0.5(\text{pH}_{ll-j_*} - \text{pH}_{ul-j_*})})}{1 + 10^{(\text{pH} - \text{pH}_{ul-j_*})} + 10^{(\text{pH}_{ll-j_*} - \text{pH})}} \quad (7.7e)$$

The volatile fraction of the feedstock, $\Phi_v = \Phi_G$ or Φ_B considered for the computation of the biogas species is between $0 < \Phi_v < 1$. Φ_G is the fraction of substrate converted to gas and Φ_B is the fraction of substrate converted to microbe biomass. Applying the various composition of biogas species, $j_* = \text{CH}_4, \text{CO}_2, \text{H}_2$, etc. to Equation (7.7b) – (7.7e) the dynamics for methane, carbon dioxide and hydrogen can be respectively deduced. Where $\Phi_v = \Phi_G$ for methane, and carbon dioxide formation. While $\Phi_v = \Phi_B$ for hydrogen formation. Literature report suggests 10% of the substrate is used for microbe formation, hence $\Phi_B = 0.1$, $\Phi_G = 0.90$, and $\Phi_G + \Phi_B = 1$ [98].

Note that feedstock rich in nitrogen such as protein-rich feedstock, the ammonia (NH_3) formed must be accounted for and it can also be computed from Equation (7.7b) – (7.7e) with $\Phi_v = \Phi_G = 0.9$. The exact number, j , and type of substrate, S_j will depend on the protein molecules. Usually dissolve ammonia formed is present as ammonium, NH_4^+ , how for simplicity, and to be able to use **Buswell and Neave (1930)** stoichiometric model

for theoretical estimation, ammonia (NH₃) is used. Furthermore, it should also be noted that there is usually an inert amount of dissolved ammonia (ammonium, NH₄⁺) present in the feedstock (regardless of whether it is lipid, carbohydrate, protein, or even mixed feedstock) that can't be accounted for by Equation (7.7b) – (7.7e). This ammonia is continuously naturally fixed from dead organisms, microbes, etc. in the sludge. The minimum required amount present in the sludge can be thought to be regenerative, and degenerative based on microbe actives, as well as this amount represents the adequate value to initiate the growth of microbes. It can be assumed that this ammonia remains dissolved in the liquid phase as ammonium, and does not evolve, the theoretical amount can be estimated via the calculated yield of ammonia from the stoichiometry of the microbe's growth, Equation (7.22a) [161,170]. Note that for a protein-rich feedstock, especially if $(a/5 - d) < 0$ i.e., NH₃ becomes a product in the reaction.

7.4.5. Component balance of water in liquid phase

The dynamics for liquid water (w) in terms of “water concentration” (kg.m⁻³) in the control volume due to water evaporation, as well as water loss associated with biogas water content can be deduced from Equation (7.8a) – (7.8b). This model is deduced by following similar derivation steps highlighted previously as well as rearranging. It is assumed water formed and consumed from anaerobic digestion is negligible as it cannot be reasonably accounted for. The dynamics for liquid water are necessary to estimate changes in liquid volume, especially when the control volume is opened to release biogas. It should be noted that the water accompanying the biogas as its inherent water content, $q_{o-GG}W_{H_2O}$, must also be accounted for.

$$\text{Water input rate} + \text{water input rate from pH controller} = \text{water accumulation rate} + \text{water output rate} + \text{water evaporation rate} + \text{water accompanying biogas outlet} \quad (7.8a)$$

$$\frac{dw}{dt} = \frac{q_{i-L}}{V_L}(w_i - w) + \frac{q_{c-L}}{V_L}(w_c - w) + \frac{w}{\rho_L} \left(R_{E-G} + \frac{R_{Evap}}{V_L} + q_{o-G}W_{H_2O} \right) - \frac{R_{Evap}}{V_L} - \frac{q_{o-GG}W_{H_2O}}{V_L} \quad (7.8b)$$

Note that the input water concentration based on the feed stream, and pH controller feed stream can be approximately estimated from the lipid feedstock and ion concentration respectively, as well as their input conditions. i.e., $w_i = (1 - (F_i/\rho_{Lipid}))\rho_w$ and $w_c = (1 - ([Z_c]M_c/\rho_c))\rho_w$. Where ρ_{Lipid} is the lipid density, ρ_w is the water density, $[Z_c]$ (kgmoles.m⁻³) is the ionic molar concentration, M_c is the molar mass, and ρ_c is the density of the pH controller feed stream.

7.5. Gas headspace component balance

The components balance for the various species present in the gas headspace are considered in the following sections, in addition to their partial pressure.

7.5.1. Component balance for biogas in gas-headspace

The dynamics of biogas specie (G_{j^*}), i.e., $j^* = CH_4, CO_2, H_2$, etc evolved from the liquid phase into the gas-headspace with concentration (kg.m⁻³) can be deduced from Equation (7.9a) – (7.9b).

$$\text{Biogas input rate} + \text{Biogas evolution rate} = \text{Biogas accumulation rate} + \text{Biogas output rate} \quad (7.9a)$$

$$\dot{m}_{i-G_{j_*}} + V_L R_{E-j_*} = \frac{dm_{G_{j_*}}}{dt} + \dot{m}_{o-G_{j_*}} \quad (7.9b)$$

Applying the necessary mathematical equivalents to Equation (7.9b) yields Equation (7.9c). Assuming that no biogas is present in the input stream, i.e., $\dot{m}_{i-G_{j_*}} = 0$.

$$0 + V_L R_{E-j_*} = \frac{d(V_G G_{j_*})}{dt} + q_{o-G} G_{j_*} \quad (7.9c)$$

Expanding the expression $d(V_L G_{j_*})/dt$, Equation (7.9d) and combining it with Equation (7.3f) yield Equation (7.9e).

$$\frac{d(V_G G_{j_*})}{dt} = V_G \frac{dG_{j_*}}{dt} + G_{j_*} \frac{dV_G}{dt} \quad (7.9d)$$

$$\frac{d(V_G G_{j_*})}{dt} = V_G \frac{dG_{j_*}}{dt} + G_{j_*} [q_{o-L} - q_{i-L} - q_{c-L} + (V_L R_{E-G} + R_{Evap} + q_{o-GG} W_{H_2O}) / \rho_L] \quad (7.9e)$$

Combining Equation (7.9e) and (7.9c), and rearranging yields Equation (7.9f).

$$\begin{aligned} V_G \frac{dG_{j_*}}{dt} + G_{j_*} [q_{o-L} - q_{i-L} - q_{c-L} + (V_L R_{E-G} + R_{Evap} + q_{o-GG} W_{H_2O}) / \rho_L] &= V_L R_{E-j_*} - q_{o-G} G_{j_*} \\ \frac{dG_{j_*}}{dt} &= \frac{G_{j_*}}{V_G} (q_{i-L} + q_{c-L} - q_{o-L} - q_{o-G}) - \frac{G_{j_*}}{\rho_L V_G} (V_L R_{E-G} + R_{Evap} + q_{o-GG} W_{H_2O}) + \frac{V_L}{V_G} R_{E-j_*} \end{aligned} \quad (7.9f)$$

The biogas species, $j_* = CH_4, CO_2, H_2$, etc. in the headspace can be deduced from Equation (7.9f).

7.5.2. Component balance of water vapour in gas headspace

The dynamics for water vapour (w_v) evaporated from the liquid phase into the gas-headspace with concentration ($kg.m^{-3}$) can be deduced from Equation (7.10a) – (7.10c) by following similar derivation steps highlighted previously for biogas species dynamic. Applying the necessary mathematical equivalents to Equation (7.10b), assuming that no liquid phase biogas is present in the input stream, i.e., $\dot{m}_{i-w_v} = 0$, and rearranging yields Equation (7.10c).

$$\begin{aligned} \text{Water vapour input rate} + \text{Water vapour evaporation rate} = \\ \text{Water vapour accumulation rate} + \text{Water vapour evaporation output rate} \end{aligned} \quad (7.10a)$$

$$\dot{m}_{i-w_v} + R_{Evap} = \frac{dm_{w_v}}{dt} + \dot{m}_{o-w_v} \quad (7.10b)$$

$$\frac{dw_v}{dt} = \frac{w_v}{V_G} (q_{i-L} + q_{c-L} - q_{o-L} - q_{o-G}) - \frac{w_v}{\rho_L V_G} (V_L R_{E-G} + R_{Evap} + q_{o-GG} W_{H_2O}) + \frac{R_{Evap}}{V_G} \quad (7.10c)$$

7.5.3. Partial pressure of biogas species, and water vapour in the gas headspace

The partial pressure of the various biogas species, P_{j^*} (pa) in the gas headspace can be deduced by assuming that the biogas species obey the ideal gas law, Equation (7.11a) and on the dynamic modelling of the ideal gas law to time to yield Equation (7.11b).

$$P_{j^*} V_G = N_{j^*} RT \quad (7.11a)$$

$$P_{j^*} \frac{dV_G}{dt} + V_G \frac{dP_{j^*}}{dt} = RT \frac{dN_{j^*}}{dt} \quad (7.11b)$$

Therefore, substituting Equation (7.3f) into (7.11b), and rearranging yield Equation (7.11c).

$$P_{j^*} [q_{o-L} - q_{i-L} - q_{c-L} + (V_L R_{E-G} + R_{Evap} + q_{o-GG} W_{H_2O}) / \rho_L] + V_G \frac{dP_{j^*}}{dt} = RT \frac{dN_{j^*}}{dt}$$

$$\frac{dP_{j^*}}{dt} = \frac{RT}{V_G} \frac{dN_{j^*}}{dt} - \frac{P_{j^*}}{V_G} [q_{o-L} - q_{i-L} - q_{c-L} + (V_L R_{E-G} + R_{Evap} + q_{o-GG} W_{H_2O}) / \rho_L] \quad (7.11c)$$

Where dN_{j^*}/dt , Equation (7.11d) is a compositional term accurately deduced from the generative expression of each biogas species formed ($dm_{G_{j^*}}/dt$), Equation (7.9b). Therefore, substituting Equation (7.11d) into Equation (7.11c), applying necessary mathematical expression and rearranging yields Equation (7.11e).

$$\frac{dN_{j^*}}{dt} = \frac{1}{M_{j^*}} \left(\frac{dm_{G_{j^*}}}{dt} \right) = \frac{1}{M_{j^*}} (V_L R_{E,j^*} - \dot{m}_{o-G_{j^*}}) \quad (7.11d)$$

$$\frac{dP_{j^*}}{dt} = \frac{RT}{V_G M_{j^*}} (V_L R_{E,j^*} - \dot{m}_{o-G_{j^*}})$$

$$- \frac{P_{j^*}}{V_G} [q_{o-L} - q_{i-L} - q_{c-L} + (V_L R_{E-G} + R_{Evap} + q_{o-GG} W_{H_2O}) / \rho_L] \quad (7.11e)$$

Therefore, by applying the various composition of biogas species, $j^* = CH_4, CO_2, H_2$, etc. their partial pressure can be deduced. In addition to the partial pressure of the biogas species is also the partial pressure exerted by water vapour pressure, P_{w_v} , and this pressure can't be obtained from component dynamics like Equation (7.11e), rather it is obtainable from saturated vapour pressure water (P_{sw}), i.e., $P_{w_v} = P_{sw}$. Where P_{sw} (pa) is thermodynamically determined from prevailing temperature, Equation (7.11f) [171] due to its instantaneous nature.

$$P_{sw} = \exp \left(73.960 - \frac{7258.2}{T(^{\circ}C) + 273.15} + 2.276 \times 10^{-3} T(^{\circ}C) - 7.3073 \ln(T(^{\circ}C) + 273.15) + 4.1653 \times 10^{-6} T(^{\circ}C)^2 \right) \quad (7.11f)$$

7.6. Computation of water evaporation rate

The evaporation rate to gas headspace can be approximated thermodynamically from the saturated vapour pressure of water, Equation (7.11f). By assuming water vapour obeys the ideal gas law, Equation (7.12a) and dynamically modelling this equation with respect to time to yield Equation (7.12b). Considering the saturated vapour pressure, P_{sw} is instantaneous and specific for a given temperature, therefore it can be assumed constant, so that $dP_{sw}/dt \approx 0$.

$$P_{sw}V_G = N_{wv}RT \quad (7.12a)$$

$$P_{sw} \frac{dV_G}{dt} + V_G \frac{dP_{sw}}{dt} = RT \frac{dN_{wv}}{dt}$$

$$P_{sw} \frac{dV_G}{dt} + 0 = RT \frac{dN_{wv}}{dt}$$

$$P_{sw} \frac{dV_G}{dt} = RT \frac{dN_{wv}}{dt} \quad (7.12b)$$

Therefore, substituting Equation (7.3f) into (7.12b), and rearranging yield, Equation (7.12c).

$$\frac{dN_{wv}}{dt} = \frac{P_{sw}}{RT} [q_{o-L} - q_{i-L} - q_{c-L} + (V_L R_{E-G} + R_{Evap} + q_{o-GG} W_{H_2O}) / \rho_L] \quad (7.12c)$$

Where dN_{wv}/dt , Equation (7.12d) is a compositional term deduced from the accumulation of water vapour in the gas headspace, (dm_{wv}/dt) , Equation (7.11b).

$$\frac{dN_{wv}}{dt} = \frac{1}{M_j} \left(\frac{dm_{wv}}{dt} \right)$$

$$\frac{dN_{wv}}{dt} = \frac{1}{M_w} (R_{Evap} - \dot{m}_{o-wv}) \quad (7.12d)$$

Therefore, substituting Equation (7.12d) into (7.12c), applying necessary mathematical expression and rearranging yield the evaporation rate, R_{Evap} , Equation (7.12e).

$$P_{sw} [q_{o-L} - q_{i-L} - q_{c-L} + (V_L R_{E-G} + R_{Evap} + q_{o-GG} W_{H_2O}) / \rho_L] = \frac{RT}{M_w} (R_{Evap} - q_{o-G} W_v)$$

$$R_{Evap,v} = \frac{M_w P_{sw}}{RT} [q_{o-L} - q_{i-L} - q_{c-L} + (V_L R_{E-G} + R_{Evap} + q_{o-GG} W_{H_2O}) / \rho_L] + q_{o-G} W_v$$

$$\left(1 - \frac{M_w P_{sw}}{\rho_L RT} \right) R_{Evap} = \frac{M_w P_{sw}}{RT} \left[q_{o-L} - q_{i-L} - q_{c-L} + \frac{V_L}{\rho_L} R_{E-G} + \frac{q_{o-GG} W_{H_2O}}{\rho_L} \right] + q_{o-G} W_v$$

$$R_{Evap} = \frac{\frac{M_w P_{sw}}{RT} \left[q_{o-L} - q_{i-L} - q_{c-L} + \frac{V_L}{\rho_L} R_{E-G} + \frac{q_{o-GG} W_{H_2O}}{\rho_L} \right] + q_{o-G} W_v}{\left(1 - \frac{M_w P_{sw}}{\rho_L RT} \right)} \quad (7.12e)$$

The Equation (7.12e), technically denotes the dynamics of the amount of water vapour to be evaporated to sustain the saturated water vapour pressure in the gas headspace. It is expected that at the given saturated water vapour pressure, P_{sw} , The rate of evaporation of water vapour, R_{Evap} , will increase or decrease with a respective increase or decrease in gas headspace.

7.7. Moisture content in the biogas

Upon removal of biogas from the bioreactor, the unavoidable water content accompanying the biogas, W_{H_2O} (kg H_2O per m^3 biogas/gases) can be deduced approximately from the thermodynamics of water-hydrocarbon phase equilibrium, Equation (7.13a) [171]. Which is defined in terms of the fugacity coefficient of water, Φ_{H_2O} , Equation (7.13b) and average molecular volume of water, v_{H_2O} ($m^3 \cdot kgmol^{-1}$), Equation (7.13c) from the total pressure of the gas-headspace, $P = P_G + P_{sw}$. Note that the amount of water vapour accompanying the

biogas, \dot{m}_{o-Gw} (i.e., $\dot{m}_{o-Gw} = q_{o-GG}W_{H_2O} = \delta_G m_{o-GG}W_{H_2O} = \delta_G q_{o-G}GW_{H_2O}$, i.e., $q_{o-GG} = \delta_G q_{o-G}G$) is inclusive of the saturated water vapour lost to the environment ($m_{o-wv} = q_{o-G}W_v$) when the gas headspace is opened to release the biogas produced. Furthermore, \dot{m}_{o-Gw} may be considered as the water vapour that would need to be dried totally or partially during biogas upgrading. Usually, the water content of raw biogas can be within 2.5 – 10v/v% [172,173]. Where $\delta_G = RT/M_G P_G$ is the ideal gas conversion factor, $R = 8314 \text{ pa} \cdot \text{kgmol}^{-1} \cdot \text{K}^{-1}$ is the ideal gas constant, T , temperature in kelvins, M_G , the average molecular weight of biogas, $P_G = (P_{CH_4} + P_{CO_2} + P_{H_2} + P_{N_2} \dots)$ is the pressure of biogas, and can be considered to be inclusive of inert gas pressure, P_{N_2} .

$$W_{H_2O} = 0.76190042 \left(\frac{P_{sw}}{\phi_{H_2O} P} \right) \exp \left(\frac{(P - P_{sw})v_{H_2O}}{8314(T + 273.15)} \right) \quad (7.13a)$$

$$\phi_{H_2O} = \exp \left[\left(0.069 - \frac{30.905}{T(^{\circ}\text{C}) + 273.15} \right) (10^{-6}P) + \left(\frac{0.3179}{T(^{\circ}\text{C}) + 273.15} - 0.0007654 \right) (10^{-6}P)^2 \right] \quad (7.13b)$$

$$v_{H_2O} = -0.5168 \times 10^{-2} + 3.036 \times 10^{-4}T(^{\circ}\text{C}) + 1.784 \times 10^{-6}T(^{\circ}\text{C})^2 \quad (7.13c)$$

7.8. Computation of biogas evolution rate

The rate of evolution of gases, $\Sigma_j R_{E-j_*} = R_{E-G}$ ($\text{kg} \cdot \text{m}^{-3} \cdot \text{s}^{-1}$) from the liquid phase to the gaseous phase is governed by Henry's law, and it is based tentatively on the assumption that biogas species formed are entrapped within spaces of clusters of liquid bubbles in the liquid phase, G_{Dj_*} and as the partial pressure of the biogas species increases, P_{j_*} they evolve to the gas headspace as given by Equation (7.14a), and as illustrated by Figure (7.3).

$$R_{E-j_*} = (K_L a)_{j_*} (G_{Dj_*} - K_{Hj_*} P_{j_*}) \quad (7.14a)$$

Where $(K_L a)_{j_*}$ (s^{-1}), is the mass transfer coefficient, and K_{Hj_*} ($\text{kg} \cdot \text{m}^{-3} \cdot \text{pa}^{-1}$), Henry's constant for biogas species.

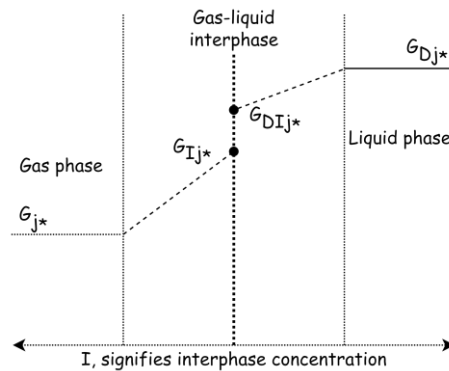


Figure 7.3. Interfacial mass transfer of biogas from a liquid to gaseous phase

The estimation of Henry's constant, K_{Hj_*} , for biogas species (CH_4 , CO_2 , H_2 , etc) of biogas produced in anaerobic digestion was extensively investigated by **Oh & Martin** [174]. According to the report, Henry's law constants in anaerobic digesters are defined based on the difference in chemical potentials, $-(\Delta\psi_{j_*}^{ovl})$ of each species, j_* , in the liquid (water) and vapour phases as given in Equation (7.14b) [174]. While ammonia gas

(NH₃) for the Henry constant for the ammonia-water system [175], Equation (7.14c) can be approximately applied. Based on a temperature reference of 298K the difference in chemical potential, ($\Delta\psi_{j_*}^{ovl}$) of each species, $j_* = \text{CH}_4, \text{CO}_2$ and H_2 was calculated as 158.084, 75.4238, and 172.7239 respectively. Where M_{j_*} is the molar mass of the biogas species and T is the temperature of the system in kelvins.

$$K_{Hj_*} = \left(\frac{M_{j_*}}{101325} \right) \exp \left\{ \frac{-(\Delta\psi_{j_*}^{ovl})}{0.0821T} \right\} \quad (7.14b)$$

$$K_{H\text{NH}_3} = \left(\frac{M_{\text{NH}_3}}{101325} \right) \exp \left(\frac{4341}{T} - 10.47 \right) \quad (7.14c)$$

While the Henry constant, K_{Hj_*} , for biogas species have been reported, and can easily be computed, the mass transfer coefficient of biogas species ($K_L a$) _{j_*} (s⁻¹) is not easily computed. It depends mainly on the operating conditions of the bioreactor, especially on the effect of stirring, as well as the exchange area between the liquid and the gaseous phase, including the size of the gas bubbles. It represents the rate of transfer in either direction (gas to liquid or liquid to gas) of the gas-liquid phase, and technically a combination of film coefficient, K_{Lj_*} (m.s⁻¹) and the specific interfacial area per unit volume of liquid, a_{j_*} (m⁻¹). Specifically, K_{Lj_*} quantifies the nature of the gas and physicochemical properties of the liquid phase, and a_{j_*} is dependent on the hydrodynamic conditions (such as stirring) and gas production rate. In AD where gas bubbles are formed from microbe activities, a_{j_*} will be influenced by the bubble formation process and gas production rate. Stirring of the liquid phase may be less important if the concentrations of the various species are kept uniform [176]. Typically, the value of K_{Lj_*} has been reported as 3.5×10^{-5} m.s⁻¹ for surface aerated stirred vessels and 3.5×10^{-4} m.s⁻¹ for sparged stirred and tower fermentors [177]. **Pauss et al.** [176] deduce ($K_L a$) _{j_*} for completely stirred reactor for hydrogen and methane as 0.16 ± 0.02 and $0.09 \pm 0.01 \text{hr}^{-1}$ respectively. **Pauss et al.** [176] used hydrogen and methane as a basis to develop Equation (7.14d) as they were expected to be the gases most sensitive to mass transfer limitations. Although the equation also applied the equation for calculation of the carbon dioxide mass transfer coefficient, ($K_L a$)_{CO₂}. Where D_{Lj_*} (m².s⁻¹) is the diffusivity of biogas species, j_* , in the liquid phase, L.

$$(K_L a)_{\text{CH}_4} = (K_L a)_{\text{H}_2} \left(D_{L\text{CH}_4} / D_{L\text{H}_2} \right)^{0.5} \quad (7.14d)$$

This expression is also like that deduced by **Weichgrebe et al.** [178] for volatile organic compounds (using methane as the basis) in wastewater treatment systems, via oxygen extrapolation, Equation (7.14e). And based on the inference that the coefficient, n_K is system specific and can range normally between 0.5 and 1.0. Therefore, the value of $n_K = 0.5$ given by Equation (7.14d) can be assumably used not only for computation of methane and carbon dioxide [176,178] but for other gaseous species such as ammonia therefore based on Equation (7.14d), a generic expression for biogas species, Equation (7.14f) can be deduced based on hydrogen gas (i.e. with ($K_L a$)_{H₂} 0.0027 – 0.36 s⁻¹ for hydrogen gas-liquid mass transfer based on gaseous dispersion impeller system [179–184]) as also reported by **Liu et al.** [185]. Where $D_{L\text{H}_2}$ and D_{Lj_*} are respectively the diffusivity of hydrogen gas, and other biogas species in the liquid.

$$(K_L a)_{\text{CH}_4} = (K_L a)_{\text{O}_2} \left(D_{L\text{CH}_4} / D_{L\text{O}_2} \right)^{n_K} \quad (7.14e)$$

$$(K_L a)_{j_*} = (K_L a)_{\text{H}_2} \left(D_{Lj_*} / D_{L\text{H}_2} \right)^{0.5} \quad (7.14f)$$

The D_{Lj^*} ($m^2.s^{-1}$) can be estimated via the **Diaz et al.** [186] correlation, [Equation \(7.14g\)](#), between the liquid and gas molar volume at their respective normal boiling temperatures, q_L and q_{j^*} ($m^3.kgmole^{-1}$), for ease of computation and accuracy the molar volume of the liquid, q_L is equivalent to that water i.e. $q_L \cong q_w$. This is because the biogas produced is entrapped more in the water portion of the liquid, with little or no dissolution in the substrate, in addition to the fact that during the gas production stage, most substrate and organic matter would have been degraded to very soluble intermediates such as acetic acid. The other liquid properties such as absolute viscosity, η_L (pa.s) and liquid density, ρ_L ($kg.m^{-3}$) can be easily measured. The values of molar volume for water $q_w = 0.0187$, for biogas species the q_{j^*} for $j^* = CH_4, CO_2, H_2$ and NH_3 are respectively 0.0377, 0.0373, 0.0143 and 0.0245 $m^3.kgmole^{-1}$ and other gases are reported in literature [186,187].

$$D_{Lj^*} = 6.43012 \times 10^{-8} \frac{q_L^{0.36} \exp(-2539/T)}{\eta_L^{0.61} q_{j^*}^{0.64}} \quad (7.14g)$$

Having determined $K_{Lj^*} a_{j^*}$ via [Equation \(7.14d\) – \(7.14g\)](#), furthermore the film coefficient, K_{Lj^*} , can be deduced via the **Hikita et al.** [188,189] correlation, [Equation \(7.14h\)](#) or the **Moo-Young and Calderbank** [190] correlation and consequently the specific interfacial area per unit volume of liquid, a_{j^*} , can be deduced using $K_{Lj^*} a_{j^*}$ deduced earlier. These correlations relate the Reynold number of mixing, $N_{Re} = \rho_L n_{st} d_{st}^2 / \eta_L$, and Schmidt number, $Sc = \eta_L / \rho_L D_{Lj^*}$. Where D_{Lj^*} is the diffusivity of gas through the liquid, d_{st} is the diameter (m) of the impeller, and n_{st} , the impeller speed (rps). In developing, [Equation \(7.14h\)](#), a_{j^*} under non-bubbling conditions was assumed to be $8.13 m^{-1}$ [188].

$$Sh = \frac{K_{Lj^*} (2\Gamma Ri)}{D_{Lj^*}} = 0.322 N_{Re}^{0.7} Sc^{1/3} \quad (7.14h)$$

7.9. Gas bubble growth and motion

Following the procedure of **Pauss et al.** [176], the gas bubble growth and motion can be deduced from the material balance on a single bubble rising vertically in the homogeneous liquid phase. It is assumed that the single spherical bubble growth initiated at a given point is an isolated bubble, with no coalescence and breakage, it moves vertically from its initial point to the top of the liquid via a terminal velocity, and the concentration of biogas species around the bubble is always constant and uniform. The rise velocity of a bubble is a function of its diameter, bubble growth and bubble motion, obeys the ideal gas law, $p_{j^*} v_{j^*} = n_{bj^*} RT$. Therefore, by differentiating the ideal gas law, the [Equation \(7.15a\)](#) is deduced. Where v_{j^*} (m^3) = $\pi d_{j^*}^3 / 6$ is the volume of a gaseous spheric bubble, for which its differential form can be expressed in terms of [Equation \(7.15b\)](#) with respect to the biogas bubble diameter. The [Equation \(7.15a\)](#) can be rearranged in terms of the partial pressure inside biogas bubble species being formed, p_{j^*} (pa), [Equation \(7.15c\)](#).

$$p_{j^*} \frac{dv_{j^*}}{dt} + v_{j^*} \frac{dp_{j^*}}{dt} = RT \frac{dn_{bj^*}}{dt} \quad (7.15a)$$

$$\frac{dv_{j^*}}{dt} = \frac{\pi d_{j^*}^2}{2} \frac{d(d_{j^*})}{dt} \quad (7.15b)$$

$$\frac{dp_{j^*}}{dt} = \frac{6}{\pi d_{j^*}^3} \left[RT \frac{dn_{j^*}}{dt} - \frac{p_{j^*} \pi d_{j^*}^2}{2} \frac{d(d_{j^*})}{dt} \right] \quad (7.15c)$$

In solving Equation (7.15c), the dynamic changes of biogas bubble species, $d(d_{j_*})/dt$ and molar mass of biogas bubble species dn_{bj_*}/dt needs to be deduced. The $d(d_{j_*})/dt$ can be estimated approximately using Equation (7.15d) via differentiation of the ideal gas law with respect to the total pressure on the biogas bubble species in the liquid phase, p_{T-j_*} and rearranging yield Equation (7.15e), where, p_{T-j_*} is given by Equation (7.15f) [191–193].

$$p_{T-j_*} \frac{dv_{j_*}}{dt} = RT \frac{dn_{bj_*}}{dt} \quad (7.15d)$$

$$\frac{d(d_{j_*})}{dt} = \frac{2}{\pi d_{j_*}^2 p_{T-j_*}} RT \frac{dn_{bj_*}}{dt} \quad (7.15e)$$

$$p_{T-j_*} = P + \rho_L g (h_L - h_{j_*}) + \frac{4\gamma_{Lj_*}}{d_{j_*}} \quad (7.15f)$$

Where γ_{Lj_*} ($N.m^{-1}$) is the interfacial tension between the biogas bubble species and liquid (approximated as water) that can be deduced as given by Equation (7.15g), (7.15h) and (7.15i) for methane [194], carbon dioxide [195,196] and hydrogen gas [197,198] respectively. Note that Equation (7.15h) – (7.15i) was developed by curve fitting data from literature [195–198]. $T_{C-CH_4}=190.56$ K is the critical temperature of methane [199]; ρ_L and ρ_{CH_4} ($kg.m^{-3}$) are the density of the liquid phase as well as methane; P and T are total pressure as well as the temperature of the bioreactor content; x_{j_*} and y_{j_*} is the liquid as well as the gaseous fraction of specie, j_* , in liquid and gaseous phase; γ , Equation (7.15j) is the average interfacial tension of the biogas with the liquid phase, calculated using the linear mixing rule, which is also applicable for all other necessary average properties of the entire system; and b_{ij} are coefficients of the polynomial models, as given in Table (7.1).

Table 7.1. Coefficients of polynomial model used for the calculation of the interfacial tension.

Coefficients, b_{ij}	Values, γ_{LCO_2}	Values, γ_{LH_2}
b_{00}	19.3506	-95.7078
b_{10}	-67.5188	14.9137
b_{01}	0.4142	1.5894
b_{20}	4.4881	-0.4375
b_{11}	0.3091	-0.1203
b_{02}	-0.0008	-0.0046
b_{30}	-0.0392	0.0056
b_{21}	-0.0202	0.0028
b_{12}	-0.0004	0.0003
b_{03}	–	3.95E-06
b_{40}	0.0001	-9.89E-05
b_{31}	8.17E-05	-9.43E-06
b_{22}	2.38E-05	-7.07E-06
b_{13}	–	-3.03E-07
b_{50}	–	2.26E-07
b_{41}	–	2.05E-07
b_{32}	–	-8.93E-09
b_{23}	–	6.75E-09

$$\gamma_{\text{LCH}_4} = 1.11 \times 10^{-4} (\rho_{\text{L}} - \rho_{\text{CH}_4})^{1.024} (T/T_{\text{C-CH}_4})^{-1.25} \quad (7.15g)$$

$$\gamma_{\text{LCO}_2} = 10^{-3} (b_{00} + b_{10}P + b_{01}T + b_{20}P^2 + b_{11}PT + b_{02}T^2 + b_{30}P^3 + b_{21}P^2T + b_{12}PT^2 + b_{40}P^4 + b_{31}P^3T + b_{22}P^2T^2) \quad (7.15h)$$

$$\gamma_{\text{LH}_2} = 10^{-3} (b_{00} + b_{10}P + b_{01}T + b_{20}P^2 + b_{11}PT + b_{02}T^2 + b_{30}P^3 + b_{21}P^2T + b_{12}PT^2 + b_{03}T^3 + b_{40}P^4 + b_{31}P^3T + b_{22}P^2T^2 + b_{13}PT^3 + b_{50}P^5 + b_{41}P^4T + b_{32}P^3T^2 + b_{23}P^2T^3) \quad (7.15i)$$

$$\gamma = \sum_{j_*} \gamma_{\text{Lj}_*} x_{j_*} \quad (7.15j)$$

Furthermore, the height of the biogas bubble specie in the liquid phase, h_{j_*} , in Equation (7.15f) can be deduced via the terminal or rising velocity of the bubble, $dh_{j_*}/dt \cong -u_b$ through the liquid. This velocity can be estimated approximately by the modified **Stokes law**, Equation (7.15k) [193,200]. As reported by **Pauss et al.** [176] on integrating Equation (7.15c), (7.15e) and (7.15k) the initial conditions of biogas bubble species diameter should be within $0.05 \leq d_{j_*} \leq 0.5\text{cm}$, alternatively the initial diameter of bubble species can be estimated from **Stokes law** approximation, $d_{j_*} = 9.52\eta_{\text{L}}^{2/3}/[g\rho_{\text{L}}(\rho_{\text{L}} - \rho_{j_*})]^{1/3}$ [201–203]. However, in this work, it is taken as $d_{j_*} = 0.05\text{cm}$ at initial condition.

$$\frac{dh_{j_*}}{dt} \cong u_b \cong \frac{\rho_{\text{L}}gd_{j_*}^2}{27\eta_{\text{L}}} \quad (7.15k)$$

Further the dn_{bj_*}/dt in Equation (7.15c) – (7.15e) is a regenerative term that can be deduced approximately from Equation (7.15l). Since a_{j_*} can't be accurately determined, combined with the bubble volume, v_{j_*} , to approximate yield $v_{j_*} a_{j_*} = \pi d_{j_*}^2$ [176,204].

$$\frac{dn_{\text{bj}_*}}{dt} = \frac{v_{j_*} R_{e-j_*}}{M_j} = \frac{v_{j_*} (K_{\text{Lj}_*} a_{j_*}) (G_{\text{Dj}_*} - K_{\text{Hj}_*} p_{j_*})}{M_{j_*}} = \frac{\pi d_{j_*}^2 K_{\text{Lj}_*} (G_{\text{Dj}_*} - K_{\text{Hj}_*} p_{j_*})}{M_{j_*}} \quad (7.15l)$$

By assuming the various possible biogas bubble specie diameters, d_{j_*h} (i.e., $d_{j_*1}, d_{j_*2}, \dots$) corresponds to the resulting diameter of each time step of the simulation, therefore the total number of bubble size categories, $h = 1, 2, \dots, H$ is considered as the total simulation time steps. Therefore, using these diameters, the Sauter mean diameter, d_{Sj_*} , Equation (7.15m) [205–207] can be approximately estimated. There are different other mean diameters than the d_{Sj_*} and their appropriate application [208]. The Sauter mean diameter is probably the most used mean diameter for the characterisation of several important chemical engineering processes [209], although the “volume moment” or **De Brouckere** mean diameter, has been reported to be a superior indicator [210].

$$d_{\text{Sj}_*} \cong \frac{\sum_{h=1}^H d_{j_*h}^3}{\sum_{h=1}^H d_{j_*h}^2} \quad (7.15m)$$

7.10. Gas bubble size distribution

On deducing the gas bubble diameters, $d_{j,h}$, an initial estimation of bubble size distribution can be deduced via a probability distribution function. A good approximation adequate to represent the size distribution is the normal distribution, Equation (7.15n) or log-normal, Equation (7.15o) [211].

$$f(d_{j,h}) = \frac{1}{\zeta_* \sqrt{2\pi}} \exp \left\{ -\frac{1}{2} \left(\frac{d_{j,h} - d_{j,m}}{\zeta_*} \right)^2 \right\} \quad (7.15n)$$

Where $d_{j,m}$ is the mean diameter of the gas bubble, which can be taken approximately as d_{Sj_*} i.e., $d_{j,m} \cong d_{Sj_*}$, and $\zeta_* = \sqrt{\sum_{h=1}^H (d_{j,h} - d_{Sj_*})^2 / H}$ is the standard deviation of the bubble diameter, $d_{j,m}$ is the mean diameter of the gas bubble, which can be taken approximately as d_{Sj_*} i.e. $d_{j,m} \cong d_{Sj_*}$, and H is the total number of bubbles (taken as simulation total time step).

$$f(d_{j,h}) = \frac{1}{d_{j,h} \zeta_{*log} \sqrt{2\pi}} \exp \left\{ -\frac{1}{2} \left(\frac{\ln d_{j,h} - d_{j,mlog}}{\zeta_{*log}} \right)^2 \right\} \quad (7.15o)$$

Where $d_{j,mlog}$ and ζ_{*log} are respectively natural logarithm of the mean and standard deviation of bubble diameter. i.e., $d_{j,mlog} \cong \ln d_{Sj_*}$ and $\zeta_{*log} \cong \ln \zeta_*$.

7.11. Estimation of biogas outflow rate

The biogas outflow rate, q_{o-G} , from the bioreactor is suggested to be dependent on the current bioreactor pressure, $P = P_G + P_{sw}$, in the headspace as given by Equation (7.16) [212]. Where P_R is the fixed or desired operating pressure of the bioreactor and k_p is the pipe resistance coefficient ($\text{pa.m}^3.\text{sec}^{-1}$).

$$q_{o-G} = k_p (P - P_R) (P / P_R) \quad (7.16)$$

7.12. Estimation of pH in the bioreactor

In modelling the dynamics of pH of the bioreactor electro balance in the liquid phase is performed. In anaerobic digestion, the electro neutrality and chemical affinity constant are utilised, and it is assumed the pH of the system, Equation (7.17k) is influenced mainly by dissolved carbon dioxide in equilibrium with bicarbonate ion molar concentration, $[\text{HCO}_3^-]$. $[\text{HCO}_3^-]$ is dependent on the presence of other cations and anions in the system as given by Equation (7.17a). Equation (7.17a) [157] is a simplified balance for the anaerobic digestion of carbohydrates, lipids, and protein, deduced from the reported generic expression for charge balances [213,214]. Where $[Z]$ (kgmoles.m^{-3}) is the molar concentration of an artificial variable i.e., considered as either cation (Na^+ , Ca^+ , etc.), and anions (such as Cl^-), $[\text{NH}_4^+]$ is the ammonium molar concentration due digestion of protein in feedstock and $[\text{Ac}^-]$ is the concentration of acetic acid. While M_{NH_4} and M_{Ac} are the molecular weight of ammonium and acetic acid in the system [215].

$$[\text{HCO}_3^-] = [Z] + [\text{NH}_4^+] - [\text{Ac}^-] \quad (7.17a)$$

In Equation (7.17a) the ammonium molar concentration, $[\text{NH}_4^+]$ can be deduced from Equation (7.17b) via Equation (7.17t) using ammonia, NH_3 , deduce from Equation (7.7m). Where $K_{a\text{NH}_4^+}$ (kgmole) is the

disassociation constant for ammonium, given by Equation (7.17o) or (7.17p). Note that in this work since the feedstock is non-proteinaceous, $G_{\text{DNH}_3} = 0$, and as such $[\text{NH}_4^+] = 0$.

$$[\text{NH}_4^+] = \frac{G_{\text{DNH}_3} [\text{H}^+]}{M_{\text{NH}_3} K_{\text{aNH}_4^+}} \quad (7.17b)$$

While the acetic ion molar concentration, $[\text{Ac}^-]$ can be approximated theoretically from the stoichiometric degradation of the given substrate since acetic acid would always be formed. This approximation is done because the SSDM does not account for the dynamics of acetic acid. Considering the illustration of LCFA ($\text{C}_{18}\text{H}_{34}\text{O}_2$), S_1 and glycerol ($\text{C}_3\text{H}_8\text{O}_3$), S_2 formed from lipid molecules, as illustrated by Equation (4.1) – (4.7). The stoichiometric balance indicates that 3, and 1 mole(s) of acetic acid molecules are formed from each LCFA and glycerol molecule respectively. Therefore, the acetic acid mass concentration, $\text{Ac} = (3S_1/M_{S_1} + S_2/M_{S_2})M_{\text{Ac}}$ can be estimated. Finally, $[\text{Ac}^-]$ can be deduced from Ac via Equation (7.17c) via Equation (4.16q). Where K_{aAc} is the disassociation constant for acetic acid, given by Equation (7.17n) or (7.17p)

$$[\text{Ac}^-] = \frac{\text{Ac}[\text{H}^+]}{M_{\text{Ac}} K_{\text{aAc}}} \quad (7.17c)$$

The artificial ionic molar concentration, $[\text{Z}]$, can be deduced from Equation (7.17d) – (7.17e).

$$\text{Cation input rate} + \text{Ion input rate from pH controller} + \text{Cation formation rate} = \text{Cation accumulation rate} + \text{Cation output rate} \quad (7.17d)$$

$$\begin{aligned} \dot{n}_{i-z} + \dot{n}_{c-z} + V_L R_Z &= \frac{dn_z}{dt} + \dot{n}_{o-z} \\ \frac{dn_z}{dt} &= \dot{n}_{i-z} + \dot{n}_{c-z} - \dot{n}_{o-z} + V_L R_Z \end{aligned} \quad (7.17e)$$

Applying the necessary mathematical expression to Equation (7.17e) yields Equation (7.17f). Where $[\text{Z}_c]$ is the molar concentration of cation ($[\text{Z}_c] = [\text{Z}]$) or anion ($[\text{Z}_c] = -[\text{Z}]$) fed by the pH controller. Typically, the choice of the ion sources is hydrochloric acid (HCl) for anion, and potassium hydroxide (KOH) for cation respectively.

$$\frac{d(V_L[\text{Z}])}{dt} = q_{i-L}[\text{Z}]_i + q_{c-L}[\text{Z}_c] - q_{o-L}[\text{Z}] + V_L R_Z \quad (7.17f)$$

Expanding the expression $d(V_L[\text{Z}])/dt$, Equation (7.17g) and combining it with Equation (7.3d) yield Equation (7.17h).

$$\frac{d(V_L[\text{Z}])}{dt} = V_L \frac{d[\text{Z}]}{dt} + [\text{Z}] \frac{dV_L}{dt} \quad (7.17g)$$

$$\frac{d(V_L[\text{Z}])}{dt} = V_L \frac{d[\text{Z}]}{dt} + [\text{Z}][q_{i-L} + q_{c-L} - q_{o-L} - (V_L R_{E-G} + R_{\text{Evap}} + q_{o-GG} W_{\text{H}_2\text{O}})/\rho_L] \quad (7.17h)$$

Combining Equation (7.17h) and (7.17f), and rearranging yields Equation (7.17i).

$$\begin{aligned}
& V_L \frac{d[Z]}{dt} + [Z][q_{i-L} + q_{c-L} - q_{o-L} - (V_L R_{E-G} + R_{Evap} + q_{o-GG} W_{H_2O})/\rho_L] \\
& \quad = q_{i-L}[Z]_i + q_{c-L}[Z]_c - q_{o-L}[Z] + V_L R_Z \\
\frac{d[Z]}{dt} & = \frac{q_{i-L}}{V_L} ([Z]_i - [Z]) + \frac{q_{c-L}}{V_L} ([Z]_c - [Z]) + \frac{[Z]}{\rho_L} \left(R_{E-G} + \frac{R_{Evap}}{V_L} + q_{o-GG} W_{H_2O} \right) + R_Z \quad (7.17i)
\end{aligned}$$

Considered in Equation (7.17i) is the inclusion of the formation of new cations, R_Z (kmole.m⁻³. s⁻¹), Equation (7.17j) – (7.17k) is associated with microbes' activities. Where Y_{cat-j} (i.e. Y_{cat-1} is the cation yield from microbes associated with the utilisation of LCFA, S_1 and Y_{cat-2} is associated with glycerol, S_2 substrates, however, it can be assumed that $Y_{cat-1} \cong Y_{cat-2} \cong Y_{cat=1}$), M_{B_j} (i.e. M_{B_1} and M_{B_2} is the molecular weight of microbes in the AD, and using the molecular formular, $C_5H_7O_2N$ [161] to represent the microbes $M_{B_1} = M_{B_2} = M_B = 113$).

$$R_Z = \sum_{j=1}^J Y_{cat-j} \mu_j B_j / M_{B_j} \quad (7.17j)$$

$$R_Z = (Y_{cat-1} \mu_1 B_1 / M_{B_1} + Y_{cat-2} \mu_2 B_2 / M_{B_2}) \cong Y_{cat} (\mu_1 + \mu_2) / M_B \quad (7.17k)$$

The hydrogen ions' molar concentration, $[H^+]$ in the anaerobic system can then be deduced via Equation (7.17l), and subsequently the pH of the system, Equation (7.17m).

$$\frac{d[H^+]}{dt} = \frac{K_{aCO_2}}{[HCO_3^-] M_{CO_2}} \frac{dG_{DCO_2}}{dt} \quad (7.17l)$$

$$pH = -\log_{10}[H^+] \quad (7.17m)$$

The estimation of the disassociation constant, $K_{aj_{\pm}}$ (kgmole), just like the Henry constant was also reported by **Oh & Martin** [174] for various components, j_{\pm} , in an anaerobic digester is given by Equation (7.17n). The equilibrium relation for the system at temperature T(K) is described by the ion association, in which the chemical potential ($\psi_{j_{\pm}}$) of components, j_{\pm} , equals the summation of chemical ions' potentials ($\psi_{j_{\pm}}^+$ and $\psi_{j_{\pm}}^-$) of its constituent ion, j_- and, j_+ , for the component j_{\pm} (i.e. $\Delta v_{j_{\pm}} \psi_{j_{\pm}}^{o\pm}$) [174]. Based on a temperature reference of 298K the summation of chemical ion potentials, $\Delta v_{j_{\pm}} \psi_{j_{\pm}}^{o\pm}$ of species, $j_{\pm} = CO_2$ (to HCO_3^-) and acetic acid was calculated as -358.8272, and -267.9815 respectively. While the disassociation constant for ammonium ($K_{aNH_4^+}$), Equation (7.17o) which applies to pure water, [216], can be approximately used. **Flores-Estrella et al.** [217] reported a typical value of 5.3×10^{-10} as the $K_{aNH_4^+}$ at 35°C for anaerobic digestion. However, **Campos & Flotats** [213] reported a generic expression, Equation (7.17p) for the computation of ions and cations for various components in anaerobic digestion, whose coefficients, Table (7.2) and some corresponding acid-base equilibrium given by Equation (7.17q) – (7.17w) [170,213,218].

$$K_{aj_{\pm}} = \exp \left\{ \frac{\Delta v_{j_{\pm}} \psi_{j_{\pm}}^{o\pm}}{0.0821T} \right\} \quad (7.17n)$$

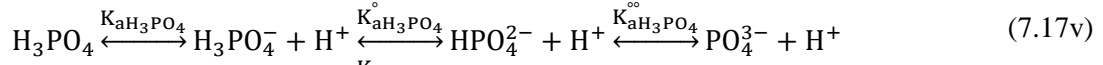
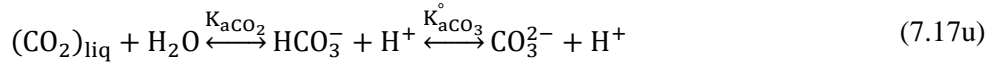
$$K_{aNH_4^+} = 10^{-\left\{ \frac{2835.76}{T} - 0.6322 + 0.001225T \right\}} \quad (7.17o)$$

$$K_{aj_{\pm}} = 10^{-\{pK_i^o(0) + a_{j_{\pm}} T(^{\circ}C) + b_{j_{\pm}} T(^{\circ}C)^2 + c_{j_{\pm}} T(^{\circ}C)^3\}} \quad (7.17p)$$

Table 7.2. Coefficients for dissociation constants of components in anaerobic digestion [213]

Components (j_{\pm})	$pK_i^0(0)$	$a_{j_{\pm}}$	$b_{j_{\pm}}$	$c_{j_{\pm}}$
Acetate, AcH	4.7803	-0.0023	6.00E-05	-2.00E-07
Ammonium, NH_4^+	10.072	-0.0356	9.00E-05	4.00E-08
Butyrate, BrH	4.8947	-0.0024	7.00E-05	-3.00E-07
Propionate, PrH	4.8063	-0.0011	8.00E-05	-4.00E-07
Carbonate, HCO_3^-	6.5787	-0.0133	0.0002	-8.00E-07
Carbonate, CO_3^{2-}	9.2839	-0.0133	9.00E-05	-2.00E-07
Phosphate, $H_3PO_4^-$	2.0473	0.0019	5.00E-05	0.0000
Phosphate, HPO_4^{2-}	7.3144	-0.0073	0.0001	-6.00E-07
Phosphate, PO_4^{3-}	12.658	0.0000	0.0000	0.0000
Water, H_2O	14.934	-0.0425	0.0002	-6.00E-07

Note that the subscript “liq” signify liquid in Equation (7.17q) – (7.17w).



7.13. Energy balance to deduce temperature dynamics

In modelling energy flow, it is assumed that the temperature distribution at every time and spatial coordinate for the bioreactor content as well as HW flowing through the HJ is the same. This is made possible in practice by adequate mixing of the bioreactor content. In general, the transfer of heat energy from fluid to fluid is based on heat flow from the hot fluid through the walls of its enclosure, and the mode of heat transfer i.e. heat loss and heat gain is assumed to be by conduction, convection, and radiation. In summary, the following phenomena are assumed.

1. Energy loss from the bioreactor content to the environment occurs, because of temperature differences between the bioreactor and the environment. The mode of heat transfer is predominantly via natural convection, forced convection as well as radiation.
2. Energy gain from HW in HJ to the bioreactor content occurs, this is due to temperature differences between the bioreactor content and the HW. This process leads to temperature increases in the bioreactor, and it is predominantly via forced convection.
3. The thermodynamic properties of the inlet stream, outlet stream and bioreactor content are approximately the same.

7.13.1. Energy balance of bioreactor

The temperature changes of the control volume can be deduced from the energy balance on the control volume via the immediate statement expression below, and applying the equivalent mathematical expression yields Equation (7.18a).

$$\begin{aligned} & \text{Input energy stream} + \text{Input energy stream from pH controller} + \text{Heat exchanger} \\ & \text{energy} + \text{Mixing energy} + \text{Heat of reaction} = \text{Energy accumulation} + \text{Output energy} \\ & \text{stream} + \text{Heat of evaporation} + \text{Energy loss to environment} \end{aligned} \quad (7.18a)$$

$$\begin{aligned} & q_{i-L}\rho_{i-L}C_{pi-L}T_i + q_{c-L}\rho_{c-L}C_{pc-L}T_c + Q_{HE} + P_{Mix} + V_L R_{AD}\Delta H_{AD} \\ & = \frac{d(m_L C_{PL} + m_G C_{PG} + m_{w_v} C_{Pw_v})T}{dt} + (q_{o-L}\rho_{o-L}C_{Po-L} + q_{o-G}G C_{Po-G} \\ & + q_{o-G}W_v C_{Po-w_v} + q_{o-GG}W_{H_2O}C_{Po-w_v})T + (R_{Evap} + q_{o-GG}W_{H_2O})\Delta H_{Evap} \\ & + Q_{R-En} \end{aligned} \quad (7.18b)$$

Therefore, based on assumption three (3) the following applies. The density, ρ ($\text{kg}\cdot\text{m}^{-3}$), and specific heat capacity, C_p ($\text{J}\cdot\text{kg}^{-1}\cdot\text{K}^{-1}$) of fluids of similar nature are considered approximately the same, i.e., $\rho_{i-L}C_{pi-L} \cong \rho_{c-L}C_{pc-L} \cong \rho_{o-L}C_{Po-L} \cong \rho_L C_{PL}$, $C_{Po-G} \cong C_{PG}$, $C_{Po-w_v} \cong C_{Pw_v}$ and rearranging Equation (7.18b) yields Equation (7.18c).

$$\begin{aligned} & \frac{d(m_L C_{PL} + m_G C_{PG} + m_{w_v} C_{Pw_v})T}{dt} \\ & = q_{i-L}\rho_L C_{pL}T_i + q_{c-L}\rho_L C_{pL}T_c - (q_{o-L}\rho_L C_{pL} + q_{o-G}G C_{PG} + q_{o-G}W_v C_{Pw_v} \\ & + q_{o-GG}W_{H_2O}C_{Pw_v})T + V_L R_{AD}\Delta H_{AD} - (R_{Evap} + q_{o-GG}W_{H_2O})\Delta H_{Evap} \\ & + (Q_{HE} + P_{Mix} - Q_{R-En}) \end{aligned} \quad (7.18c)$$

Expanding the expression, $d(m_L C_{PL} + m_G C_{PG} + m_{w_v} C_{Pw_v})T/dt$, Equation (7.18d) and rearranging yields Equation (7.18e) i.e., by substituting in Equation (7.3c), Equation (7.8c) based all gases and Equation (7.11c).

$$\begin{aligned} & \frac{d(m_L C_{PL} + m_G C_{PG} + m_{w_v} C_{Pw_v})T}{dt} \\ & = TC_{PL} \frac{dm_L}{dt} + TC_{PG} \frac{dm_G}{dt} + TC_{Pw_v} \frac{dm_{w_v}}{dt} + (m_L C_{PL} + m_G C_{PG} \\ & + m_{w_v} C_{Pw_v}) \frac{dT}{dt} \end{aligned} \quad (7.18d)$$

$$\begin{aligned} & \frac{d(m_L C_{PL} + m_G C_{PG} + m_{w_v} C_{Pw_v})T}{dt} \\ & = TC_{PL} [(q_{i-L} + q_{c-L} - q_{o,L})\rho_L - (V_L R_{E-G} + R_{Evap} + q_{o-GG}W_{H_2O})] \\ & + TC_{PG} [V_L R_{E-j_*} - q_{o-G}G_{j_*}] + TC_{Pw_v} [R_{Evap} - q_{o-G}W_v] + (V_L \rho_L C_{PL} \\ & + V_G G C_{PG} + V_G W_v C_{Pw_v}) \frac{dT}{dt} \end{aligned} \quad (7.18e)$$

Substituting Equation (7.18e) into Equation (7.18c) and rearranging yields Equation (7.18f).

$$\begin{aligned}
& \text{TC}_{\text{PL}}[(q_{i-L} + q_{c-L} - q_{o,L})\rho_L - (V_L R_{E-G} + R_{\text{Evap}} + q_{o-GG} W_{\text{H}_2\text{O}})] \\
& \quad + \text{TC}_{\text{PG}}[V_L R_{E-j_*} - q_{o-G} G_{j_*}] + \text{TC}_{\text{PW}_v}[R_{\text{Evap}} - q_{o-G} W_v] + (V_L \rho_L C_{\text{PL}} \\
& \quad + V_G G C_{\text{PG}} + V_G W_v C_{\text{PW}_v}) \frac{dT}{dt} \\
& = q_{i-L} \rho_L C_{\text{PL}} T_i + q_{c-L} \rho_L C_{\text{PL}} T_c - (q_{o-L} \rho_L C_{\text{PL}} + q_{o-G} G C_{\text{PG}} + q_{o-G} W_v C_{\text{PW}_v} \\
& \quad + q_{o-GG} W_{\text{H}_2\text{O}} C_{\text{PW}_v}) T + V_L R_{\text{AD}} \Delta H_{\text{AD}} - (R_{\text{Evap}} + q_{o-GG} W_{\text{H}_2\text{O}}) \Delta H_{\text{Evap}} \\
& \quad + (Q_{\text{HE}} + P_{\text{Mix}} - Q_{\text{R-En}}) \\
& (V_L \rho_L C_{\text{PL}} + V_G G C_{\text{PG}} + V_G W_v C_{\text{PW}_v}) \frac{dT}{dt} \\
& = q_{i-L} \rho_L C_{\text{PL}} (T_i - T) + q_{c-L} \rho_L C_{\text{PL}} (T_c - T) + q_{o-GG} W_{\text{H}_2\text{O}} (C_{\text{PL}} - C_{\text{PW}_v}) T \\
& \quad + R_{\text{Evap}} (C_{\text{PL}} - C_{\text{PW}_v}) T + V_L R_{E-G} (C_{\text{PL}} - C_{\text{PG}}) T + V_L R_{\text{AD}} \Delta H_{\text{AD}} \\
& \quad - (R_{\text{Evap}} + q_{o-GG} W_{\text{H}_2\text{O}}) \Delta H_{\text{Evap}} + (Q_{\text{HE}} + P_{\text{Mix}} - Q_{\text{R-En}}) \\
\frac{dT}{dt} & = \frac{1}{(V_L \rho_L C_{\text{PL}} + V_G G C_{\text{PG}} + V_G W_v C_{\text{PW}_v})} [q_{i-L} \rho_L C_{\text{PL}} (T_i - T) + q_{c-L} \rho_L C_{\text{PL}} (T_c - T) \\
& \quad + q_{o-GG} W_{\text{H}_2\text{O}} (C_{\text{PL}} - C_{\text{PW}_v}) T + R_{\text{Evap}} (C_{\text{PL}} - C_{\text{PW}_v}) T + V_L R_{E-G} (C_{\text{PL}} \\
& \quad - C_{\text{PG}}) T + V_L R_{\text{AD}} \Delta H_{\text{AD}} - (R_{\text{Evap}} + q_{o-GG} W_{\text{H}_2\text{O}}) \Delta H_{\text{Evap}} \\
& \quad + (Q_{\text{HE}} + P_{\text{Mix}} - Q_{\text{R-En}})] \tag{7.18f}
\end{aligned}$$

Where $Q_{\text{HE}}(\text{W})$ is heating energy from hot water, $Q_{\text{R-En}}(\text{W})$ is the heat loss to the environment from the bioreactor, $P_{\text{Mix}}(\text{W})$ is the stirring power, $\Delta H_{\text{AD}}(\text{J.kgmoles}^{-1})$ is the heat of reaction of the anaerobic reaction (dependent on feedstock type), $\Delta H_{\text{Evap}}(\text{J.kg}^{-1})$ is the latent heat of vapourisation of water, C_{PW_v} is the specific heat capacity of water vapour, C_{PL} is the specific heat capacity of the liquid phase (i.e. sludge), $G = \sum_{j_*}^J G_{j_*}$ is the sum of all gaseous species concentration in the headspace, inert gas inclusive, $C_{\text{PG}} = \sum_{j_*}^J y_{j_*} C_{\text{P-j}_*}$ is the specific heat capacity of biogas species only, y_{j_*} is the gaseous fraction of biogas species, and $R_{\text{AD}}(\text{kg.m}^{-3}.\text{s}^{-1})$ is the rate of anaerobic digestion, Equation (7.18g) – (7.18h).

$$R_{\text{AD}} = \sum_j^J \frac{1}{Y_{\text{S}_j/\text{F}}} \left(\frac{\mu_j B_j}{Y_{\text{B}_j/\text{S}_j}} \right) = \frac{1}{Y_{\text{S}_1/\text{F}}} \left(\frac{\mu_1 B}{Y_{\text{B}/\text{S}_1}} \right) + \frac{1}{Y_{\text{S}_2/\text{F}}} \left(\frac{\mu_2 B}{Y_{\text{B}/\text{S}_2}} \right) \tag{7.18g}$$

$$\Delta H_{\text{AD}} = \sum_{j_o} \omega_{\text{F}_{j_o}} (1/M_{\text{F}_{j_o}}) \frac{m_{\text{F}_{j_o}}}{m_{\text{Ref}_{j_o}}} \Delta H_{\text{AD-Ref}_{j_o}} \tag{7.18h}$$

The ΔH_{AD} for a given feedstock, F_{j_o} can be calculated from reference values, $\Delta H_{\text{AD-Ref}_{j_o}}$ for $j_o =$ carbohydrates, protein, and lipid feedstock as reported by **Lindorfer et al.** [219], Equation (7.18h) applicable for mixed or single feedstock. Where $m_{\text{Ref}_{j_o}}$ is the stoichiometric mass of the reference (j_o) molecule, $m_{\text{F}_{j_o}}$ and $\omega_{\text{F}_{j_o}}$ are respectively the stoichiometric mass as well as the mass fraction of the specific (j_o) molecule in the feedstock. As an illustration of an AD system with lipid ($\text{C}_{57}\text{H}_{104}\text{O}_6$, $M_{\text{F}_{\text{lip}}} = 884$, i.e. $m_{\text{F}_{\text{lip}}} = 884$ based on a mole basis) and xanthan gum ($\text{C}_{35}\text{H}_{49}\text{O}_{29}$, $M_{\text{F}_{\text{carb}}} = 933$, i.e. $m_{\text{F}_{\text{carb}}} = 933$ based on a mole basis) as an emulsifier in a mass ratio of 50:50 (i.e. $\omega_{\text{F}_{\text{lip}}} = \omega_{\text{F}_{\text{carb}}} = 0.5$). Therefore, lipid reference ($2\text{C}_{16}\text{H}_{12}\text{O}_6$, $m_{\text{Ref}_{\text{lip}}} = 600$ & $\Delta H_{\text{AD-Ref}_{\text{lip}}} = +544.5 \text{ kJ.gmole}^{-1}$) and carbohydrates reference ($\text{C}_6\text{H}_{12}\text{O}_6$, $m_{\text{Ref}_{\text{carb}}} = 180$ & $\Delta H_{\text{AD-Ref}_{\text{carb}}}^{\text{Ro}} = -138.5 \text{ kJ.gmole}^{-1}$). Therefore $\Delta H_{\text{AD}} = 0.0690 \text{ kJ.g}^{-1}$.

7.14. Power supplied by mixer or stirrer

The power (W) of the mixer, P_{Mix} , can be estimated from either Equation (7.19a), (7.19b), for laminar range i.e., $N_{\text{Re}}(\rho_L n_{\text{st}} d_{\text{st}}^2 / \eta_L) \leq 10$ or Equation (7.19c) for over the laminar range [220–222]. Where n_{st} (rps) is the stirrer speed, d_{st} (m) is the diameter of the stirrer and η_L (pa.s) is the viscosity of the bioreactor liquid content.

$$P_{\text{Mixer}} = 2\pi n_{\text{st}} \tau \quad (7.19a)$$

$$P_{\text{Mix}} = N_p \eta_L n_{\text{st}}^2 d_{\text{st}}^3 \quad (7.19b)$$

$$P_{\text{Mix}} = N_p \rho_L n_{\text{st}}^3 d_{\text{st}}^5 \quad (7.19c)$$

The Equation (7.19a) is a general equation of stirrer power, when the torque, τ (N.m) is known, and N_p is the power number of the stirrer, which is determined based on correlation with N_{Re} [220,223,224], however for simplicity it will be taken as $N_p = 0.309$.

7.15. Material balance on energy jacket

The changes in hot water level can be deduced using the immediate statement expression below and applying the equivalent mathematical expression yields Equation (7.20a) – (7.20b).

$$\text{Input hot water} = \text{Accumulation of hot water} + \text{Output hot water} \quad (7.20a)$$

$$\dot{m}_{\text{i-hw}} = \frac{dm_{\text{hw}}}{dt} + \dot{m}_{\text{o-hw}} \quad (7.20b)$$

The flow of heating water in the heating jacket is assumed to be in a steady state, hence $dm_{\text{HW}}/dt = 0$, therefore Equation (7.20b) reduces to (7.20c).

$$\begin{aligned} \dot{m}_{\text{i-hw}} &= \dot{m}_{\text{o-hw}} \\ q_{\text{i-hw}} \rho_{\text{i-hw}} &= q_{\text{o-hw}} \rho_{\text{o-hw}} \\ \rho_{\text{i-hw}} &\cong \rho_{\text{o-hw}} \cong \rho_{\text{hw}} \\ q_{\text{i-hw}} &= q_{\text{o-hw}} = q_{\text{hw}} \end{aligned} \quad (7.20c)$$

Where $q_{\text{i-hw}}$, $q_{\text{o-hw}}$, q_{hw} are input, output, generic volumetric flowrates and $\rho_{\text{i-hw}}$, $\rho_{\text{o-hw}}$, as well as ρ_{hw} are their respective density.

7.16. Energy balance for heating jacket

The temperature changes of the heating jacket can be deduced from the energy balance on the control volume via Equation (7.21a) – (7.21e).

$$\text{Input energy} = \text{Energy accumulation} + \text{Energy output} + \text{Energy loss to reactor} + \text{Energy loss to environment} \quad (7.21a)$$

$$q_{\text{i-hw}} \rho_{\text{i-hw}} C_{\text{P-i-hw}} T_{\text{i-hw}} = \frac{d(m_{\text{hw}} C_{\text{P-hw}} T_{\text{hw}})}{dt} + q_{\text{o-hw}} \rho_{\text{o-hw}} C_{\text{P-o-hw}} T_{\text{hw}} + Q_{\text{HE}} + Q_{\text{EN}} \quad (7.21b)$$

Expanding the expression $d(m_{\text{hw}} C_{\text{P-hw}} T_{\text{hw}})/dt$, Equation (7.21c) and substituting in $dm_{\text{hw}}/dt = 0$ and necessary mathematical expression yield Equation (7.21d).

$$\frac{d(m_{\text{hw}} C_{\text{P-hw}} T_{\text{hw}})}{dt} = m_{\text{hw}} C_{\text{P-hw}} \frac{dT_{\text{hw}}}{dt} + C_{\text{P-hw}} T_{\text{hw}} \frac{dm_{\text{hw}}}{dt} = m_{\text{hw}} C_{\text{P-hw}} \frac{dT_{\text{hw}}}{dt} \quad (7.21c)$$

$$\frac{d(m_{hw}C_{P-hw}T_{hw})}{dt} = \rho_{hw}V_{hw}C_{P-hw}\frac{dT_{hw}}{dt} \quad (7.21d)$$

Substituting Equation (7.21d) into (7.21b), noting that $\rho_{i-hw}C_{Pi-hw} = \rho_{o-hw}C_{Po-hw} \cong \rho_{hw}C_{P-hw}$ and rearranging yields Equation (7.21e).

$$q_{i-hw}\rho_{i-hw}C_{Pi-hw}T_{i-hw} = \rho_{hw}V_{hw}C_{P-hw}\frac{dT_{hw}}{dt} + q_{o-hw}\rho_{o-hw}C_{Po-hw}T_{hw} + Q_{HE} + Q_{H-En}$$

$$\frac{dT_{hw}}{dt} = \frac{q_{hw}(T_{i-hw} - T_{hw})}{V_{hw}} - \frac{(Q_{HE} + Q_{H-En})}{\rho_{hw}V_{hw}C_{P-hw}} \quad (7.21e)$$

Where T_{i-hw} , T_{hw} , V_{hw} , C_{P-hw} , ρ_{hw} , Q_{H-En} are inlet hot water temperature, heating jacket temperature, the volume of the heating jacket, specific heat capacity, density of water, and heat loss from the heating jacket to the environment or surrounding.

7.17. Estimation of bioreactor heat transfer with wall temperatures

Considering a jacketed bioreactor, Figures (7.1) and (7.2) with the same length as the reactor, h_R , whose cross-sectional area is also shown in Figure (7.4) as applicable to this work. Given that the heating jacket's hydraulic inner diameter, $D_{H-i} \cong 0.02m$, and the outer diameter $D_{H-o} \cong 0.02+x_H$ are specified with x_H being its thickness.

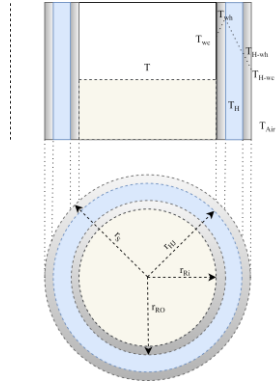


Figure 6.4. Cross-sectional area of the bioreactor with material and heat transfer

The estimation of heat transfer between bioreactor content and heating jacket, Q_{HE} , can be deduced via Equation (7.22a) – (7.22c) or (7.22d) – (7.22f). Furthermore, based on Figure (7.4), it is assumed that heat loss from the bioreactor content to the environment $Q_{R-En} = 0$ is negligible. However, the heat transfer from the heating jacket to the environment, Q_{H-En} would need to be estimated as detailed in Equation (7.22o) – (7.22q) or (7.22r) – (7.22t).

7.17.1. Computation of heat transfer from heating fluid to bioreactor content

Heat flux based on bioreactor internal area

The heat flux based on the internal area, $A_{Ri} = \pi D_{Ri} h_R$, of the bioreactor is given as, Q_{HE}/A_{Ri} , expressed in Equation (7.22a) or (7.22b), the overall heat transfer coefficient based on the internal area of the bioreactor, U_{HE-i} is given by Equation (7.22c).

$$\frac{Q_{HE}}{A_{Ri}} = U_{HE-i}(T_{hw} - T) \quad (7.22a)$$

$$\frac{Q_{HE}}{A_{Ri}} = \dot{h}_R(T_{wc} - T) \quad (7.22b)$$

$$U_{HE-i} = \frac{1}{\frac{1}{\dot{h}_R} + \frac{x_R}{\dot{k}_R} \left(\frac{D_{Ri}}{\bar{D}_R} \right) + \frac{1}{\dot{h}_{Hi}} \left(\frac{D_{Ri}}{D_{Ro}} \right)} \quad (7.22c)$$

Heat flux based on bioreactor outer area

The heat flux based on the internal area, $A_{Ro} = \pi D_{Ro} h_R$, of the bioreactor is given as, Q_{HE}/A_{Ro} , expressed in Equation (7.22d) or (7.22e), the overall heat transfer coefficient based on the internal area of the bioreactor, U_{HE-o} is given by Equation (7.22f).

$$\frac{Q_{HE}}{A_{Ro}} = U_{HE-o}(T_{hw} - T) \quad (7.22d)$$

$$\frac{Q_{HE}}{A_{Ro}} = \dot{h}_{Hi}(T_{wh} - T) \quad (7.22e)$$

$$U_{HE-o} = \frac{1}{\frac{1}{\dot{h}_{Hi}} + \frac{x_R}{\dot{k}_R} \left(\frac{D_{Ro}}{\bar{D}_R} \right) + \frac{1}{\dot{h}_R} \left(\frac{D_{Ro}}{D_{Ri}} \right)} \quad (7.22f)$$

Where U_{HE-i} ($W \cdot m^{-2} \cdot K^{-1}$), U_{HE-o} , x_R , \dot{k}_R ($W \cdot m^{-1} \cdot K^{-1}$), D_{Ri} , D_{Ro} , $\bar{D}_R = (D_{Ro} - D_{Ri}) \ln(D_{Ro}/D_{Ri})$, T_{wh} (K), and T_{wc} are the inner overall heat coefficient, outer overall heat coefficient, thickness, thermal conductivity, inner diameter, outer diameter, logarithmic mean diameter, hot side wall temperature and cold side wall temperature of the bioreactor respectively. While \dot{h}_R ($W \cdot m^{-2} \cdot K^{-1}$) and \dot{h}_{Hi} are the heat transfer coefficient for the liquid content in the bioreactor as well as that of the heating fluid of the heating jacket based on the inner area.

7.17.2. Computation of bioreactor heat transfer coefficient

The effective heat transfer coefficient for the bioreactor, \dot{h}_R can be deduced from Equation (7.22k) [225], for which \dot{h}_L , Equation (7.22g) represents the stirred liquid portion while \dot{h}_G , depending on the criteria either Equation (7.22h) for $D/h_L \geq 35/Gr^{1/3}$ or Equation (7.22i) for $10^4 < GrPr < 10^8$ or Equation (7.22j) for $10^8 < GrPr < 10^{12}$ [226–228] represent the gas-vapour portion. Where $N_{Re} = \rho_j n_{st} d_{st}^2 / \eta_j$ is the Reynold number of the stirred bioreactor as earlier defined, $Pr = C_{pj} \eta_j / \dot{k}_L$, Prandtl number, \dot{k}_j is the thermal conductivity of fluid in the bioreactor, $Gr = g \beta \rho_j^2 |\Delta T| L_c^3 / \eta_j$ is the Grashof number, ΔT is the temperature difference between fluid and wall, $\beta = \Delta \rho_j / (\rho_{avj} \Delta T)$ [229] for liquid or $\beta \cong 1/T_f$ for gases [230] is the fluid thermal expansion coefficient, ρ_{avj} is the average density of liquid between temperature changes, Θ_1 and Θ_2 are the stirrer characteristics, assuming a single paddle-type propeller, $\Theta_1 = 0.36$ and $\Theta_2 = 0.21$ [231–233]. The characteristic length, L_c , for Equation (7.22g), is the inner diameter of the reactor, while for Equation (7.22h) – (7.22j) is the height of the gas headspace. Note that all physiochemical properties of fluids in these equations are calculated at the film temperature, $T_f = 0.5(T_{wc} + T)$, j indicates specific fluid in the bioreactor (i.e. either liquid, $j=L$ or gas, $j=G$), and η_{wj} is the viscosity of the fluid at the inner wall temperature of the heating jacket, T_{wc} .

$$\text{Nu} = \left(\frac{\dot{h}_j L_c}{k_j} = \Theta_1 \text{Re}^{2/3} \text{Pr}^{1/3} \left(\frac{\eta_j}{\eta_{wj}} \right)^{\Theta_2} \right)_{j=L} \quad (7.22g)$$

$$\text{Nu} = \left(\frac{\dot{h}_j L_c}{k_j} = \left(0.825 + \frac{0.387(\text{GrPr})^{1/6}}{(1 + (0.492/\text{pr})^{9/16})^{8/27}} \right)^2 \right)_{j=G} \quad (7.22h)$$

$$\text{Nu} = \left(\frac{\dot{h}_j L_c}{k_j} = 0.555(\text{GrPr})^{0.25} \right)_{j=G} \quad (7.22i)$$

$$\text{Nu} = \left(\frac{\dot{h}_j L_c}{k_j} = 0.129(\text{GrPr})^{0.33} \right)_{j=G} \quad (7.22j)$$

$$\dot{h}_R = \sqrt[4]{\dot{h}_L^4 + \dot{h}_G^4} \quad (7.22k)$$

7.17.3. Computation of heating jacket heat transfer coefficient

The value for \dot{h}_{Hi} can be deduced from the correlation given by Equation (7.22l) [234] for lamina ($\text{Re} < 2300$) or Equation (7.22m) [234–236] for turbulent flow regime.

$$\text{Nu} = \left(\frac{\dot{h}_j L_c}{k_j} = \left\{ 3.66 + \frac{0.065 \text{RePr} D_{H-i}/h_R}{1 + 0.04(\text{RePr} D_{H-i}/h_R)^{2/3}} \right\} \left(\frac{\eta_j}{\eta_{wj}} \right)^{0.11} \right)_{j=Hi} \quad (7.22l)$$

$$\text{Nu} = \left(\frac{\dot{h}_j L_c}{k_j} = 0.0243 \text{Re}^{c_1} \text{Pr}^{c_2} \left(\frac{\eta_j}{\eta_{wj}} \right)^{0.14} \right)_{j=Hi} \quad (7.22m)$$

Where $c_1 = 0.8$, $c_2 = 0.4$ for heating or 0.3 for cooling (which is applicable in this work). The characteristic length, $L_c = D_{H-i}$, k_j is the thermal conductivity, $\text{Re} = \rho_j u_j D_{H-i} / \eta_j$, Reynold's number, $u_H = 4q_{hw} / \pi D_{H-i}^2$, $\text{Pr} = C_{pj} \eta_j / k_j$, Prandtl number of hot water and all physiochemical properties are calculated at the film temperature, $T_f = 0.5(T_{wh} + T_{hw})$, $j=Hi$ indicates all thermodynamic properties are for heating fluid in the heater jacket (in this case heating water, i.e., $j=Hi$ or hw) based on heat loss reactor (i.e. the outer surface of the reactor and heating fluid), η_{wj} is the viscosity of water on the outer/inner wall temperature of the reactor/heating jacket, T_{wh} , and η_j the viscosity of bulk water flowing through the heating jacket. Adequate estimation of T_{wh} is therefore important to ensure accurate prediction or estimation of heat transfer from the heating jacket to the bioreactor, hence T_{wh} is usually computed iteratively. The computation of either wall temperature of a bioreactor can be deduced (if one of the other is known, T_{wh} or T_{wc}) by Equation (7.22n).

$$\frac{Q_{HE}}{\bar{A}} = \frac{k_R (T_{wh} - T_{wc})}{x_R} \quad (7.22n)$$

Where $\bar{A} = \pi \bar{D} h_R$, $\bar{D} = (D_o - D_i) \ln(D_o/D_i)$, and k_R is the logarithmic area, logarithmic diameter, and thermal conductivity of bioreactor material evaluated at its hot (T_{wh}) or cold (T_{wc}) wall temperature depending on which wall temperature reactor is readily available. However, a more rigorous and accurate procedure is the estimation of k_R via the average wall temperature of the bioreactor, $T_w = 0.5(T_{wh} + T_{wc})$.

7.17.4. Computation of heat transfer from heating fluid to environment

Heat flux based on the internal area

The heat flux based on the internal area, $A_{H-i} = \pi D_{H-i} h_R$, of the bioreactor is given as Q_{H-En}/A_{H-i} , expressed in Equation (7.22o) or (7.22p), the overall heat transfer coefficient based on the internal area of the heating jacket, U_{H-Eni} is given by Equation (7.22q).

$$\frac{Q_{H-En}}{A_{H-i}} = U_{H-Eni}(T_{hw} - T_{Air}) \quad (7.22o)$$

$$\frac{Q_{H-En}}{A_{H-i}} = \dot{h}_{Ho}(T_{hw} - T_{H-wh}) \quad (7.22p)$$

$$U_{H-Eni} = \frac{1}{\frac{1}{\dot{h}_{Ho}} + \frac{x_{Ho}}{\dot{k}_{Ho}} \left(\frac{D_{H-i}}{\bar{D}_H} \right) + \frac{1}{\dot{h}_{Air}} \left(\frac{D_{H-i}}{D_{H-o}} \right)} \quad (7.22q)$$

Heat flux based on the external area

The heat flux based on the External area ($A_{H-o} = \pi D_{H-o} h_R$) of the bioreactor is given as Q_{H-En}/A_{H-o} , expressed in Equation (7.22r) or (7.22s), the overall heat transfer coefficient based on the outer area of the heating jacket, U_{H-Eno} is given by Equation (7.22t).

$$\frac{Q_{H-En}}{A_{H-o}} = U_{H-Eno}(T_{hw} - T_{Air}) \quad (7.22r)$$

$$\frac{Q_{H-En}}{A_{H-o}} = \dot{h}_{Air}(T_{H-wc} - T_{Air}) \quad (7.22s)$$

$$U_{H-Eno} = \frac{1}{\frac{1}{\dot{h}_{Air}} + \frac{x_{Ho}}{\dot{k}_{Ho}} \left(\frac{D_{H-o}}{\bar{D}_H} \right) + \frac{1}{\dot{h}_{Ho}} \left(\frac{D_{H-o}}{D_{H-i}} \right)} \quad (7.22t)$$

Where U_{HEN-i} , U_{HEN-o} , x_{Ho} , \dot{k}_{Ho} , D_{H-i} , D_{H-o} , $\bar{D}_H = (D_{H-o} - D_{H-i}) \ln(D_{H-o}/D_{H-i})$, T_{H-wh} , and T_{H-wc} are the inner overall heat coefficient, outer overall heat coefficient, thickness, thermal conductivity, inner diameter, outer diameter, logarithmic mean diameter, hot side wall temperature and cold side wall temperature of the heating jacket respectively. While \dot{h}_{Ho} is the heat transfer coefficient for the heating fluid in the heating jacket due to heat loss to surrounding and \dot{h}_{Air} is the heat transfer coefficient for the environmental air surrounding the bioreactor.

The \dot{h}_{Ho} is computed using Equation (7.22l) – (7.22m) in a similar procedure highlighted earlier, however in this case, the calculation is performed based on thermodynamic properties, $j=Ho$ i.e., properties for heating fluid in heater jacket (in this case water, i.e., $j=Ho$ or hw) based on heat loss surrounding (i.e., the temperature of the heating fluid and that of the surface of heating jacket in contact with the surrounding). Specifically, it is based on wall temperature, T_{H-wh} and film temperature, $T_f = 0.5(T_{H-wh} + T_{hw})$. While \dot{h}_{Air} is computed via Equation (7.22h) – (7.22j), with properties, $j=Air$ i.e., properties for air at wall temperature, T_{H-wc} and $T_f = 0.5(T_{H-wc} + T_{Air})$, as well as the length of the bioreactor, h_R , as its characteristic length, L_c . Furthermore, the computation of either wall temperature of the heating jacket can be deduced (if one of the other is known, T_{H-wh} or T_{H-wc}) by Equation (7.22u). Where, $\bar{A}_H = \pi \bar{D}_H h_R$, \dot{k}_H is the thermal conductivity of the heating jacket material evaluated at either wall temperature, T_{H-wh} or T_{H-wc} depending on which wall temperature is readily available.

$$\frac{Q_{H-En}}{\bar{A}_H} = \frac{k_H(T_{H-wh} - T_{H-wc})}{x_{H_0}} \quad (7.22u)$$

7.18. Experimental analysis of lipid hydrolysis

To deduce the kinetic constant, K_{lipid} , for the hydrolysis of the lipid into substates as introduced in [Equation \(7.4f\)](#), an experimental investigation to describe the reaction quantitatively and qualitatively as a function of temperature is considered. The kinetics model as highlighted earlier will be described using the first-order model. The first-order kinetic model can be modelled as a single-step model in which one kinetic constant is deduced, which is simple and more practical for AD [76]. It can also be modelled as consecutive degradation of tri-, di-, and mono-glycerides into LCFA, following the procedure described by **Moate et al.** [237].

8. Experimental framework – Materials and methods

8.1. Collection and storage of sludge sample

A substantial amount of industrial-activated sludge samples was sourced from a biogas production plant. To enhance the homogeneity of the sludge sample, it was filtered using a 16-mesh size filter. The sample pH (via the Hanna 213 pH meter with CHS FermPro Lab probe), density and other properties were measured as given in Table (8.1). It was then sealed and stored in a refrigerator at 4 °C to minimise its activity [238].

Table 8.1. Average physicochemical properties, and composition of sludge sample

Properties, unit	Results
pH, 19.7°C	7.3200
Density, 20 °C H ₂ O	0.9900
Total suspended solids (TSS), kg.m ⁻³	22.391
Volatile suspended solids (VSS), kg.m ⁻³	13.459
Biochemical oxygen demand (BOD), kg.m ⁻³	1.5700
Chemical oxygen demand (COD), kg.m ⁻³	21.300
Total kjeldahl nitrogen (TKN), kg.m ⁻³	0.5660
Triglyceride, kg.m ⁻³	0.0105
Diglyceride, kg.m ⁻³	0.0102
Monoglyceride, kg.m ⁻³	0.1194
LCFA, kg.m ⁻³	0.0918

8.2. Determination of TSS, and VSS

The total suspended solids (TSS) and volatile suspended solids (VSS) of sludge are essential characteristics of active sludge. The essential characteristic of the sludge sample, such as the total suspended solids (TSS) and volatile suspended solids (VSS), which are good criteria to quantify microbes in the sludge as they exclude soluble solids both organic and “inorganic”, typically the VSS test is better for such purpose as it indicates the organic-solids concentrations [239,240]. The TSS and VSS were measured following APHA standard methods 2540D and 2540E respectively [241,242].

8.3. Determination of BOD, COD, and TKN

The concentration, kg.m⁻³ of the sludge biochemical oxygen demand (BOD), chemical oxygen demand (COD), and Total Kjeldahl Nitrogen (TKN) were respectively determined using the ISO 5815-1 [243,244], and ISO 15705 standards [245,246], and the ISO 11732 ISO 11732 (for NH₄⁺N) standard together with the ISO 13395 (for NO₂⁻-N and NO₃⁻-N).

8.4. Dispersion of lipid sample in sludge

To standardise the procedure of monitoring lipid hydrolysis, a known amount of lipid (specifically, rapeseed oil) is added to the sludge sample. Considering the low solubility and consequently inhomogeneity of lipids in aqueous solutions, the lipid was emulsified and stabilised using xanthan gum, in a similar procedure described by Putra et al [247]. In the presence of a continuous flow of nitrogen, 130 g of stored sludge placed in a beaker was stirred at 2000 rpm in a temperature-controlled stirrer to 25, 30, 35, 45, and 50 °C. At each condition, 0.33 g (i.e., 2.5 kg.m⁻³ of lipid) of lipid was slowly added, while stirring continued for 15 minutes. Furthermore, 0.33 g of xanthan gum powder was slowly added with stirring for another 15 minutes before the process was stopped.

8.5. Setup of the anaerobic hydrolysis system

The prepared oil-sludge emulsion was then transferred to a 250 mL Fisherbrand glass reactor (FB-800-250) and placed in a temperature-controlled water bath (Memmert, WNB 22) with an inbuilt shaking device. The reactor was stirred horizontally at 160 strokes per minute and each temperature (i.e., 25, 30, 35, 45, and 50 °C). Finally, to monitor the hydrolysis kinetics, samples were collected from the reactor periodically (i.e., 0.00, 0.50, 1.00, ..., 24.0 hours) in the presence of nitrogen.

8.6. Analysis of hydrolysed lipid

The qualitative and quantitative analysis of lipid hydrolysis was performed using gas chromatography (GC). In the GC analysis, 0.2 g of samples in duplicate were withdrawn from the reactor periodically. Each sample was mixed with 4 mL propanol, 6 mL hexane solvents, and shaken for 2 hours with a mechanical shaker to extract the lipid as well as its subsidiary component into the solvent. The sample residue after solvent extraction was filtered with a 0.45 μm nylon syringe filter. The filtrate was left to evaporate through laminar airflow and the remaining non-volatile fraction was dissolved in heptane (3 mL). Furthermore, to remove non-lipid components, sodium sulfate solution (3 mL; 7% w/w) was added to the heptane mixture, and vigorously stirred for several seconds, and its aqueous layer was separated by centrifugation at 3500 rpm for 10 minutes. The heptane layer, rich in lipids, was evaporated using laminar airflow. Finally, 0.8 mL of heptane, 0.1 mL of internal standard, and 0.1 mL of BSTFA (derivatisation agent) were added to the resulting sample, before being analysed in duplicate by the GC, as described by Šánek et al. [248].

8.7. Measurement of produced biogas, and methane content

The overall gaseous outlet on a volumetric basis was measured using a simplified volumetric displacement of water from an air-tight sealed water displacement bottle based on the volume of biogas produced, as illustrated in Figures (7.2) and (8.1). Methane content was determined by Fourier-transform infrared spectroscopy (FTIR) technique on a Thermo-Fisher Nicolet iS50 spectrometer equipped with a DTGS KBr detector. A 5 cm long gas cell with BaF₂ windows was used for measurement, the sample was measured with a resolution of 4 cm⁻¹ and 25 scans per sample. The area of the absorption band between 3002-3024 cm⁻¹ was used for quantification. The method was calibrated using calibration gas mixtures supplied by SIAD company as well as in-house prepared gas mixtures. Note that using this developed method, the FTIR could only be used to measure the methane and carbon dioxide content.

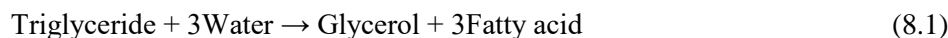


Figure 8.1. Experimental setup utilised for the anaerobic digestion

8.8. Modelling lipid hydrolysis kinetics

The results from the GC analysis, i.e., the dynamics of sample concentration can be modelled into a first-order kinetic model by curve fitting the deduced result. The model can be developed based on triglyceride degradation, or formation of LCFA using the single-step first-order model, or based on consecutive degradation, and formation of Tri-, Di-, Mono-glyceride into LCFA via the multi-step first-order model (i.e., a consecutive model). Developing either of these models is dependent on the ease and availability of data or measurement techniques, however, in this work, the single-step first-order model will be considered.

The reaction kinetics, R_F of the lipid feedstock (i.e., triglyceride = F) in the sludge was investigated using the generic single-step first-order kinetic model, Equation (8.2). In Equation (8.2), it is assumed the rate constants, k_{Lipid} is temperature dependent, as such can be modelled by the 1st term Gaussian model, Equation (8.3) [249,250].



$$R_F = dF/dt = -k_{Lipid}F \quad (8.2)$$

$$k_{Lipid} = k_0 e^{-\left(\frac{T-T_0}{K_T}\right)^2} \quad (8.3)$$

Where $T(K)$ is the reaction temperature, $T_0(K)$ is the reference temperature, $k_0(\text{hr}^{-1})$ is the preexponential factor of the reaction, and $k_T(K^{-1})$ is a temperature constant. Furthermore, considering the report by **Enebu et al.** [250], the single-step curve-fitting method (i.e., fitting Equation (8.1) and (8.3) as one combined equation), as opposed to the multi-step curve-fitting method will be applied to developing the kinetic models. The curve-fitting procedure can be implemented in MATLAB through the Lsqcurvefit function and the ode45 numerical non-stiff solver [251].

8.9. Evaluation of models

The accuracy or evaluation metrics for the proposed kinetic models, as do other curve-fitted models in this work can be checked using R-squared (R^2) value, Equation (8.4). The R^2 value can range from 0 to 1, with values closer to unity indicating a better model fit. Where y is the output, \bar{y} is the mean output of the data set, and \hat{y} is model output.

$$R^2 = 1 - \Sigma(y - \hat{y})^2 / \Sigma(y - \bar{y})^2 \quad (8.4)$$

8.10. Simulation of model

The Equations (7.1) – (7.22) of develop dynamic models as well as analytical/empirical models together with Equation (A.41) – (A.44) were solved using ODE15s (a stiff numerical solver) as well as lsqnonlin function (an iterative estimation of the bioreactor and heating jacketing wall temperature) in MATLAB via data in Table (6.3), (7.1), (7.2), (8.2), (9.1) and (9.2), including the thermochemical properties of components given in Equation (A.1) – (A.38) of the Appendix section.

Table 8.2. Simulation parameters based on laboratory scale, and literature review

Symbols	Description	Values (units)
r_{Ri} and r_{Ro}	Inner and outer radius of Bioreactor (BR)	0.0300 and 0.0307 m
r_{Hi} and r_{Ho}	Hydraulic radius of heating jacket (HJ)	0.01 and 0.0107 m
h_R	Total height of BR=HJ	0.0218 m
h_L	Liquid level in BR	0.082 m
q_{i-L} and q_{o-L}	Inflow and outflow rate of liquid in the BR	0 m ³ .hr ⁻¹
q_{c-L}	pH inflow rate	0 m ³ .hr ⁻¹
g & R	Acceleration due to gravity & Ideal gas constant	9.81m.s ⁻² & 8314 J.kgmol ⁻¹ . K ⁻¹
F	Initial concentration of lipid	2.5385 kg.m ⁻³
B	Initial concentration of microbes	0.01 kg.m ⁻³
M_B	Molecular weight of microbes, C ₅ H ₇ O ₂ N [161]	113
$[Z]$	Molar concentration of artificial ion	0.00035 kgmoles.m ⁻³
$[Z_c]$	pH controller artificial ion	0.000 kgmoles.m ⁻³
T and T_{hw}	Initial temperature of fluid in BR, and HJ	35 and 60 °C
T_{Air}	Environment or surround air temperature	25 °C
Φ_v	Volatile fraction of the feedstock [98]	$\Phi_G = 0.9$ and $\Phi_B = 0.1$
pH	Initial pH of BR	8.23
Y_{cat}	Cation yield from microbes	1.000
i_{pH-j_*}	Ideal inhibition of various biogas species	$i_{pH-j_*} = 1$
pH_{ll}	Lower pH limit for CH ₄ , CO ₂ , and H ₂	6.5, 5.0, and 5.0
pH_{ul}	Upper pH limit for CH ₄ , CO ₂ , and H ₂	7.5, 7.5, and 7.5
$-(\Delta\psi_j^{ovl})$	Chemical potential difference for CH ₄ , CO ₂ , and H ₂	158.084, 75.4238, and 172.7239
$\Delta v_{j\pm} \psi_{j\pm}^{o\pm}$	Summation of chemical ion potentials for HCO ₃ ⁻ and acetic acid	-358.8272, and -267.9815
$(K_L a)_{H_2}$	Hydrogen gas-liquid mass transfer coefficient [181–184]	0.0027 s ⁻¹
K_{d-1} & K_{d-2}	Death rate for microbes of substrates (1) and (2)	$K_d=0.05\mu_{max}$
K_{S_1} & K_{S_2}	Half-saturation coefficient for substrate (1) and (2) [252,253]	3.18 & 1.00 kg.m ⁻³
K_p	Pipe resistance coefficient	0.000001 Pa.m ³ .hr ⁻¹
d_{j_*}	Initial bubble diameter	0.00050 m
ΔH_{AD}	Heat of reaction of the anaerobic	0.0690 kJ.g ⁻¹
N_p	Power number of the bioreactor stirrer	0.309
n_{st}	Stirrer speed	100 rpm
d_{st}	Diameter of stirrer	0.65(2r _{Ri})

* Generically well-known parameters are not given in this table but are found in appropriate sections

9. Results and discussion

9.1. Hydrolysis kinetics

Evaluation of the developed kinetic model with experimental data given in Table (A.3) of the Appendix section, indicates a significant fit as shown in Figure (9.1), and Table (9.1) with an average $R^2 = 0.9895$. The kinetics model reveals the lower temperature regime, i.e., 25 – 30 °C, showed a better fit with 30 °C being the optimal condition. In contrast, the higher temperature regime, i.e., 35 – 50 °C resulted in poorer fit, with 50 °C being the least favourable.

Table 9.1. Estimated parameters and evaluation metrics of hydrolysis model

	Gaussian model constants				
	k_0, h^{-1}	k_T, K^{-1}			T_0, K
	2.5667	20.1518			320.0911
	Temperature, °C				
	25	30	35	45	50
k_{Lipid}, hr^{-1}	0.7717	1.2502	1.7907	2.5392	2.5138
R^2	0.9964	0.9901	0.9912	0.9942	0.9756

The deduced k_{Lipid} indicate that increasing the temperature enhances the rate of hydrolysis, as also reported in literature for both mesophilic (< 40 °C) and thermophilic (55 – 60 °C) AD systems [254,255]. It is well known that as reaction temperature increases, reactant molecules acquire sufficient kinetic energy to overcome the reaction activation energy barrier. Thus, increasing the reaction rate, especially in mass transfer-driven regimes. This principle is however limited in biochemical reactions due to less tolerance of microbes or enzymes to higher temperatures [256].

The result of this work shows that as the temperature increases, the hydrolysis rate increase with the rate more than doubling at 45 °C from 25 °C, also with considerable increase from 30 °C to 25 °C, slight increase from 30 °C to 35 °C and observable decrease from 45 °C as it approaches 50 °C. This observation suggests mass transfer-driven hydrolysis dominates at higher temperature regimes [257], reaching optimum at 45 °C. On further increases in temperature after this point, the benefits of higher thermal energy on the reaction begin to diminish from 45 °C, due to microbial tolerance, as observed at 50 °C.

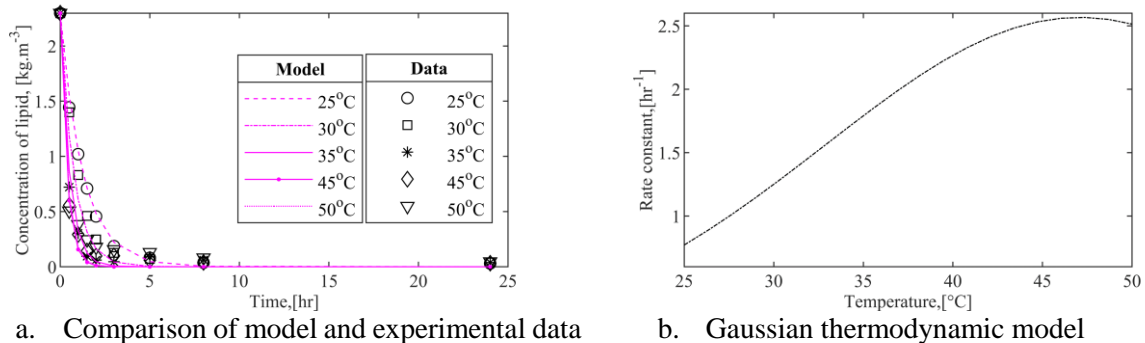


Figure 9.1. Illustration of hydrolysis kinetic, and Gaussian model for lipid degradation

The resulting biogas production for the oil-sludge emulsion at 35 °C beyond the time limit of lipid hydrolysis is also illustrated in Figure (9.2a). The methane and carbon dioxide volumetric content in the

produced biogas were respectively found cumulatively (i.e., at the end of the biogas production process) to be about 62% and 38% using the methodology developed via FTIR.

Furthermore, the Ratkowsky model, Equation (7.5e), was applied to theoretically approximate the maximum microbe specific growth rate, μ_{max} , required for the calculation of the microbe specific growth rate, μ , for the anaerobic digestion (AD) process. The model was curve-fitted based on hypothetical data for LCFA and glycerol, as illustrated in Figure (9.2b) – (9.2c), with parameters, as well as the estimated R^2 values as given in Table (9.2). Based on the R^2 values, the developed model seems adequate with the applied data. Note that these models are applicable within the temperature range of 273 – 333.15 K.

Table 9.2. Ratkowsky constants for estimation of maximum specific growth rate

Substrate/parameter	R^2	$B_1(K^{-1}.h^{-1/2})$	$B_2(K^{-1})$	$T_{min}(K)$	$T_{max}(K)$
LCFA	0.9571	0.0037	0.1331	274.1496	333.3498
Glycerol	0.9525	0.0021	0.1558	273.6860	332.8614

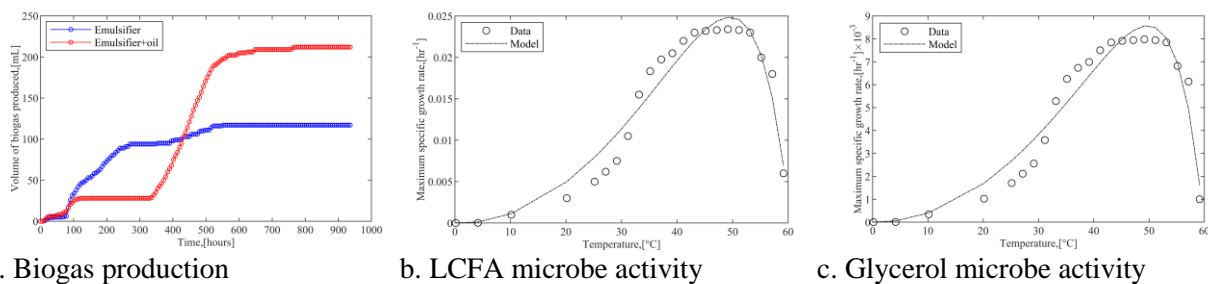


Figure 9.2. Biogas production, and maximum microbe specific growth rate

9.2. Anaerobic digestion simulation

The SSDM was developed such that it could be applied for both the simulation and control of anaerobic digestion. Specifically, the model can be applied to control the pressure, pH, and temperature of the bioreactor by manipulating the bioreactor gas outlet, q_{o-G} , pH control inlet, q_{c-L} , and heating water flowrate, q_{hw} , respectively.

9.2.1. Effect of pressure

To elaborate on the effect of pressure, the developed SSDM model was simulated in MATLAB based on three (3) case studies at 35 °C (i.e., based on heating water flowrate, $q_{hw} = 0.0000000040 \text{ m}^3.s^{-1}$), and negligible pH inhibition. These case studies include Case-study-A(P) (Complete batch system without output of biogas, i.e., overpressure), Case-study-B(P) (Semi-batch system with output of biogas at atmospheric pressure), and Case-study-C(P) (Semi-batch system with output of biogas below atmospheric pressure, typically 30% atmospheric pressure). It is assumed that the bioreactor is initially operated at atmospheric pressure, simulated by Nitrogen as an inert gas i.e., Nitrogen gas is initially present in the bioreactor in an amount equivalent to 101325 Pa of pressure. The inert concentration and corresponding pressure in the headspace are modelled using Equation (7.9f) but with $R_{E-j_*} = 0$, and the ideal gas law equation respectively.

Case-study-A(P)

Case-study-A(P) considers a complete batch system without output of biogas, i.e., $q_{o-G} = 0$. Figure (9.3a) illustrates a slight decrease (i.e., by about 0.26%) in the bioreactor liquid level, mainly due to the formation

of biogas from substrates (LCFA and glycerol), evolution of biogas from the liquid phase, and evaporation of water vapour to the gas headspace.

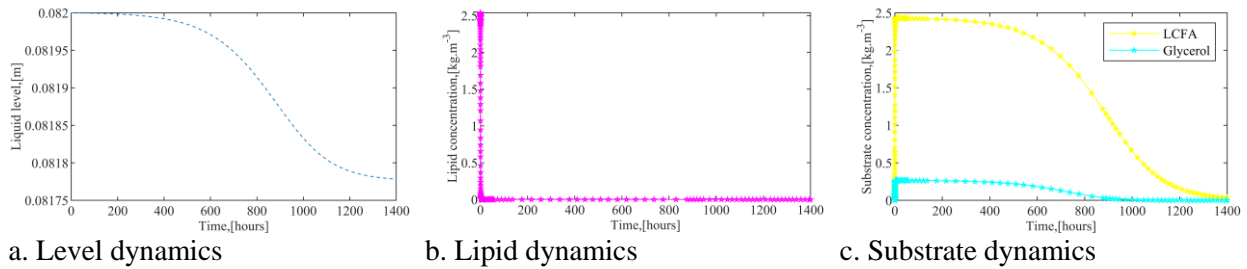


Figure 9.3. Changes in liquid level, lipid, and microbes in the liquid phase (1)

The substrates utilised for biogas formation were a result of the hydrolysis of lipid feedstock, [Figure \(9.3b\)](#). The result shows that the rate of hydrolysis is very fast, i.e., about 2.5 – 5.5 hours for completion of the reaction, [Figure \(9.1a\)](#). This extracellular step of AD is much faster than the intracellular steps which are facilitated by microbe's growth, [Figure \(9.4a\)](#). The resulting substrate formation from the lipid hydrolysis and subsequent utilisation into biogas is illustrated in [Figure \(9.3c\)](#). The result shown in [Figure \(9.3c\)](#) indicates that the amount of glycerol formed is smaller in comparison to the LCFA formed, as such glycerol diminishes faster. This is because for every mole of glycerol formed, three moles of LCFAs are formed alongside based on the molecule of triglyceride (C₅₇H₁₀₄O₆) used to illustrate lipid, as well as the stoichiometry of the reaction, [Equation \(5.1\)](#).

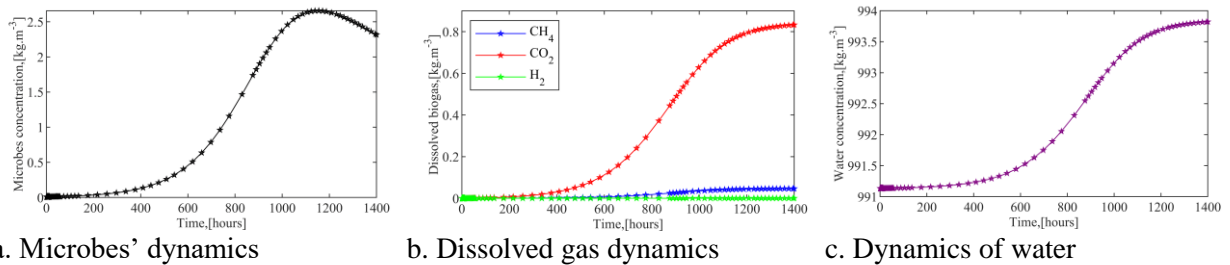


Figure 9.4. Concentration dynamics for microbes, biogas formation and water (1)

Subsequently in the intracellular steps, the substrates being formed are assumed to be transformed into microbe's biomass during the biochemical transformation of substrates to biogas as illustrated by [Figure \(9.4a\)](#). The result shows that microbes will continue to grow provided substrates are present in the system, and as the substrates get depleted, their growth begins to decline, due to the rapid death of microbes.

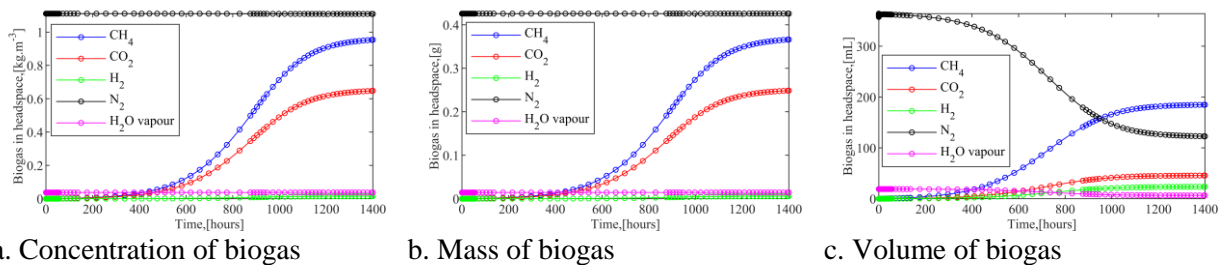


Figure 9.5. Concentration, mass, and volume of biogas obtainable in headspace (1)

* H₂O vapour and H₂O-biogas respectively indicate water vapour and inherent biogas water

The resulting biogas formed, accompanying inert and water vapour present or flowing from the bioreactor are shown in Figure (9.4b) – (9.6c), which comprises the total biogas formed in the AD process. Figure (9.4b) shows the concentration of biogas dissolved in the liquid phase, i.e., the amount of biogas unevolved, and Figure (9.4c) shows the changing concentration of water (i.e., amount of water per liquid volume) predominately present in the liquid phase, because of biogas formation as well as evolution. It is observed that there is an increase in water concentration, due to a decrease in liquid level caused by the evolution of biogas and vapour. As expected, as the nonwatery components are being used or evolve from the liquid phase, the water concentration increases. While Figures (9.5a) – (9.6a) correspondingly indicate the concentration, mass, volume and resulting partial pressure of biogas evolved from the liquid phase to the gas headspace based on the Henry law.

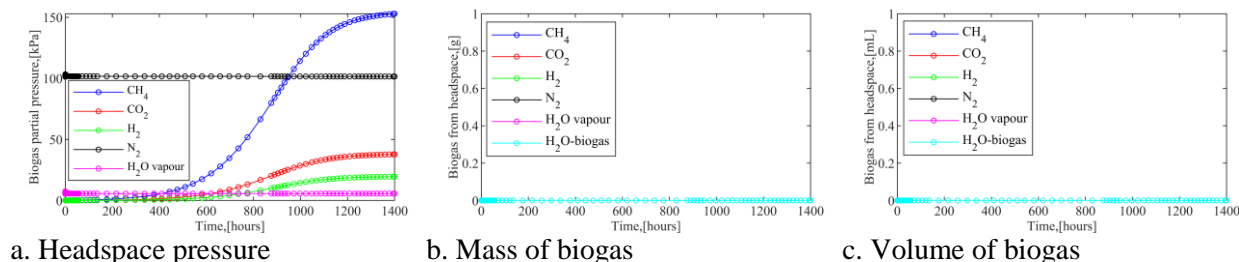


Figure 9.6. Pressure in headspace, mass, and volume of biogas from headspace (1)

The results in Figure (9.4b) show that a higher amount of the carbon dioxide formed remains dissolved in the liquid phase in comparison to methane and hydrogen gas. This is because carbon dioxide is more soluble in aqueous media than the other species. Notwithstanding the fact the theoretical yield of carbon dioxide gas from lipids is also higher than the other species (followed by methane gas with hydrogen gas being the least), Table (6.3). However due to the lower solubility and lighter density of methane gas in comparison to carbon dioxide, more methane gas evolves from the liquid phase to the gas headspace, Figure (9.5a) – (9.6a). Although hydrogen gas has the lowest solubility, and density, as such by following the preceding analogy, one would expect hydrogen gas to be more in the headspace, however, this is contradicted by the very low yield of hydrogen gas.

Furthermore, aside from the biogas species formed other components are accounted for in the gas headspace, Figure (9.5a) – (9.6a). Water vapour that evaporated from the liquid phase is estimated based on saturated water pressure via the prevailing temperature. The amount of water vapour in the headspace is estimable by the ideal gas law, hence the adequacy of the model seems reasonable. The developed model for water vapour formed is particularly novel and can be used to generally estimate the rate of water evaporation or other solvents from their liquid phase in a closed or partially closed vessel. It is expected that as the liquid level decreases due to the evolution of biogas, the corresponding amount of water needed to sustain the saturated water pressure of the bioreactor at its prevailing temperature is carried off the liquid phase to the gas headspace.

Figure (9.6a) shows the corresponding partial pressure of the biogas species (methane, carbon dioxide, and hydrogen), inert gas, and water vapour. Considering that more methane gas is present in the gas headspace, followed by carbon dioxide, and hydrogen, the corresponding pressures are also in this order. However, in addition, water vapour via its saturated pressure also exerts pressure, which is instantaneously estimated from the prevailing temperature of the bioreactor. Therefore, the total pressure on the bioreactor gas headspace is the sum of the biogas species, water-saturated vapour pressure, and as well as the prevailing pressure of the Nitrogen/inert gas. Regarding the inert gas, it can be observed that the initial amount (i.e., concentration, and mass) and pressure of inert gas used to initiate the system remain approximately the same, Figure (9.5a) – (9.5b), and (9.6a). This is because there is no release of gases from the bioreactor.

Therefore, as the biogas species are being formed and evolved from the liquid phase to the gas headspace, their pressure begins to increase, as such based on the volumetric balance of the gas headspace, the initially constant inert gas will undergo compression, Figure (9.5c). Note that the consideration of no outflow of biogas from the bioreactor is also simulated, as shown in Figure (9.6b) – (9.6c) in terms of mass and volumetric balances.

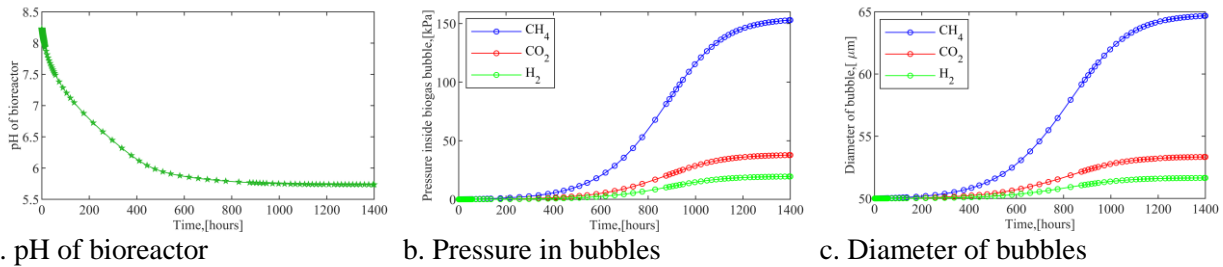


Figure 9.7. pH bioreactor, pressure in bubbles, and diameter of biogas bubbles (1)

Considering that a sustainable amount of carbon dioxide remains in the liquid phase, Figure (9.4b), forming bicarbonate ions, $[\text{HCO}_3^-]$, due to the overpressure on the bioreactor, as such the pH of the bioreactor decreases significantly (i.e., by about 31%), Figure (9.7a). Figure (9.7b) – (9.9a) indicates the dynamics of biogas bubble growth in the liquid phase. In modelling and describing the bubble growth phenomena, it is initially assumed that the biogas bubble grows as a single bubble, Figure (9.7b) – (9.7c), and (9.8c) – (9.9a). However, the probable number of biogas bubbles, Figure (9.8a) – (9.8b) can be estimated based on the probability distribution function model. The result of the bubble distributions shows that the bigger the biogas bubble grows, the tendency of its multiplicity in the liquid phase reduces, assuming no breakage of bubbles occurs. Specifically, the methane and hydrogen, which are the largest and smallest in size respectively have the lowest, and highest number of bubbles respectively.

In estimating biogas bubble growth, the partial pressure inside the bubble (emanating from its centre or originating point) needs to be initially estimated. The result, Figure (9.7b), is similar to that of the partial pressure of biogas species in the headspace, Figure (9.6a). A detailed explanation of this similarity is based on the consideration that the dissolved biogas bubbles, which can be assumed to exist in the interface between the gas and liquid phase, would remain in the interface, as well as continue to grow until biogas production ends, Figure (9.7c), provided biogas does not exit the bioreactor. Therefore, the dissolved biogas bubbles would have similar thermodynamic changes as the biogas in the headspace, hence their similarity.

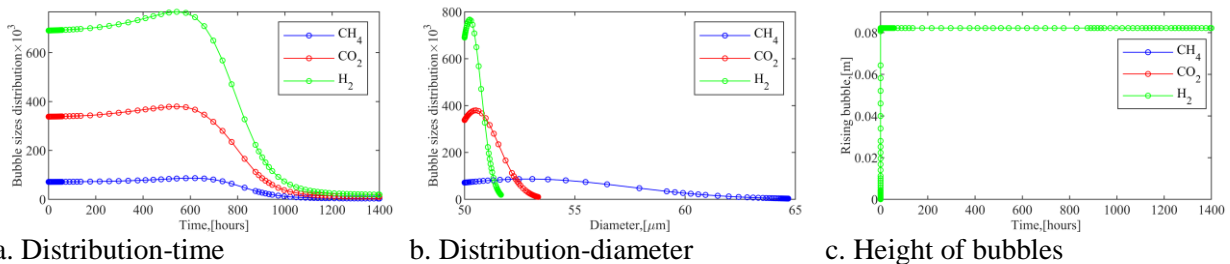


Figure 9.8. Biogas bubbles distribution and its rising height in liquid phase (1)

Furthermore, having deduced the pressure inside the bubbles and pressure in the headspace, the corresponding pressure on the surface of the biogas bubble from its originating point can also be estimated. The surface pressure on the biogas bubble is the summation of the headspace pressure, liquid hydraulic

pressure, as well as pressure due to the resistive effect of interfacial tension between the biogas and liquid solvent. However, because the rise velocity of the biogas bubbles from the liquid phase to the gas headspace is instantaneous as observed in Figure (9.8c), the effect of the liquid hydraulic pressure on the bubbles is also instantaneous and almost negligible. Furthermore, because the pressure due to the interfacial effect is much smaller than the headspace pressure due to no outlet of biogas from the bioreactor, the pressure on individual biogas bubble surfaces is there same as the headspace pressure, as such approximately the same for all biogas species, Figure (9.9a).

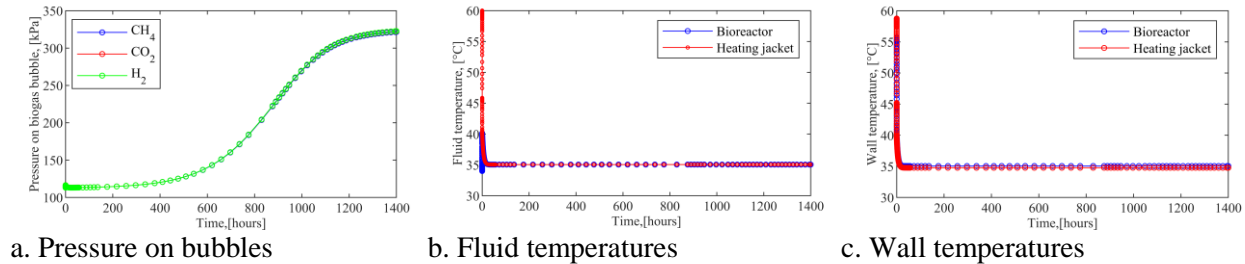


Figure 9.9. Bubbles surface pressure, fluid, and wall temperature of reaction system (1)

Figure (9.9b) – (9.9c), shows the resulting fluid and wall temperature. The heating fluid or water was fed at a specific flow rate such that the fluid temperature of the bioreactor is regulated to 35 °C, as required for this study, Figure (9.9b). This attained temperature is made possible, by the temperature equilibrium between the bioreactor content and heating fluid. Furthermore, it can be observed that the heat of the reaction, vapourisation of water, and input energy of stirring, are negligible to the heat energy supplied by the heating fluid. The resulting wall temperature of the bioreactor, and heating jacket, which were iteratively computed are well within the limit of the bioreactor reactor, suggestive of the accuracy of the result. Also, Figure (9.9c) shows that the bioreactor wall temperature is slightly higher than the heating jacket temperature. This is because the bioreactor is enclosed around its curve surface area by the heating jacket, Figure (7.4), as such the heating jacket wall is exposed to the prevailing ambient or surrounding temperature (assumed as 25 °C), and therefore loses heat to the surrounding.

Case-study-B(P)

Case-study-B(P) is a semi-batch reactor, whose biogas outflow, q_{o-G} , is regulated by the total pressure of the gas headspace as given by Equation (7.16). The bioreactor is assumed to operate at atmospheric pressure like the experimental condition considered in this work. Biogas is discharged from the bioreactor once the total pressure in the gas headspace minutely exceeds atmospheric pressure (i.e., 101325 Pa).

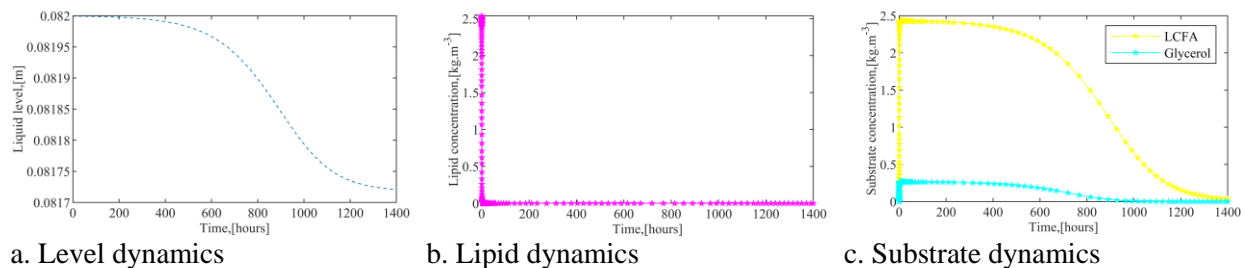
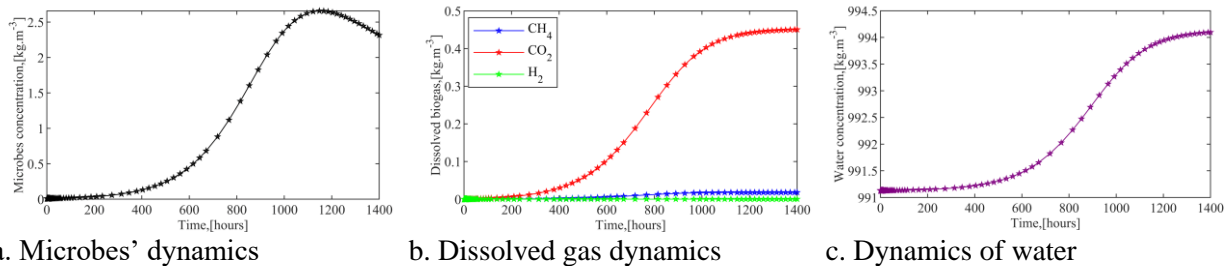


Figure 9.10. Changes in liquid level, lipid, and microbes in the liquid phase (2)

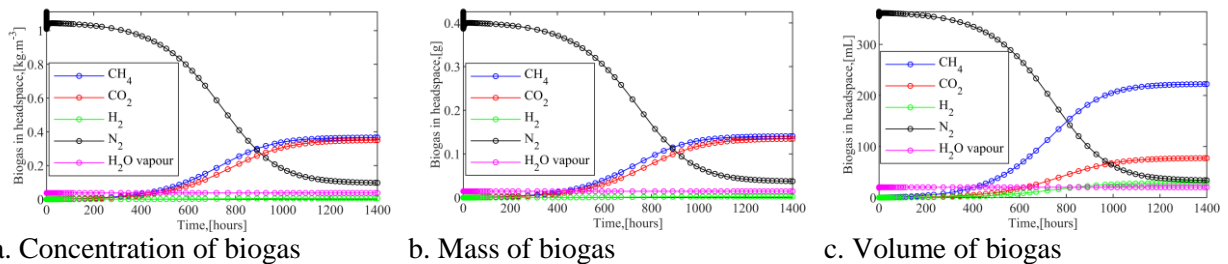
While Figure (9.10a) – (9.11c), in this case study, is identical to that of Case-study-A(P). In this case study, the liquid level (i.e., decreased by 0.34%), Figure (9.10a) and concentration of dissolved biogas species, Figure (9.11b), are however more depleted. This is due to the continuous outflow of biogas from the

bioreactor to maintain the atmospheric operating pressure of the bioreactor. In Figure (9.11c), It can be observed that the water concentration increased more than in Case-study-A(P), Figure (9.4b), due to more decrease in liquid level caused by evolution, and outflow of biogas, water vapour, as well as accompanying water content from the bioreactor. Although the gas outlet is opened, it would have been expected that the concentration would decrease, however, this is not so in this case, because the influence due to the decrease in liquid level is significantly more than the influence caused by the outflow of water vapour and inherent water content accompanying the biogas leaving the system.



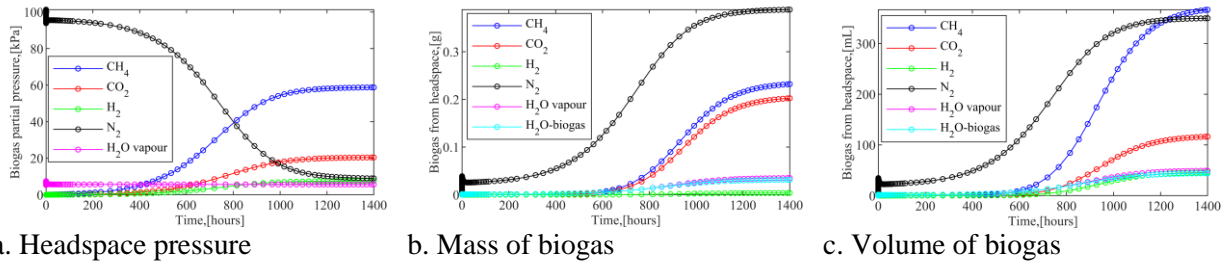
a. Microbes' dynamics b. Dissolved gas dynamics c. Dynamics of water
Figure 9.11. Concentration dynamics for microbes, biogas formation and water (2)

Considering that the required operating pressure of this case study is lower than that of Case-study-A(P), the solubility of carbon dioxide in the liquid phase is reduced following Henry's law, and as such enhance the evolution of more carbon dioxide to the gas headspace. This explains why the carbon dioxide content, Figure (9.11b), unlike the other biogas species is significantly lower, i.e., ~44% lower than Case-study-A(P), Figure (9.4b). Furthermore, the reason why the methane and carbon dioxide contents on a mass basis in the gas headspace are almost the same, Figure (9.12a) – (9.12b) unlike that of Case-study-A(P), Figure (9.5a) – (9.5b). However, due to the lower molecular weight/density of methane in comparison to carbon dioxide, the volumetric amount of methane gas in the headspace is higher than that of carbon dioxide, Figure (9.12c), following the ideal gas law.



a. Concentration of biogas b. Mass of biogas c. Volume of biogas
Figure 9.12. Concentration, mass, and volume of biogas obtainable in headspace (2)

Based on the volumetric balance of the biogas species in the headspace, their resulting partial pressures are also simultaneously deduced accordingly. However, considering that in this case the bioreactor is operated at lower pressure, the partial pressures of the biogas species, Figure (9.13a), are considerably lower than for Case-study-A(P), Figure (9.6a). Although it can be observed that the partial pressure of water vapour is the same. This is because the saturated pressure of water is dependent mainly on the temperature of the bioreactor, as well as instantaneously deduced.

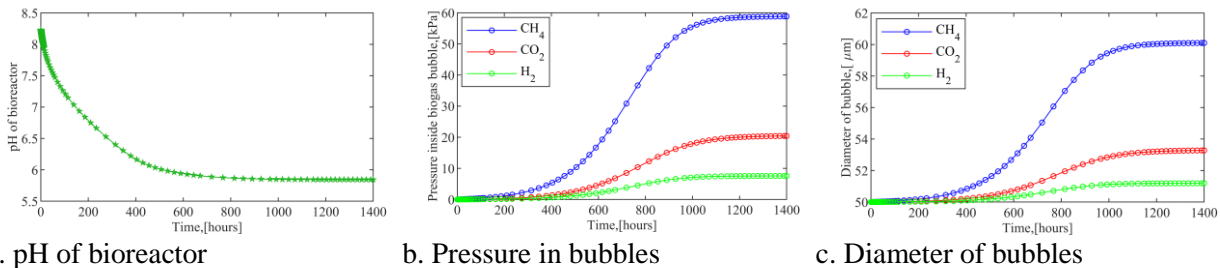


a. Headspace pressure b. Mass of biogas c. Volume of biogas
Figure 9.13. Pressure in headspace, mass, and volume of biogas from headspace (2)

The resulting outflow of biogas species and other components that are released from the bioreactor to ensure the bioreactor remains at atmospheric pressure are illustrated in Figure (9.13b) – (9.13c). And as expected, based on the volumetric balance, Figure (9.13b), more methane is released from the bioreactor than other biogas species.

Furthermore, the inherent biogas water content, Figure (9.13b) – (9.13c), is approximately estimated from the thermodynamics of water-hydrocarbon phase equilibrium. Note that the biogas water content is assumed as well as calculated to not be inclusive of the amount of water vapour. However, in terms of its mechanism of formation, it is assumed to be formed from an intermediary water vapour medium, that is formed from the water liquid phase. The estimated biogas water content (~10v/v%), is within reasonable limit of the raw biogas water content reported (5 – 10 v/v %) [172,258,259]. Therefore, suggestive of the adequacy of this simulated estimation.

Considering the Nitrogen/inert gas, which is used to initiate the atmospheric pressure of the system, on the opening of the biogas outlet, it is expected that there will be an instantaneous decrease in its amount, as well as its pressure due to the instantaneous effect of saturated water vapour pressure on the gas headspace, Figure (9.12a) – (9.13a). The unsteady changes in the inert gas amount and pressure, apart from the instantaneous effect of the saturated water vapour pressure influenced by the initial changes in system temperature (i.e., increase of initial temperature from 34 to 45 and then to 35 °C), Figure (9.16b). Furthermore, as biogas is being produced, the inert gas will also be gradually released from the bioreactor, Figure (9.13b) – (9.13c). Consequently, being also reduced in the headspace, Figure (9.12a) – (9.13a).



a. pH of bioreactor b. Pressure in bubbles c. Diameter of bubbles
Figure 9.14. pH bioreactor, pressure in bubbles, and diameter of biogas bubbles (2)

Operating the bioreactor at a lower pressure in this case study, causes a slight increase in its pH, Figure (9.14a). Specifically, the pH decreases from its initial condition by ~29%, i.e., 2% less than Case-study-A(P). This implies the reduction of pressure in this case study causes only a slight increase in the pH of the system, due to a lesser amount of dissolved carbon dioxide in the liquid phase. Furthermore, regarding the growth of biogas bubble, there is an observable reduction of biogas bubble sizes, and consequently the bubble size distribution increase, Figure (9.14c) – (9.15b), in comparison to Case-study-B(P), Figure (9.7c) – (9.8b).

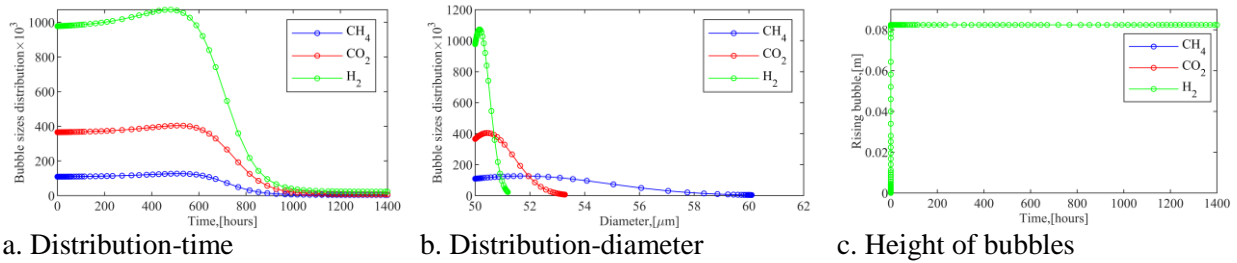


Figure 9.15. Biogas bubbles distribution and its rising height in liquid phase (2)

Furthermore, the pressure inside the biogas bubbles as assumed for the previous case study rises to and grows at the interface of the gas-liquid phase. This growth continues provided biogas is being formed, however considering that in the cases study biogas is also being released from the bioreactor. It implies that it can be assumed that during the outflow of biogas, portions of the bubbles will break off, and flow away from the source or assumed single originating bubbles of each biogas species. This explains why the bubble pressure is lower in this case, Figure (9.14b) than in Case-study-A(P), Figure (9.7a). Also, the assumption that the bubble grows at the interface, may explain why the bubble pressure of each biogas species is similar to that of the partial pressure of the biogas species in the headspace, Figure (9.14b) and (9.13a).

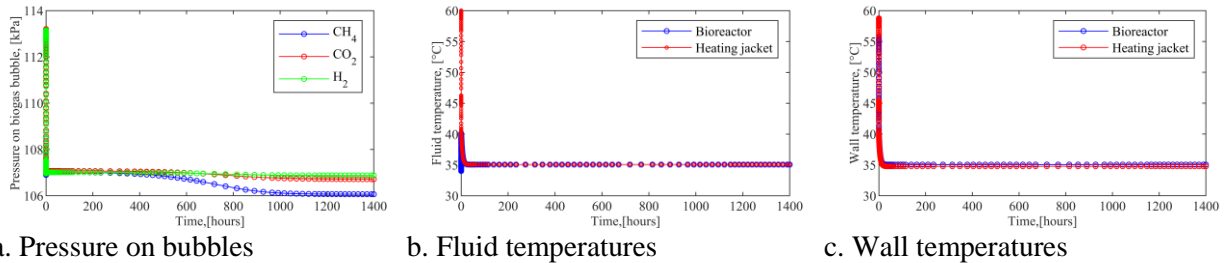


Figure 9.16. Bubbles surface pressure, fluid, and wall temperature of reaction system (2)

The pressure on the biogas bubble surface as observed in Case-study-A(P), is also within the limit of the headspace pressure in this case study. However, in this case, it can be observed that there is a slight dispersity among the biogas species, Figure (9.16a). This is because the operating atmospheric pressure on the headspace is not high enough to significantly make the pressure due to the interfacial effect negligible. The pressure due to interfacial tension is particularly more observable in methane gas than in the other biogas species. Considering that the methane bubble diameter is higher than the other biogas species, Figure (9.14c), and that the interfacial pressure is inversely proportional to the bubble diameter. It, therefore, implies that the reason for the higher pressure on the methane bubble is due to methane having a higher interfacial tension with water than the other biogas species.

Finally, from the result of fluid and wall temperature, Figure (9.16b) – (9.16c) of the bioreaction system. It is observed that there is no difference between this case study and that of Case-study-A(P), hence the effect of pressure on the temperature of the system is negligible.

Case-study C(P)

Case-study-C(P) is also a semi-batch reactor, whose biogas outflow, q_{o-G} , is regulated by the total pressure of the gas headspace. However, in this case, the bioreactor is assumed to operate at some vacuum, specifically 30% atmospheric pressure. Although this case study might not be practicable commercially, and expensive to operate, the essence of this simulation is to evaluate the robustness of the model, as well as further elucidate the effect of pressure.

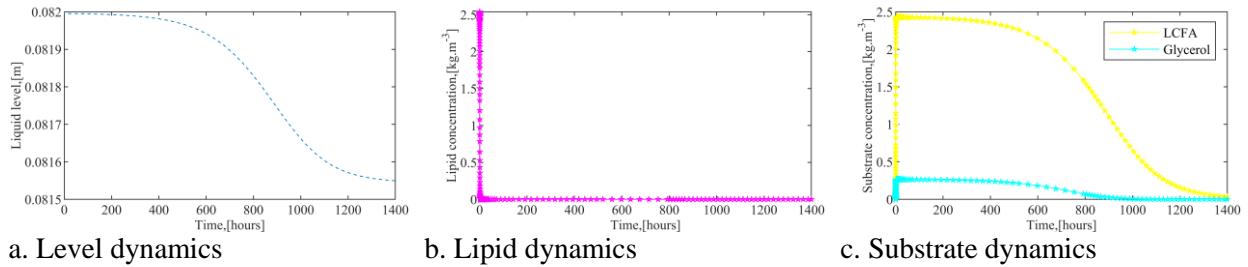


Figure 9.17. Changes in liquid level, lipid, and microbes in the liquid phase (3)

While Figure (9.17a) – (9.18c), in this case study is also similar to that of Case-study-B(P). The liquid level (i.e., decreased by ~ 0.54%), Figure (9.17a) and concentration of dissolved biogas species (only ~ 0.14 kg.m⁻³ CO₂ is in the liquid phase), Figure (9.18b), are more depleted than in the other case studies. This is due to the larger continuous outflow of biogas from the bioreactor caused by the lower operating pressure of the bioreactor. Also, Figure (9.18c), indicates that the water concentration increased to ~ 993.1 kg.m⁻³, which is lesser than the other case studies. This is significantly due to more loss of water from the outflow of water vapour and inherent biogas water content, as such counteracting the effect of decreasing liquid level or volume (caused by the release of all vapour, and gaseous component from the bioreactor), which due have increased the concentration of water in the liquid phase.

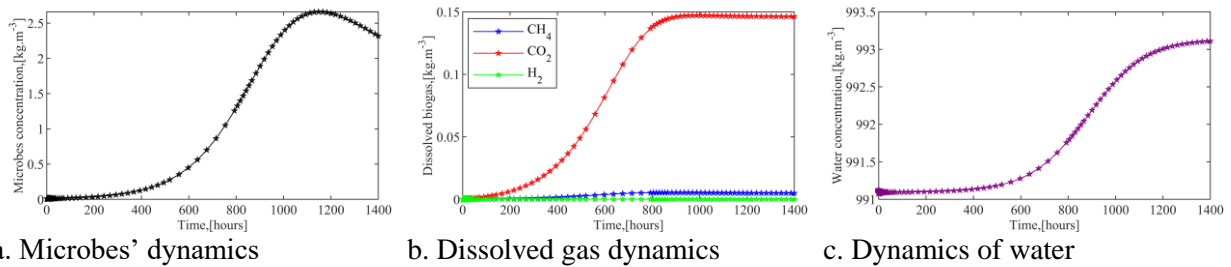


Figure 9.18. Concentration dynamics for microbes, biogas formation and water (3)

As stated earlier, following Henry's law, the lower operating pressure in this case study greatly reduced the solubility of carbon dioxide, to the extent that its amount exceeded that of methane, Figure (9.19a) – (9.19b). However, due to the relative lightness of methane gas, it is present more on a volumetric basis than carbon dioxide, Figure (9.19c).

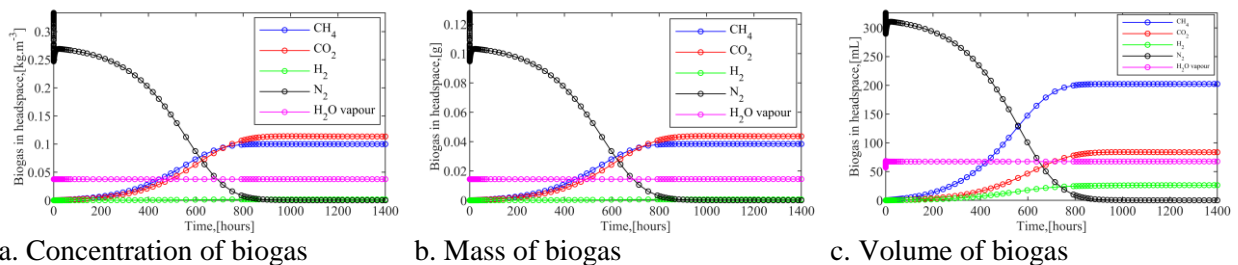


Figure 9.19. Concentration, mass, and volume of biogas obtainable in headspace (3)

Considering the higher volume ratio of methane in the gas headspace, it implies that methane would exert higher pressure than the other components, Figure (9.20a). Figure (9.20b) – (9.20c), shows the outflow of gaseous and vapour species from the bioreactor gas outlet. In this case, as opposed to previous case studies more water accompanies the biogas from the reactor, and the outlet is comprised of a high amount of water

(i.e., ~ 30 v/v% water content, and ~ 12 v/v% water vapour). A possible explanation for this high-biogas water content and water vapour is due to lower headspace pressure on the liquid phase. This causes less exertion on the vapourisation of water vapour, according to Equation (7.13a). However, considering the limited practicality of this case study, this result should be subjected to experimental validation.

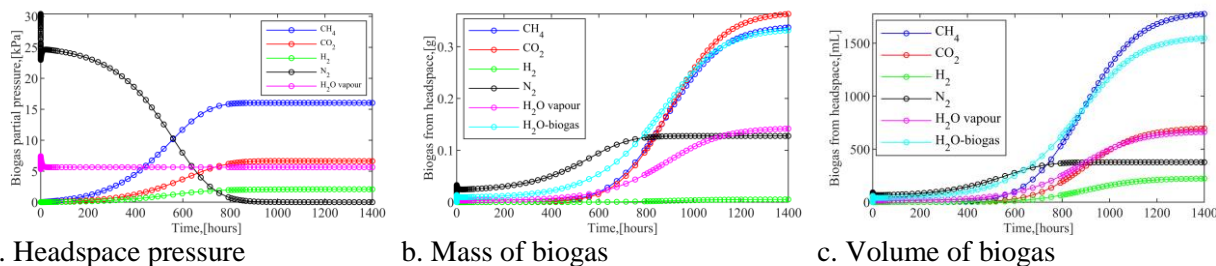


Figure 9.20. Pressure in headspace, mass, and volume of biogas from headspace (3)

The pH in this case study, Figure (9.21a), in comparison to other cases, is expectedly higher (with a decrease from its initial condition by ~27%), as there is a lesser amount of dissolved carbon dioxide in the liquid phase, caused by its lesser solubility at the lower operating pressure.

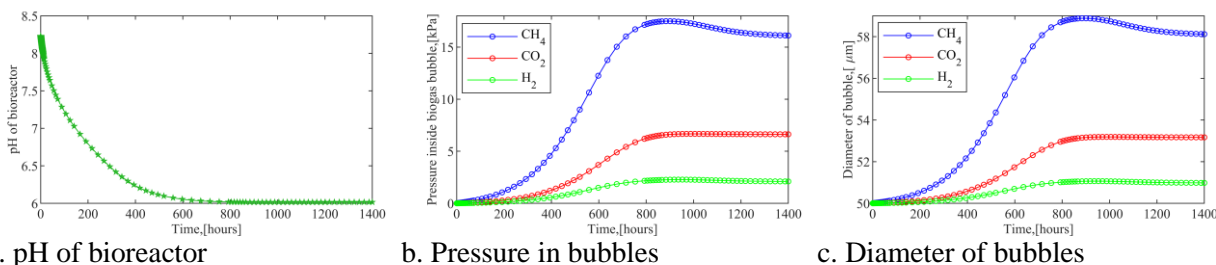


Figure 9.21. pH bioreactor, pressure in bubbles, and diameter of biogas bubbles (3)

Regarding the pressure inside the biogas bubbles, and their diameter, in Figure (9.21b) – (9.21c), the pressure inside the bubble seems to be more significantly influenced by the rapid breakage of bubbles due to the lower operating pressure of the bioreactor. Therefore, the sizes of the biogas bubbles are smaller in this case, than other case studies, Figure (9.21c). This further explains, the larger bubble size distribution of the biogas species, Figure (9.22a) – (9.22b), than in Case-study-A(P). However, the lower operating pressure in this case study seems to have caused a slightly lesser bubble size distribution than in Case-study-B(P). This may be due to the operating pressure being attained faster in this case study.

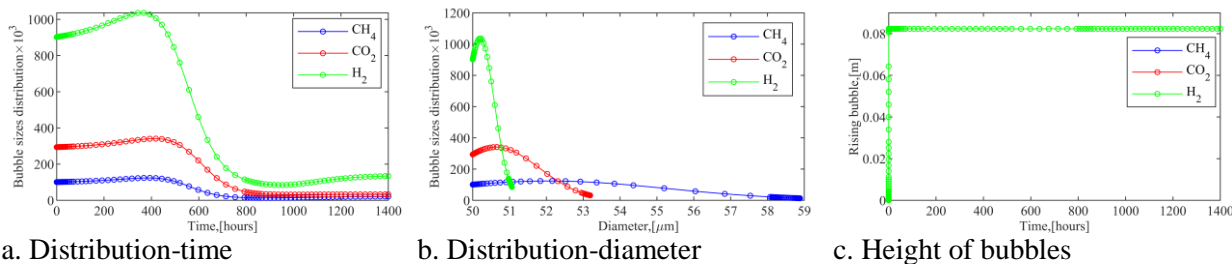


Figure 9.22. Biogas bubbles distribution and its rising height in liquid phase (3)

The pressure inside the biogas bubble species, [Figure \(9.21b\)](#), at the interface of the gas-liquid phase, also shows proximity with the headspace pressure of each biogas species, [Figure \(9.20a\)](#). Furthermore, regarding the pressure on the biogas bubbles, as observed in Case-study-B(P), it is also significantly influenced by the headspace pressure, and the interfacial pressure of each biogas species, [Figure \(9.23a\)](#). Furthermore, the fluid and wall temperature, [Figure \(9.23b\) – \(9.23c\)](#) of the bioreactor, like the previous case studies, is not influenced by the effect of pressure.

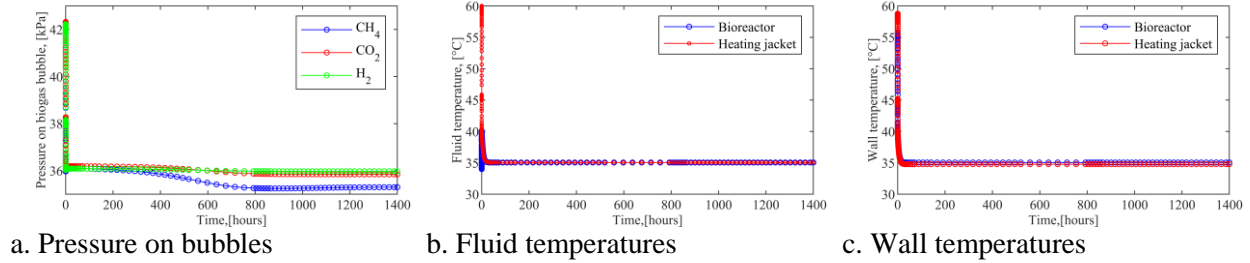


Figure 9.23. Bubbles surface pressure, fluid, and wall temperature of reaction system (3)

In summary of the effect of pressure on AD, it can be inferred that operating the AD process at higher pressure enhances the solubility of the carbon dioxide in the liquid phase. Thus, resulting in a higher proportion of methane gas in the headspace, but at the expense of lowering the pH of the system due to higher dissolved carbon dioxide. In turn, lower pH can also result in the inhibition of methane production, as would be discussed in the proceeding section. Regarding biogas bubble growth, higher pressure leads to larger biogas bubbles, which correspondingly limit the bubble size distribution in the system. Furthermore, operating the bioreactor as a semi-batch process with reduced operating pressure enhances biogas production, as well as the release of more biogas from the bioreactor.

9.2.2. Effect of pH inhibition

Considering that the Case-study-B(P) is the exact experimental condition applied in this work, therefore its conditions (i.e., 35 °C, and 101325 Pa) would be used to illustrate the effect of pH inhibition on the AD process.

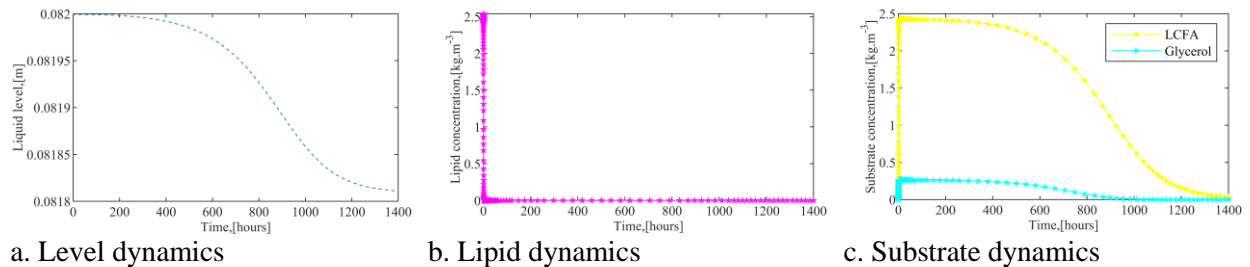


Figure 9.24. Changes in liquid level, lipid, and microbes in the liquid phase (4)

Typically, from [Equation \(7.7d\)](#), and [\(7.7e\)](#), it is expected that consideration of pH inhibition will limit the reaction completion or conversion from the substrate into the various biogas species. Therefore, it is expected that less amount of biogas will be produced. This explains why the liquid level is less depleted (~0.22%) in this case study than in Case-study-B(P). This is because if the biogas production is hindered, it would also result in little or no evolution of biogas from the liquid phase to the headspace, thus a resulting in minute decrease in liquid level. This higher liquid level also explains why the water concentration is lower in this case study (i.e., ~ 993.2 kg.m⁻³) than in Case-study-B(P) (i.e., ~ 994.1 kg.m⁻³). Considering

that lipid, substrate, and microbes are not affected by the pH inhibition, their results, Figure (9.24b) – (9.25a), are exactly same as Case-study-B(P).

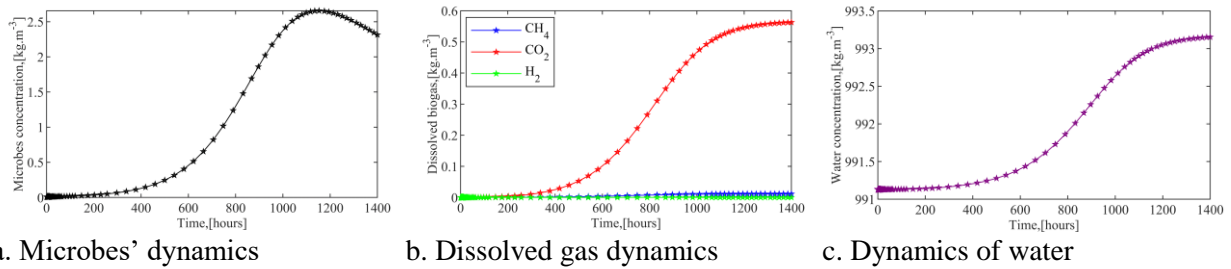


Figure 9.25. Concentration dynamics for microbes, biogas formation and water (4)

Regarding dissolved biogas in the liquid phase, Figure (9.25b), it can be observed that more carbon dioxide is in the liquid than in Case-study-B(P). It would have been expected that since the reaction did not proceed to completion, a lesser amount of carbon dioxide would be present. However, this is not so, because methane is inhibited more than carbon dioxide, as such more carbon dioxide is produced as well as evolves more into the gas headspace, Figure (9.26a) – (9.26b) than in Case-study-B(P) as such exerted more partial pressure, Figure (9.27a). And following Henry's law, a lesser amount of carbon dioxide would evolve into the headspace with higher partial pressure.

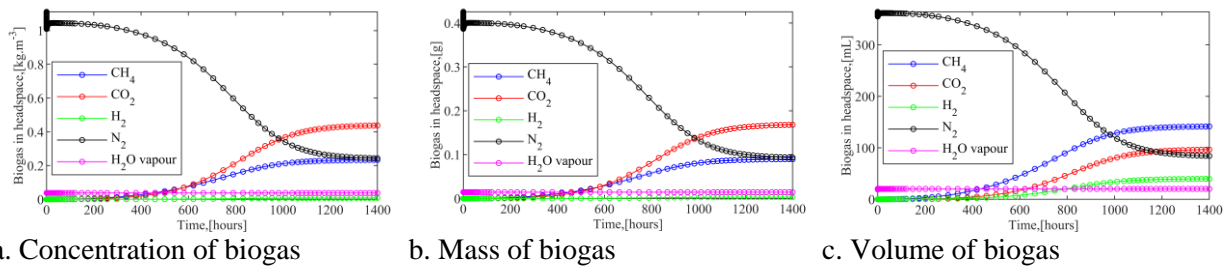


Figure 9.26. Concentration, mass, and volume of biogas obtainable in headspace (4)

Furthermore, as observed in previous case studies, the volumetric balance of methane is also higher than carbon dioxide, Figure (9.26c) because methane is considerably lighter than carbon dioxide. And according to the Ideal gas law also explains why the partial pressure of methane is higher than that of carbon dioxide, Figure (9.27a).

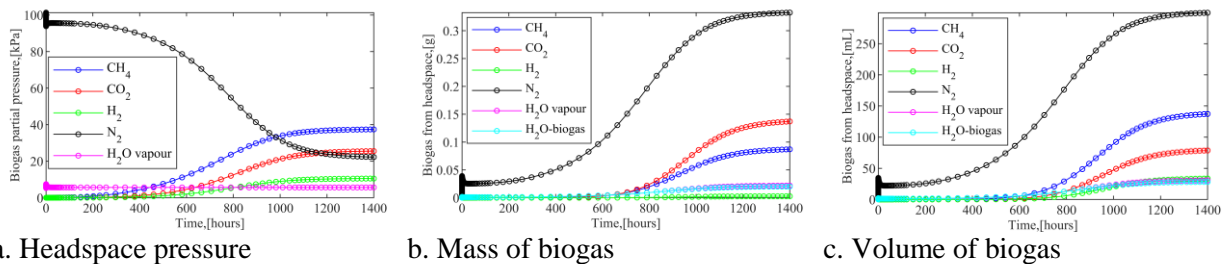


Figure 9.27. Pressure in headspace, mass, and volume of biogas from headspace (4)

Consequent to the higher production of carbon dioxide than methane, due to its lesser pH inhibition explains why more carbon dioxide is released from the gas outlet than methane on a mass basis, Figure (9.27b) as

opposed to Case-study-B(P). However, on a volumetric basis more methane is released, [Figure \(9.27c\)](#), due to its lesser molecular weight.

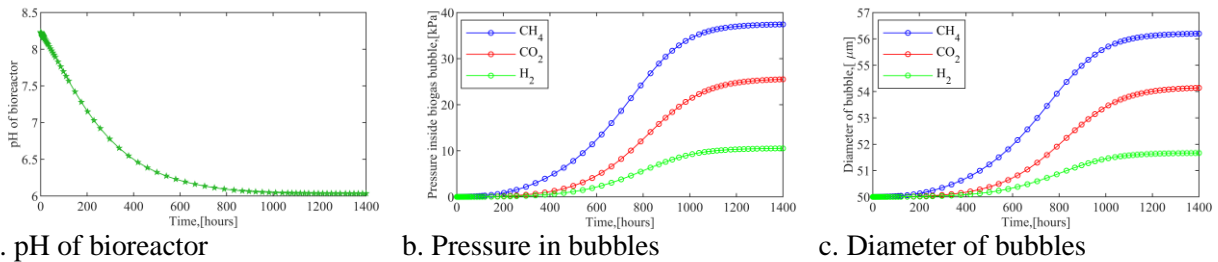


Figure 9.28. pH bioreactor, pressure in bubbles, and diameter of biogas bubbles (4)

The pH of the bioreactor, [Figure \(9.28a\)](#), is higher (i.e., decreased by ~ 27%) than Case-study-B(P). This is mainly due to the limitation of the reaction, rather than the amount of carbon dioxide dissolved in the liquid phase. It can be thought that the limited reaction, causes more formation of other ions, thus limiting the amount of bicarbonate ions, [HCO₃⁻] formed, [Equation \(7.17a\)](#).

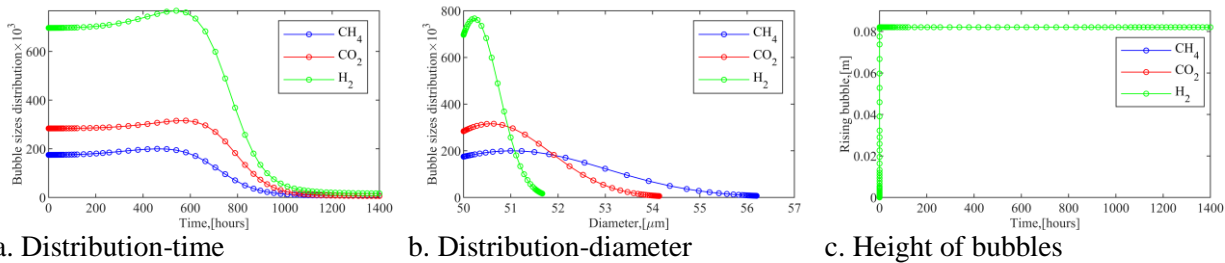


Figure 9.29. Biogas bubbles distribution and its rising height in liquid phase (4)

Furthermore, similar to other cases, in this case study the biogas bubble evolves instantaneously to the interface of the gas-liquid phase, [Figure \(9.29c\)](#). The biogas bubble pressure and diameter are expectedly smaller, [Figure \(9.28b\) – \(9.28c\)](#) than in Case-study-B(P), due to the lesser amount of biogas formed. This also explains why the bubble size distribution are also smaller in comparison to [Case-study-B\(P\)](#).

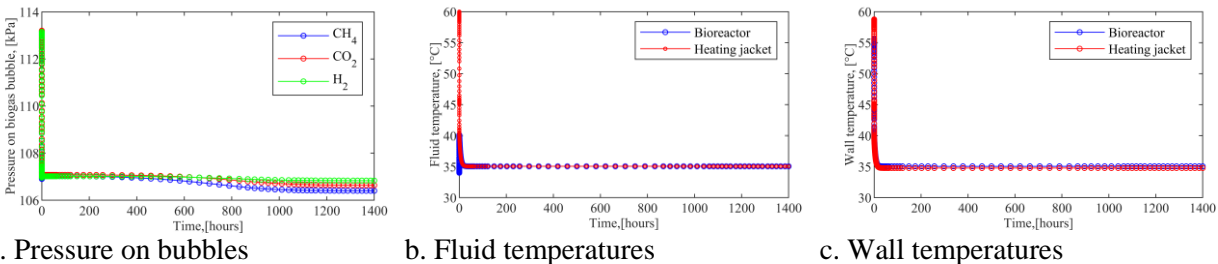


Figure 9.30. Bubbles surface pressure, fluid, and wall temperature of reaction system (4)

The pressure on the biogas bubbles is approximately closer to the headspace pressure as observed in Case-study-B(P), however in this case due to the smaller diameter of the bubbles, the effect of the interfacial pressure of each biogas species is less obvious, [Figure \(9.30a\)](#), than in Case-study-B(P). Finally, the fluid and wall temperature, [Figure \(9.30b\) – \(9.30c\)](#) are not influenced by pH inhibition.

This case study is more realistic, and closely simulates the experimental condition highlighted in [Figures \(7.2\) and \(8.1\)](#) as well as the result given in [Figure \(9.2a\)](#). Therefore, by comparing the amount of biogas

produced experimentally (230 mL) to that simulated in this case study (575 mL). It can be observed that the simulation produced about 2.7 times the amount of biogas produced experimentally. This implies that the anaerobic digestion process proceeded only by about 40%, which is not too far off the reported percentage conversion of AD, i.e., about 49.97% [260].

In summary, regarding the pH inhibition, considering that methanogenesis operates at higher pH conditions (i.e., close to neutral pH). Methane production is, therefore, more inhibited in the bioreactor, especially since the simulated pH is between 5.6 – 6.0 approximately. Therefore, with the limitation of biogas production, the biogas bubble growth as well as its size distribution is limited. In retrospect, while increasing the operating pressure limit the evolution of carbon dioxide, it also results in lowering the pH of the system. Which in turn limits methane production. It is expected that increasing the pH until the maximum allowable limit (i.e., 7.5) would enhance the production of biogas in general, thus increasing the biogas bubble size, and reducing the bubble size distribution. However, decreasing the pH below 6.5 (i.e., the minimum allowable limit for methanogenesis) would limit methane production, as well as carbon dioxide and hydrogen gas for pH below 5.0 (i.e., the minimum allowable limit for acidogenesis and acetogenesis).

9.2.3. Effect of temperature

Case-study-A(T)

This case study focuses on applying atmospheric pressure to investigate the effect of temperature on the AD process, the conditions of Case-study-B(P) are applied based on the reasons highlighted earlier. To increase the temperature of the bioreactor, the flow rate of the heating water into the heating jacket is increased. Specifically, the temperature of the system is increased to 45 °C (i.e., based on heating water flowrate, $q_{hw} = 0.000000158 \text{ m}^3 \cdot \text{s}^{-1}$), as shown in Figure (9.37b) – (9.37c) with the corresponding wall temperatures.

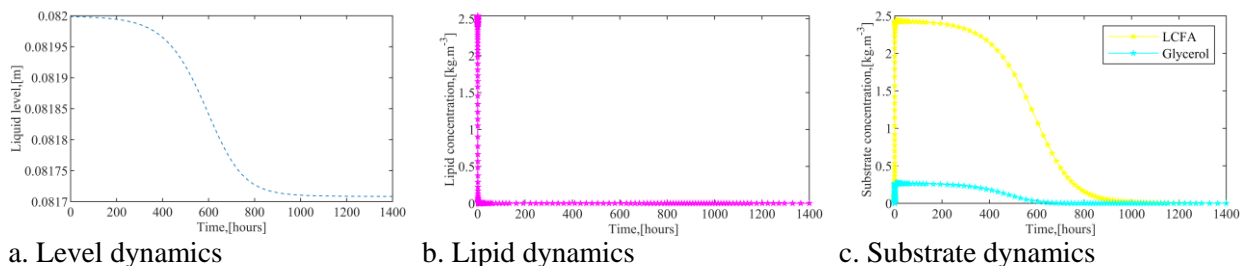
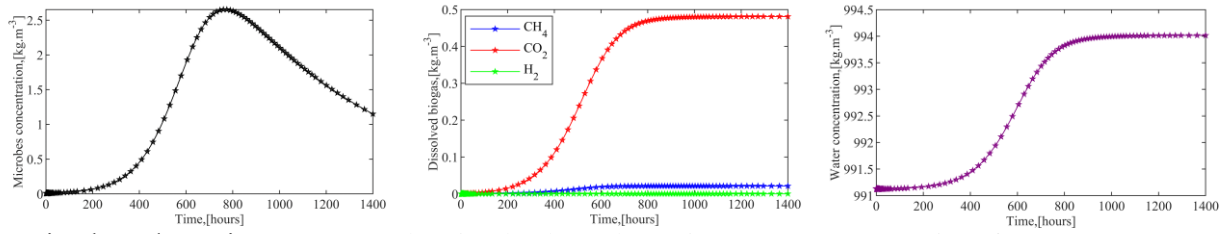


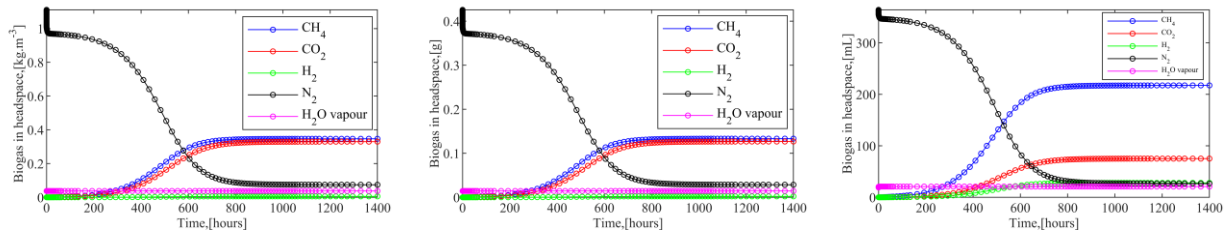
Figure 9.31. Changes in liquid level, lipid, and microbes in the liquid phase (5)

It can be observed that operating the AD process at higher temperatures, primarily increased the rate of reaction. This is evident in the result for microbe growth, and dissolve biogas, Figure (9.32a) – (9.32b). Specifically, it can be observed that microbes reached their maximum concentration quickly at about 800 hours, as well as depleting very quickly, afterwards. It is this fast microbe activity that explains the reaction speed. This fast reaction rate is also evident in all results, especially in Figure (9.32b) – (9.34c), considering that all estimated components, or parameters plateaus (which signifies no further changes) at lesser time than Case-study-B(P). This is also observable for the result of liquid level, Figure (9.31c), as well as for substrate utilisation, Figure (9.31b), but not clearly obvious for lipid degradation, Figure (9.31b), because of its faster reaction rate.



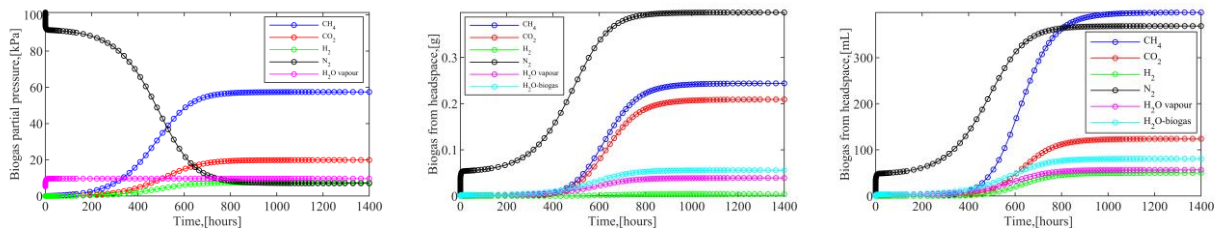
a. Microbes' dynamics b. Dissolved gas dynamics c. Dynamics of water
Figure 9.32. Concentration dynamics for microbes, biogas formation and water (5)

The amount of carbon dioxide remaining in the liquid phase, as well as water concentration, [Figure \(9.32b\)](#) and [\(9.32c\)](#), is higher in this case study than in Case-study-B(P). This is because of the accelerated reaction rate due to increased temperature. This is also applicable to the components in the headspace, [Figure \(9.33a\)](#) – [\(9.34a\)](#). The obvious difference between these results and that of Case-study-B(P) is the speed at which the estimated components or parameters reach their peak.



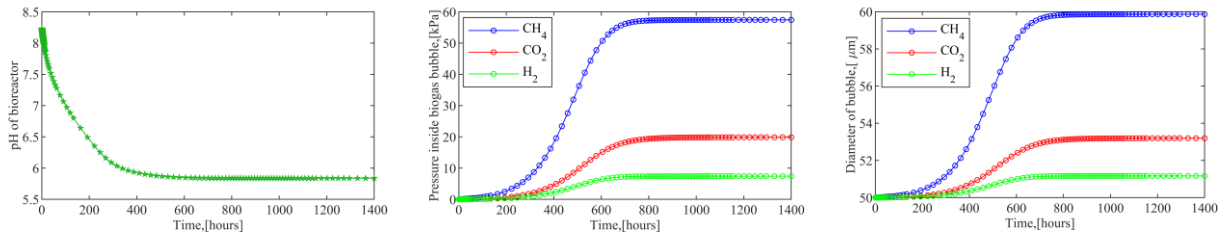
a. Concentration of biogas b. Mass of biogas c. Volume of biogas
Figure 9.33. Concentration, mass, and volume of biogas obtainable in headspace (5)

Regarding the estimated biogas water content, the value is higher than in Case-study-B(P), as well as higher than the estimated saturated water vapour, [Figure \(9.34b\)](#) – [\(9.34c\)](#). The reason for this could be attributed to the fact that higher temperature facilitates the vapourisation of water, as such more water is released with the biogas as water content.



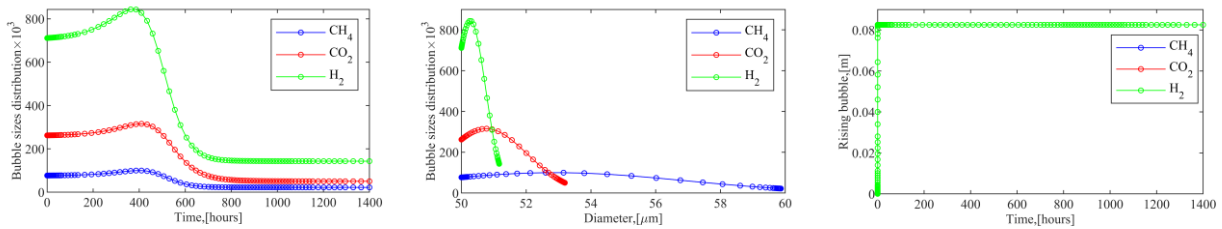
a. Headspace pressure b. Mass of biogas c. Volume of biogas
Figure 9.34. Pressure in headspace, mass, and volume of biogas from headspace (5)

Furthermore, the pH of the bioreactor, [Figure \(9.35a\)](#), as do the partial pressure, [Figure \(9.35b\)](#), and the bubble diameter, [Figure \(9.35c\)](#), are also similar in this case study in comparison to Case-study-B(P). It would have been expected that higher temperature would result in higher pressure, as such enhance the solubility of carbon dioxide. This, in turn, would have resulted in lower pH in this case, however, because the system pressure is regulated, the influence of temperature on the operating pressure becomes negligible.



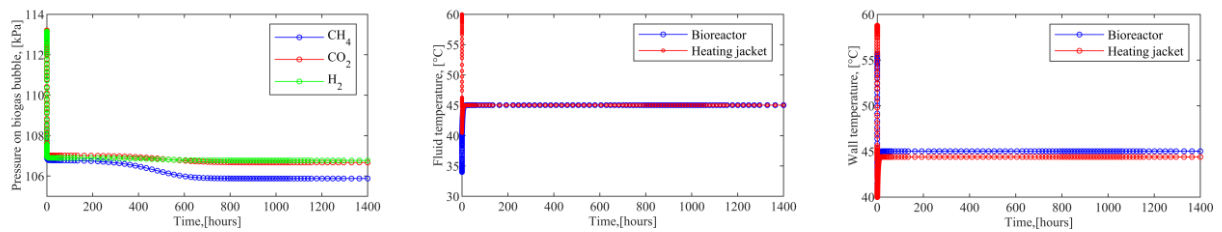
a. pH of bioreactor b. Pressure in bubbles c. Diameter of bubbles
Figure 9.35. pH bioreactor, pressure in bubbles, and diameter of biogas bubbles (5)

Furthermore, as do other case studies the effect of temperature on the rising velocity of bubbles is also negligible, Figure (9.36c), however its effect is obvious on the bubble size distribution, Figure (9.36a) – (9.36b) as the size distribution in this case study are smaller than in Case-study-B(P). This is because, at this high operating temperature, the bubbles grew faster to their respective maximum sizes, Figure (9.35c), hence with a higher probability of larger bubbles in the liquid, the lesser space they will occupy.



a. Distribution-time b. Distribution-diameter c. Height of bubbles
Figure 9.36. Biogas bubbles distribution and its rising height in liquid phase (5)

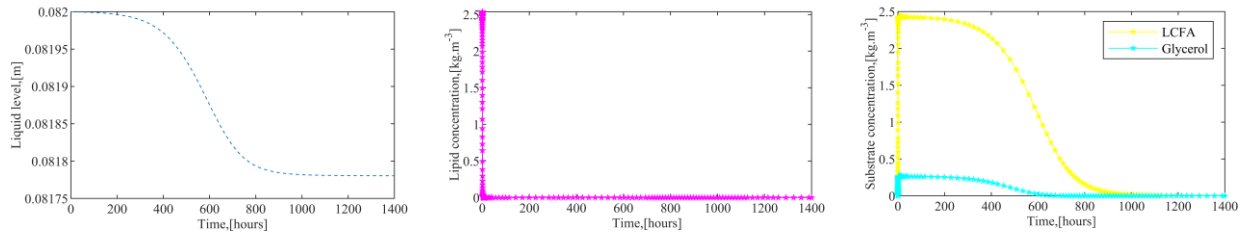
Finally, the pressure on the biogas bubbles is approximately closer to the headspace pressure as observed in Case-study-B(P), and the effect of interfacial pressure of each biogas species is also obvious, Figure (9.37a).



a. Pressure on bubbles b. Fluid temperatures c. Wall temperatures
Figure 9.37. Bubbles surface pressure, fluid, and wall temperature of reaction system (5)

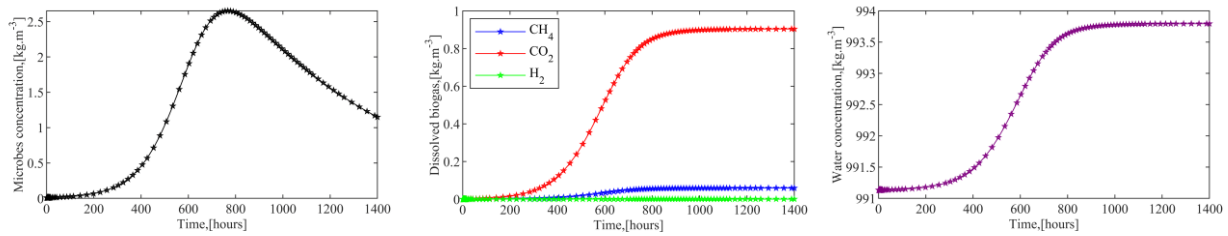
Case-Study-B(T)

This case study focuses on applying overpressure to investigate the effect of temperature on a complete-batch system. Considering that for the previous system, i.e., a semi-batch system with the regulation of the system to atmospheric pressure, it can be observed that its effects on the headspace pressure are negligible as opposed to the expectation of the Ideal gas law. Therefore, to further elucidate the effect of temperature, its influence is also considered for a complete batch system, with increased temperature to 45 °C as shown in Figure (9.44b) – (9.44c).



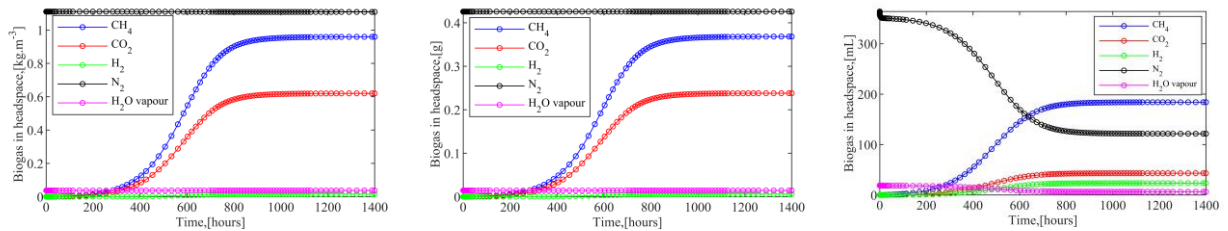
a. Level dynamics b. Lipid dynamics c. Substrate dynamics
Figure 9.38. Changes in liquid level, lipid, and microbes in the liquid phase (6)

As observed previously, increasing the temperature increased the reaction rate as signified by the faster plateauing (~800 hours) of results presented in Figures (9.38a) – (9.42a) as opposed to Case-study-A(P). Although not quite observable in Figure (9.38b), due to the very fast reaction of lipid degradation.



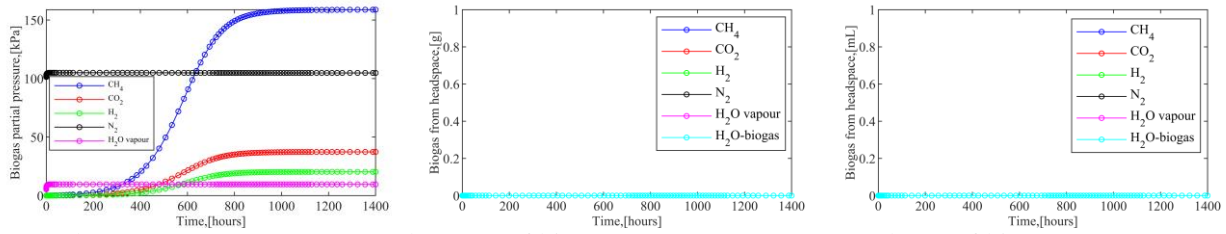
a. Microbes' dynamics b. Dissolved gas dynamics c. Dynamics of water
Figure 9.39. Concentration dynamics for microbes, biogas formation and water (6)

The increase in temperature is also expected to influence the pressure of the system as observed in Figure (9.41a). The headspace pressure is higher in this case study than that of Case-study-A(P). This increase in pressure is evident in the higher amount of dissolved carbon dioxide in the liquid phase, Figure (9.39b), than in Case-study-A(P), following Henry's law.



a. Concentration of biogas b. Mass of biogas c. Volume of biogas
Figure 9.40. Concentration, mass, and volume of biogas obtainable in headspace (6)

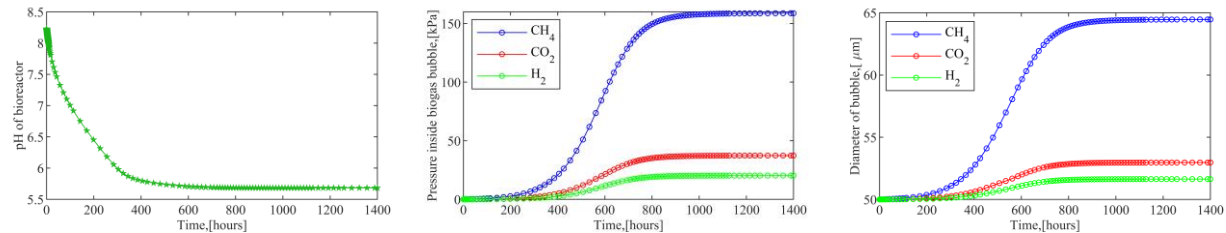
Consequent to the increased amount of carbon dioxide in the liquid phase, the amount of methane gas in the headspace is, therefore, higher in this case study, Figure (9.40a) – (9.40c) than in Case-study-A(P). The deduce corresponding pressure is, therefore, higher for the methane gas, Figure (9.41a) than in Case-study-A(P). Considering that the gas outlet is shut, Figure (9.41b) – (9.41c), therefore indicates no gaseous or vapour outlet from the system.



a. Headspace pressure b. Mass of biogas c. Volume of biogas

Figure 9.41. Pressure in headspace, mass, and volume of biogas from headspace (6)

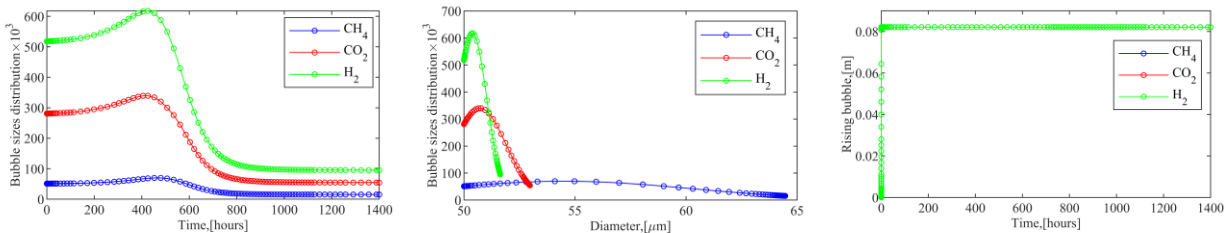
Furthermore, since higher temperature increases pressure, the increased temperature of the system therefore enhanced the solubility of carbon dioxide in the liquid phase. As such the pH of the system decreased a bit slightly (~ 31.5%), [Figure \(9.42a\)](#), in this case study than in Case-study-A(P).



a. pH of bioreactor b. Pressure in bubbles c. Diameter of bubbles

Figure 9.42. pH bioreactor, pressure in bubbles, and diameter of biogas bubbles (6)

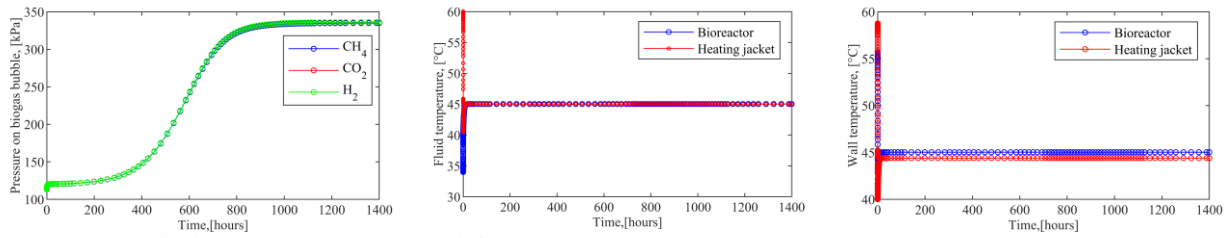
Regarding the biogas bubble growth, the bubble rose quickly to the gas-liquid interface, [Figure \(9.43c\)](#) and grew faster, [Figure \(9.42c\)](#), resulting in increased partial pressure of biogas species, [Figure \(9.42b\)](#), in equilibrium with pressure at the headspace, [Figure \(9.41a\)](#).



a. Distribution-time b. Distribution-diameter c. Height of bubbles

Figure 9.43. Biogas bubbles distribution and its rising height in liquid phase (6)

The resulting biogas bubble distribution is lesser in this case study, [Figure \(9.43a\) – \(9.43b\)](#), than in Case-study-A(P), as explained earlier. Bigger biogas bubbles are quickly formed in the system due to the speed of reaction, thus limiting the probability of higher bubble size distribution. Furthermore, the pressure on the biogas bubble is significantly influenced by the total headspace pressure, [Figure \(9.44a\)](#), similar to Case-study-A(P), but a little bit higher in this case study.

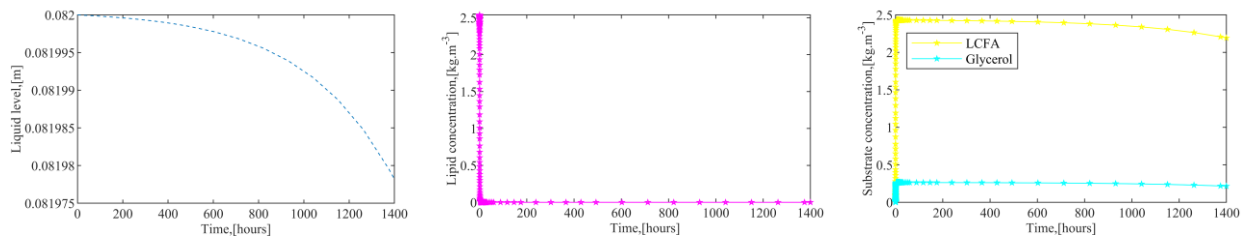


a. Pressure on bubbles b. Fluid temperatures c. Wall temperatures
Figure 9.44. Bubbles surface pressure, fluid, and wall temperature of reaction system (6)

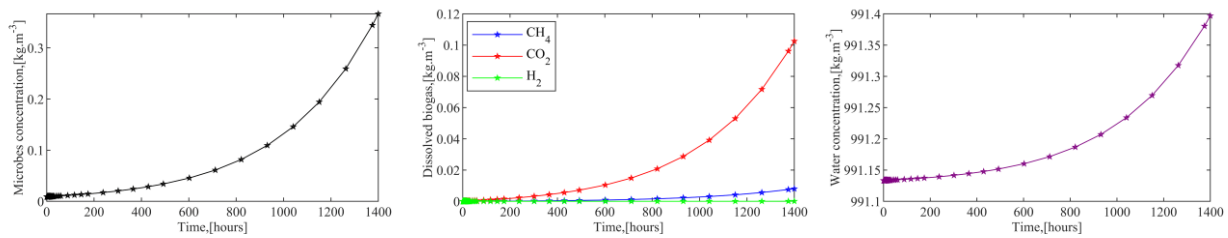
In summary of the effect of temperature, increasing the temperature of the AD enhances the reaction rate. This favours the production of all biogas species, with a rapid increase in bubble growth, as such a more reduced bubble size distribution. However, too high a temperature, specifically from about 50 °C begins to limit the reaction rate and gets worse with higher temperature. A typical illustration of the adverse effect of temperature on AD is illustrated in the results presented in Figure (9.45) – (9.51) for ~ 59 °C. Furthermore, increasing the temperature also increases the pressure of the system, thus also lowering its pH, especially for a closed system. It should be noted that based on the model for lipid hydrolysis, Equation (8.2) – (8.3), and maximum microbe activity, Equation (7.5e), the model applies accurately from 25 to 60 temperature limits as illustrated in Figure (9.1), (9.2b) and (9.2c). However, with appropriate parameter values outside this limit, the SSDM can also be applied.

Case-study-C(T)

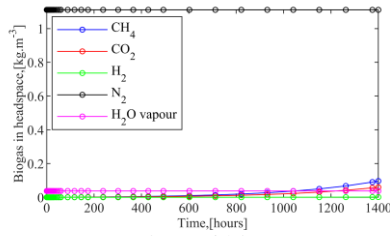
The Figure (9.45) – (9.51) is an illustration of AD process at ~ 59 °C. This temperature as shown in Figure (9.51b) was attained by setting the heating water flowrate, $q_{hw} = 0.00000050 \text{ m}^3 \cdot \text{s}^{-1}$. It can be observed in all the results, especially Figure (9.46a) that the system has been greatly inhibited by operating the system at this high temperature. Figure (9.46a) shows the microbes' growth is slower in comparison to previous case studies.



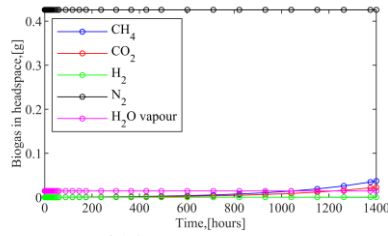
a. Level dynamics b. Lipid dynamics c. Substrate dynamics
Figure 9.45. Changes in liquid level, lipid, and microbes in the liquid phase (7)



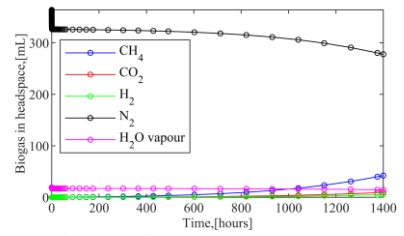
a. Microbes' dynamics b. Dissolved gas dynamics c. Dynamics of water
Figure 9.46. Concentration dynamics for microbes, biogas formation and water (7)



a. Concentration of biogas

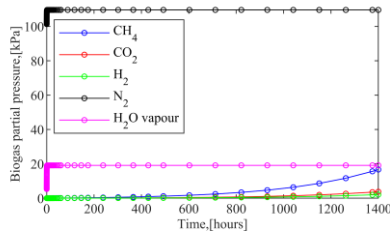


b. Mass of biogas

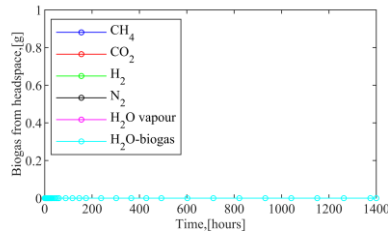


c. Volume of biogas

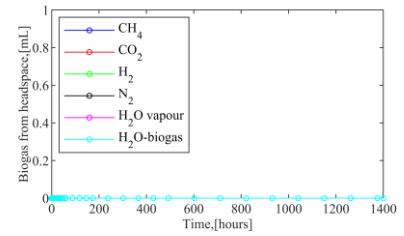
Figure 9.47. Concentration, mass, and volume of biogas obtainable in headspace (7)



a. Headspace pressure

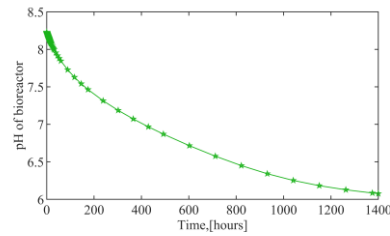


b. Mass of biogas

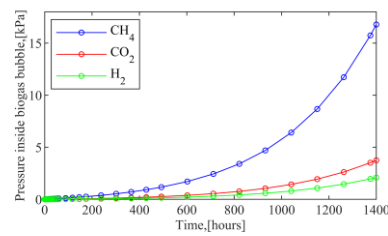


c. Volume of biogas

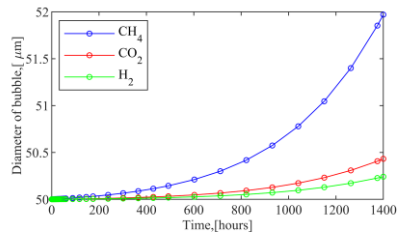
Figure 9.48. Pressure in headspace, mass, and volume of biogas from headspace (7)



a. pH of bioreactor

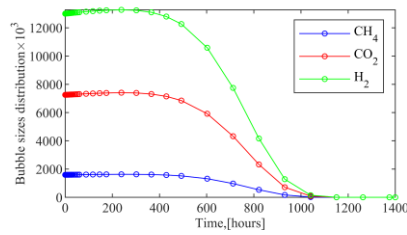


b. Pressure in bubbles

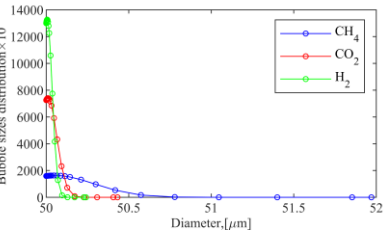


c. Diameter of bubbles

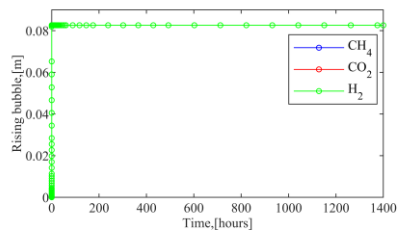
Figure 9.49. pH bioreactor, pressure in bubbles, and diameter of biogas bubbles (7)



a. Distribution-time

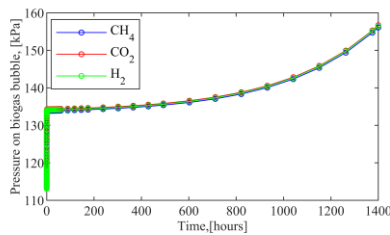


b. Distribution-diameter

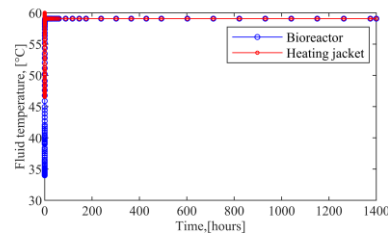


c. Height of bubbles

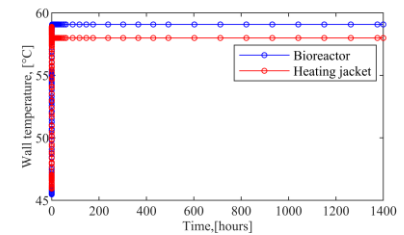
Figure 9.50. Biogas bubbles distribution and its rising height in liquid phase (7)



a. Pressure on bubbles



b. Fluid temperatures



c. Wall temperatures

Figure 9.51. Bubbles surface pressure, fluid, and wall temperature of reaction system (7)

Finally, the estimated result for heat transfer coefficients for the fluids (bioreactor lipid phase, and heating water) and overall heat transfer coefficients for the AD bioreactor based on its outer surface, as deduced from iterative calculations are as presented in [Table \(9.3\)](#). The result shows that the heat transfer coefficients of the fluids and the overall heat transfer coefficient of the bioreactor increased with temperature.

Table 9.3. Iteratively estimated heat transfer properties for the AD process

Temperature, °C	Heat transfer coefficient, W.m ⁻² . K ⁻¹		Overall heat transfer coefficient, W.m ⁻² . K ⁻¹
	Bioreactor content	Heating water	Bioreactor outer surface
35	1457.640	114.3820	98.98090
45	1570.870	117.6940	101.9860
59	1718.060	133.9400	114.7090

10. Conclusion

In conclusion, an adequate review of various reported anaerobic digestion models has been performed in this work. Specifically, this work focused on the Multi-step dynamic model (i.e., Single-step-degradation model, SSDM, Two-step-degradation model, TSDM, and Multi-step-degradation model, MSDM) rather than the Single-based equation model (i.e., Dynamic-, and Cumulative-single-equation models). The SSDM was considered since in terms of solvability, measurability, and controllability of the AD the SSDM > TSDM > MSDM, as it allows for simpler, quicker, as well as adequate evaluation of unknown parameters, due to fewer number dynamic equations. Specifically, the developed SSDM is simpler than the standard Anaerobic digestion model no.1 (ADM1) and can estimate the outflow of biogas from the reactor based on deduced headspace pressure, as do the ADM1. In addition, the SSDM can estimate water evaporation rate, pH dynamic, and can elaborately account for the effect of temperature on the entire AD better than other reported AD models.

In modelling the anaerobic digestion (AD) process with the SSDM, in addition to the biochemical stage (i.e., substrate conversion to biogas in this case), other processes such as the hydrolysis of lipid, mass transfer, heat transfer, and pH of the process were modelled. The microbial activity, physicochemical, and thermodynamic parameters necessary for the model were also modelled (especially as a function of temperature, and pressure). Furthermore, the SSDM was developed such that it could be easily applied to control the pressure, pH, and temperature of the bioreactor.

The model development started with an experimental investigation as well as modelling the hydrolysis of lipids into LCFA and glycerol as a function of temperature, and the model showed excellent proximity with experimental data. The result of the lipid hydrolysis showed that 45 °C was the optimal reaction temperature because the hydrolysis rate more than doubled at 45 °C from 25 °C. The specific physiochemical, and biochemical properties (pH, biological oxygen demand (BOD), chemical oxygen demand (COD), etc.) of the sludge sample used, were also analysed before the experimental investigation of the lipid hydrolysis.

Having modelled the lipid hydrolysis, it was followed by the modelling of mass transfer (specifically, the dissolution and evolution of biogas species, as well as water vapour, together with the water content that is constituted in the biogas), as well as heat transfer (e.g., bioreactor temperature) models, and parameters. Additionally, the biogas bubble growth and motion dynamics, which enable the estimation of biogas bubble diameter, rising velocity, and pressure inside and on the bubble at the gas-liquid interface, were also estimated. Furthermore, physiochemical (such as density, and viscosity), thermodynamic (such as specific heat capacity, and thermal conductivity), and biochemical (e.g., maximum microbe activity) parameters were as modelled as a function of temperature, with good adequacy to ensure the robustness of the model.

Furthermore, once the constitute models have been developed, and interconnected, the SSDM was simulated for different scenarios to evaluate the robustness of the developed model. The simulation was performed to evaluate the effect of pressure, temperature, and pH inhibition on biogas production.

To evaluate the effect of operating pressure on the bioreactor, three case studies were considered. These case studies include Case-study-A(P) (i.e., a complete batch system without output of biogas), Case-study-B(P) (i.e., a semi-batch system with an output of biogas at atmospheric pressure), and Case-study-C(P) (i.e., a semi-batch system with an output of biogas below atmospheric pressure, typically about 30% atmospheric pressure). It was found that higher pressure increased the solubility of carbon dioxide in the liquid phase, thus increasing the proportion of methane gas in the gas phase, assuming pH inhibition is negligible. However, with a realistic consideration of pH inhibition, increasing the operating pressure of the bioreactor also results in lowering the pH of the system, as such can limit methane production. Furthermore, increasing

the pressure of the system or limiting the outlet of biogas will result in the formation of larger biogas bubbles, which correspondingly limit the bubble size distribution in the system.

On evaluating the effect of pH on the bioreactor, it was found that the methane production was more susceptible to the pH of the system considering that methanogenesis is favourable close to the neutral pH. Therefore, methane production was found to be inhibited in the bioreactor, considering that the simulated pH of the system was between 5.6 – 6.0 approximately. As such biogas bubble growth as well as its size distribution were also limited, i.e., reduce with pH inhibition.

Regarding the effect of temperature, increasing the operating temperature of the bioreactor (from 35 to 45 °C) was found to increase the reaction rate for the production of all biogas species. As such rapidly increasing the biogas bubble growth, with a resulting reduction of bubble size distribution. Although it was found that increasing the temperature too high would reduce the reaction rate. The adverse effect of temperature inhibition on the AD was illustrated by setting the bioreactor temperature to 59 °C. In addition to temperature influencing the reaction rate, increasing the temperature also increased the pressure of the system, lowering its pH slightly, especially for a batch system.

Furthermore, considering that the estimated water vapour, as well as the estimated biogas water content, are within the numerical limit of the biogas produced, especially at atmospheric conditions. It can be inferred that the model for water vapour and especially the biogas water content can be tentatively considered adequate.

Finally, based on the simulation results in response to changes in the operating temperature, pressure, and pH. It can be inferred that the developed SSDM is adequate in modelling the AD process, especially regarding the expected theoretical responses according to Henry's and Ideal gas laws. In addition to the simplified comparison of the simulation result (at atmospheric pressure and consideration of pH inhibition) to the experimental result, which was found to be approximately 40 v/v% of the experimentally produced biogas. Furthermore, to adequately validate the developed SSDM, a comprehensive comparison or optimisation of the model to experimental data on real-time dynamics (i.e., dynamics of substrate, microbes, dissolved and evolved biogas species concentrations, as well as water vapour together with biogas water content) is necessary. Performing such comprehensive model optimisation to fit experimental results would require specialised analytical equipment, as well as a careful development of methodologies. Which are currently beyond the time, and financial limit of this thesis.

11. Contribution to science and practice

As a contribution to science, a new simplified AD model based on SSDM has been developed. This model can serve as an alternative to the popular standard Anaerobic digestion model no.1 (ADM1), as it can also estimate biogas evolution, as well as its headspace pressure. Furthermore, unlike the ADM1 or other multi-step dynamic models. The SSDM developed in this work incorporated a novel model to predict the water evaporation rate from the liquid phase in a closed or partially closed vessel. The model can also be applied to other liquid systems apart from water. Additionally, the model can predict inherent water content in biogas based on the thermodynamics of water-hydrocarbon phase equilibrium. The pH dynamic in this model has been developed, such that the control of pH via this model is simplified. Also, the hydrolysis dynamic of the feedstock (i.e., lipid) has been developed to elucidate the effect of temperature. Furthermore, most fluid properties have been modelled as a function of temperature, in addition to modelling the temperature dynamics of the AD, unlike other reported AD models. Therefore, this developed SSDM is most likely to outperform other AD models in evaluating the effect of temperature.

Finally, as a contribution to practice, the SSDM developed in this work can be effectively applied in simulating, optimisation, and control of industrial AD plants. Therefore, it could be used for design and sizing, as well as cost estimation of anaerobic bioreactors (as such the AD plant economics) for laboratory-scaled, medium to large-scale industrial biogas plants.

Bibliography

- [1] Demirbaş A, Şahin-Demirbaş A, Hilal Demirbaş A. Global Energy Sources, Energy Usage, and Future Developments. *Energy Sources* 2010;26:191–204. <https://doi.org/10.1080/00908310490256518>.
- [2] Dincer I, Aydin MI. New paradigms in sustainable energy systems with hydrogen. *Energy Convers Manag* 2023;283:116950. <https://doi.org/10.1016/J.ENCONMAN.2023.116950>.
- [3] Borowski PF. Mitigating Climate Change and the Development of Green Energy versus a Return to Fossil Fuels Due to the Energy Crisis in 2022. *Energies (Basel)* 2022;15:9289. <https://doi.org/10.3390/EN15249289>.
- [4] Kumar S, Smith SR, Fowler G, Velis C, Kumar SJ, Arya S, et al. Challenges and opportunities associated with waste management in India. *R Soc Open Sci* 2017;4. <https://doi.org/10.1098/RSOS.160764>.
- [5] Atchike DW, Irfan M, Ahmad M, Rehman MA. Waste-to-Renewable Energy Transition: Biogas Generation for Sustainable Development. *Front Environ Sci* 2022;10:840588. <https://doi.org/10.3389/FENVS.2022.840588>.
- [6] Azzuni A, Breyer C. Definitions and dimensions of energy security: a literature review. *Wiley Interdiscip Rev Energy Environ* 2018;7:e268. <https://doi.org/10.1002/WENE.268>.
- [7] Ang BW, Choong WL, Ng TS. Energy security: Definitions, dimensions and indexes. *Renewable and Sustainable Energy Reviews* 2015;42:1077–93. <https://doi.org/10.1016/J.RSER.2014.10.064>.
- [8] Yang M, Chen L, Wang J, Msigwa G, Osman AI, Fawzy S, et al. Circular economy strategies for combating climate change and other environmental issues. *Environmental Chemistry Letters* 2022 21:1 2022;21:55–80. <https://doi.org/10.1007/S10311-022-01499-6>.
- [9] Bull SR. Renewable energy today and tomorrow. *Proceedings of the IEEE* 2001;89:1216–26. <https://doi.org/10.1109/5.940290>.
- [10] Siler-Evans K, Azevedo IL, Morgan MG, Apt J. Regional variations in the health, environmental, and climate benefits of wind and solar generation. *Proc Natl Acad Sci U S A* 2013;110:11768–73. <https://doi.org/10.1073/PNAS.1221978110>.
- [11] Hersh MA. The Economics and Politics of Energy Generation. Improving Stability in Developing Nations through Automation 2006 2006:77–82. <https://doi.org/10.1016/B978-008045406-1/50011-2>.
- [12] Fridleifsson IB. Geothermal energy for the benefit of the people. *Renewable and Sustainable Energy Reviews* 2001;5:299–312. [https://doi.org/10.1016/S1364-0321\(01\)00002-8](https://doi.org/10.1016/S1364-0321(01)00002-8).
- [13] Bishoge OK, Kombe GG, Mvile BN. Renewable energy for sustainable development in sub-Saharan African countries: Challenges and way forward. *Journal of Renewable and Sustainable Energy* 2020;12. <https://doi.org/10.1063/5.0009297/1017497>.
- [14] Van Der Schoor T, Scholtens B. Power to the people: Local community initiatives and the transition to sustainable energy. *Renewable and Sustainable Energy Reviews* 2015;43:666–75. <https://doi.org/10.1016/J.RSER.2014.10.089>.

- [15] Pearson RJ, Eisaman MD, Turner JWG, Edwards PP, Jiang Z, Kuznetsov VL, et al. Energy storage via carbon-neutral fuels made from CO₂, Water, and Renewable Energy. *Proceedings of the IEEE* 2012;100:440–60. <https://doi.org/10.1109/JPROC.2011.2168369>.
- [16] Gielen D, Boshell F, Saygin D, Bazilian MD, Wagner N, Gorini R. The role of renewable energy in the global energy transformation. *Energy Strategy Reviews* 2019;24:38–50. <https://doi.org/10.1016/J.ESR.2019.01.006>.
- [17] Bioenergy. International Energy Agency 2023. <https://www.iea.org/energy-system/renewables/bioenergy> (accessed August 9, 2023).
- [18] Ng'andwe P, Ratnasingam J, Mwitwa J, Tembo JC. Wood and Wood Products, Markets and Trade. *Forest Policy, Economics, and Markets in Zambia* 2015:27–66. <https://doi.org/10.1016/B978-0-12-804090-4.00002-1>.
- [19] Luo Z, Zhou J. Thermal conversion of biomass. *Handbook of Climate Change Mitigation* 2012;2:1001–42. https://doi.org/10.1007/978-1-4419-7991-9_27.
- [20] Donate PM. Green synthesis from biomass. *Chemical and Biological Technologies in Agriculture* 2014;1:1–8. <https://doi.org/10.1186/S40538-014-0004-2>.
- [21] Basu P. Biomass Gasification Design Handbook. *Biomass Gasification Design Handbook*, Elsevier; 2010, p. 1–25. <https://doi.org/10.1016/B978-0-12-374988-8.00001-5>.
- [22] Tambone F, Scaglia B, D'Imporzano G, Schievano A, Orzi V, Salati S, et al. Assessing amendment and fertilizing properties of digestates from anaerobic digestion through a comparative study with digested sludge and compost. *Chemosphere* 2010;81:577–83. <https://doi.org/10.1016/J.CHEMOSPHERE.2010.08.034>.
- [23] Solé-Bundó M, Salvadó H, Passos F, Garfi M, Ferrer I. Strategies to Optimize Microalgae Conversion to Biogas: Co-Digestion, Pretreatment and Hydraulic Retention Time. *Molecules* 2018;23:2096. <https://doi.org/10.3390/MOLECULES23092096>.
- [24] Saritha M, Arora A, Lata. Biological Pretreatment of Lignocellulosic Substrates for Enhanced Delignification and Enzymatic Digestibility. *Indian J Microbiol* 2012;52:122–30. <https://doi.org/10.1007/S12088-011-0199-X>.
- [25] Zhang Q, Asian Development Bank. *Rural biomass energy 2020*. 2020.
- [26] Adeniyi OM, Azimov U, Burluka A. Algae biofuel: Current status and future applications. *Renewable and Sustainable Energy Reviews* 2018;90:316–35. <https://doi.org/10.1016/J.RSER.2018.03.067>.
- [27] Luque R, Lovett JC, Datta B, Clancy J, Campelo JM, Romero AA. Biodiesel as feasible petrol fuel replacement: a multidisciplinary overview. *Energy Environ Sci* 2010;3:1706–21. <https://doi.org/10.1039/C0EE00085J>.
- [28] Awogbemi O, Von Kallon DV, Onuh EI, Aigbodion VS. An Overview of the Classification, Production and Utilization of Biofuels for Internal Combustion Engine Applications. *Energies (Basel)* 2021;14:5687. <https://doi.org/10.3390/EN14185687>.
- [29] Sindhu R, Binod P, Pandey A, Ankaram S, Duan Y, Awasthi MK. Biofuel Production From Biomass: Toward Sustainable Development. *Current Developments in Biotechnology and*

- Bioengineering: Waste Treatment Processes for Energy Generation 2019:79–92.
<https://doi.org/10.1016/B978-0-444-64083-3.00005-1>.
- [30] Lee RA, Lavoie JM. From first- to third-generation biofuels: Challenges of producing a commodity from a biomass of increasing complexity. *Animal Frontiers* 2013;3:6–11.
<https://doi.org/10.2527/AF.2013-0010>.
- [31] Nanda S, Rana R, Sarangi PK, Dalai AK, Kozinski JA. A broad introduction to first-, second-, and third-generation biofuels. *Recent Advancements in Biofuels and Bioenergy Utilization* 2018:1–25.
https://doi.org/10.1007/978-981-13-1307-3_1.
- [32] Lee OK, Seong DH, Lee CG, Lee EY. Sustainable production of liquid biofuels from renewable microalgae biomass. *Journal of Industrial and Engineering Chemistry* 2015;29:24–31.
<https://doi.org/10.1016/J.JIEC.2015.04.016>.
- [33] Kan T, Strezov V. Gasification of biomass. *Biomass Processing Technologies* 2014:81–121.
<https://doi.org/10.1201/B17093>.
- [34] Grosser A, Neczaj E. Enhancement of biogas production from sewage sludge by addition of grease trap sludge. *Energy Convers Manag* 2016;125:301–8.
<https://doi.org/10.1016/J.ENCONMAN.2016.05.089>.
- [35] Pienkos PT, Darzins A. The promise and challenges of microalgal-derived biofuels. *Biofuels, Bioproducts and Biorefining* 2009;3:431–40. <https://doi.org/10.1002/BBB.159>.
- [36] Alves MM, Mota Vieira JA, Alvares Pereira RM, Pereira MA, Mota M. Effects of lipids and oleic acid on biomass development in anaerobic fixed-bed reactors. Part II: Oleic acid toxicity and biodegradability. *Water Res* 2001;35:264–70. [https://doi.org/10.1016/S0043-1354\(00\)00242-6](https://doi.org/10.1016/S0043-1354(00)00242-6).
- [37] Astals S, Batstone DJ, Mata-Alvarez J, Jensen PD. Identification of synergistic impacts during anaerobic co-digestion of organic wastes. *Bioresour Technol* 2014;169:421–7.
<https://doi.org/10.1016/J.BIORTECH.2014.07.024>.
- [38] Awe OW, Lu J, Wu S, Zhao Y, Nzihou A, Lyczko N, et al. Effect of Oil Content on Biogas Production, Process Performance and Stability of Food Waste Anaerobic Digestion. *Waste Biomass Valorization* 2018;9:2295–306. <https://doi.org/10.1007/S12649-017-0179-4>.
- [39] Wang J, Singer SD, Souto BA, Asomaning J, Ullah A, Bressler DC, et al. Current progress in lipid-based biofuels: Feedstocks and production technologies. *Bioresour Technol* 2022;351:127020. <https://doi.org/10.1016/J.BIORTECH.2022.127020>.
- [40] Materazzi M, Foscolo PU. The role of waste and renewable gas to decarbonize the energy sector. *Substitute Natural Gas from Waste: Technical Assessment and Industrial Applications of Biochemical and Thermochemical Processes* 2019:1–19. <https://doi.org/10.1016/B978-0-12-815554-7.00001-5>.
- [41] Bušić A, Kundas S, Morzak G, Belskaya H, Mardetko N, Šantek MI, et al. Recent Trends in Biodiesel and Biogas Production. *Food Technol Biotechnol* 2018;56:152–73.
<https://doi.org/10.17113/FTB.56.02.18.5547>.
- [42] Wu N, Moreira CM, Zhang Y, Doan N, Yang S, Philips EJ, et al. Techno-Economic Analysis of Biogas Production from Microalgae through Anaerobic Digestion. *Anaerobic Digestion* 2019.
<https://doi.org/10.5772/INTECHOPEN.86090>.

- [43] Al-Sakkari EG, Mohammed MG, Elozeiri AA, Abdeldayem OM, Habashy MM, Ong ES, et al. Comparative Technoeconomic Analysis of Using Waste and Virgin Cooking Oils for Biodiesel Production. *Front Energy Res* 2020;8:583357. <https://doi.org/10.3389/FENRG.2020.583357>.
- [44] Allah FUM, Alexandru G. Waste cooking oil as source for renewable fuel in Romania. *IOP Conf Ser Mater Sci Eng* 2016;147:012133. <https://doi.org/10.1088/1757-899X/147/1/012133>.
- [45] Varbanov PS, Wang Q, Zeng M, Seferlis P, Ma T, Klemeš JJ, et al. Cooking Oil and Fat Waste Management: A Review of the Current State. *Chem Eng Trans* 2020;81:763–8. <https://doi.org/10.3303/CET2081128>.
- [46] Singh-Ackbarali D, Maharaj R, Mohamed N, Ramjattan-Harry V. Potential of used frying oil in paving material: solution to environmental pollution problem. *Environmental Science and Pollution Research* 2017;24:12220–6. <https://doi.org/10.1007/S11356-017-8793-Z>.
- [47] Dalke R, Demro D, Khalid Y, Wu H, Urgan-Demirtas M. Current status of anaerobic digestion of food waste in the United States. *Renewable and Sustainable Energy Reviews* 2021;151:111554. <https://doi.org/10.1016/J.RSER.2021.111554>.
- [48] Lin L, Xu F, Ge X, Li Y. Improving the sustainability of organic waste management practices in the food-energy-water nexus: A comparative review of anaerobic digestion and composting. *Renewable and Sustainable Energy Reviews* 2018;89:151–67. <https://doi.org/10.1016/J.RSER.2018.03.025>.
- [49] Wu D, Li L, Zhao X, Peng Y, Yang P, Peng X. Anaerobic digestion: A review on process monitoring. *Renewable and Sustainable Energy Reviews* 2019;103:1–12. <https://doi.org/10.1016/J.RSER.2018.12.039>.
- [50] Surendra KC, Takara D, Jasinski J, Kumar Khanal S. Household anaerobic digester for bioenergy production in developing countries: opportunities and challenges. *Environ Technol* 2013;34:1671–89. <https://doi.org/10.1080/09593330.2013.824012>.
- [51] Pilloni M, Hamed TA, Pilloni M, Hamed TA. Small-Size Biogas Technology Applications for Rural Areas in the Context of Developing Countries. *Anaerobic Digestion in Built Environments* 2021. <https://doi.org/10.5772/INTECHOPEN.96857>.
- [52] Jain S, Newman D, Nizhou A, Dekker H, Feuvr P, Richter H, et al. *Global Potential of Biogas*. 2019.
- [53] European Biogas Association. *EBA Statistical report 2018*. 2018.
- [54] Lobo MG, Dorta E. Utilization and Management of Horticultural Waste. *Postharvest Technology of Perishable Horticultural Commodities* 2019:639–66. <https://doi.org/10.1016/B978-0-12-813276-0.00019-5>.
- [55] Van Hulle SWH, Vesvikar M, Poutiainen H, Nopens I. Importance of scale and hydrodynamics for modeling anaerobic digester performance. *Chemical Engineering Journal* 2014;255:71–7. <https://doi.org/10.1016/J.CEJ.2014.06.041>.
- [56] Wade MJ. Not Just Numbers: Mathematical Modelling and Its Contribution to Anaerobic Digestion Processes. *Processes* 2020;8:888. <https://doi.org/10.3390/PR8080888>.

- [57] Fedailaine M, Moussi K, Khitous M, Abada S, Saber M, Tirichine N. Modeling of the Anaerobic Digestion of Organic Waste for Biogas Production. *Procedia Comput Sci* 2015;52:730–7. <https://doi.org/10.1016/J.PROCS.2015.05.086>.
- [58] Cervantes F, Pavlostathis S, van Haandel A. Advanced Biological Treatment Processes for Industrial Wastewaters - Principles & Applications. *Water Intelligence Online* 2006;5:9781780402345–9781780402345. <https://doi.org/10.2166/9781780402345>.
- [59] Jain S, Lala AK, Bhatia SK, Kudchadker AP. Modelling of hydrolysis controlled anaerobic digestion. *Journal of Chemical Technology & Biotechnology* 1992;53:337–44. <https://doi.org/10.1002/JCTB.280530404>.
- [60] Yang G, Sun Y, Li L, Lv P, Kong X, Huang D. Hydrolysis dynamics for batch anaerobic digestion of elephant grass. *RSC Adv* 2018;8:22670–5. <https://doi.org/10.1039/C8RA01115J>.
- [61] Meegoda JN, Li B, Patel K, Wang LB. A Review of the Processes, Parameters, and Optimization of Anaerobic Digestion. *International Journal of Environmental Research and Public Health* 2018, Vol 15, Page 2224 2018;15:2224. <https://doi.org/10.3390/IJERPH15102224>.
- [62] Ma J, Frear C, Wang ZW, Yu L, Zhao Q, Li X, et al. A simple methodology for rate-limiting step determination for anaerobic digestion of complex substrates and effect of microbial community ratio. *Bioresour Technol* 2013;134:391–5. <https://doi.org/10.1016/J.BIORTECH.2013.02.014>.
- [63] Batstone DJ, Keller J, Angelidaki I, Kalyuzhnyi S V., Pavlostathis SG, Rozzi A, et al. The IWA Anaerobic Digestion Model No 1 (ADM1). *Water Science and Technology* 2002;45:65–73. <https://doi.org/10.2166/WST.2002.0292>.
- [64] Jiunn-Jyi L, Yu-You L, Noike T. Influences of pH and moisture content on the methane production in high-solids sludge digestion. *Water Res* 1997;31:1518–24. [https://doi.org/10.1016/S0043-1354\(96\)00413-7](https://doi.org/10.1016/S0043-1354(96)00413-7).
- [65] Nielfa A, Cano R, Fdz-Polanco M. Theoretical methane production generated by the co-digestion of organic fraction municipal solid waste and biological sludge. *Biotechnology Reports* 2015;5:14–21. <https://doi.org/10.1016/J.BTRE.2014.10.005>.
- [66] Hill DT, Barth CL. A Dynamic Model for Simulation of Animal Waste Digestion. *Water Pollution Control Federation* 1977;49:2129–43.
- [67] Havlík I, Votruba J, Sobotka M. Mathematical modelling of the anaerobic digestion process: Application of dynamic mass-energy balance. *Folia Microbiol (Praha)* 1986;31:56–68. <https://doi.org/10.1007/BF02928680>.
- [68] Emebu S, Pecha J, Janáčová D. Review on anaerobic digestion models: Model classification & elaboration of process phenomena. *Renewable and Sustainable Energy Reviews* 2022;160:112288. <https://doi.org/10.1016/J.RSER.2022.112288>.
- [69] Holohan BC, Duarte MS, Szabo-Corbacho MA, Cavaleiro AJ, Salvador AF, Pereira MA, et al. Principles, Advances, and Perspectives of Anaerobic Digestion of Lipids. *Environ Sci Technol* 2022;56:4749–75. <https://doi.org/10.1021/ACS.EST.1C08722>.
- [70] Rasit N, Idris A, Harun R, Wan Ab Karim Ghani WA. Effects of lipid inhibition on biogas production of anaerobic digestion from oily effluents and sludges: An overview. *Renewable and Sustainable Energy Reviews* 2015;45:351–8. <https://doi.org/10.1016/J.RSER.2015.01.066>.

- [71] Angelidaki I, Petersen SP, Ahring BK. Effects of lipids on thermophilic anaerobic digestion and reduction of lipid inhibition upon addition of bentonite. *Appl Microbiol Biotechnol* 1990;33:469–72. <https://doi.org/10.1007/BF00176668>.
- [72] Cirne DG, Paloumet X, Björnsson L, Alves MM, Mattiasson B. Anaerobic digestion of lipid-rich waste—Effects of lipid concentration. *Renew Energy* 2007;32:965–75. <https://doi.org/10.1016/J.RENENE.2006.04.003>.
- [73] Hejnfelt A, Angelidaki I. Anaerobic digestion of slaughterhouse by-products. *Biomass Bioenergy* 2009;33:1046–54. <https://doi.org/10.1016/J.BIOMBIOE.2009.03.004>.
- [74] Capson-Tojo G, Torres A, Muñoz R, Bartacek J, Jeison D. Mesophilic and thermophilic anaerobic digestion of lipid-extracted microalgae *N. gaditana* for methane production. *Renew Energy* 2017;105:539–46. <https://doi.org/10.1016/J.RENENE.2016.12.052>.
- [75] Usman M, Zha L, Abomohra AEF, Li X, Zhang C, Salama ES. Evaluation of animal- and plant-based lipidic waste in anaerobic digestion: kinetics of long-chain fatty acids degradation. *Crit Rev Biotechnol* 2020;40:733–49. <https://doi.org/10.1080/07388551.2020.1756215>.
- [76] Zeeman G, Sanders W. Potential of anaerobic digestion of complex waste(water). *Water Science and Technology* 2001;44:115–22. <https://doi.org/10.2166/WST.2001.0479>.
- [77] Béline F, Rodriguez-Mendez R, Girault R, Bihan Y Le, Lessard P. Comparison of existing models to simulate anaerobic digestion of lipid-rich waste. *Bioresour Technol* 2017;226:99–107. <https://doi.org/10.1016/J.BIORTECH.2016.12.007>.
- [78] Demirbas A. Waste management, waste resource facilities and waste conversion processes. *Energy Convers Manag* 2011;52:1280–7. <https://doi.org/10.1016/J.ENCONMAN.2010.09.025>.
- [79] Arvanitoyannis IS, Tserkezou P. Cereal Waste Management: Treatment Methods and Potential Uses of Treated Waste. *Waste Management for the Food Industries* 2008:629–702. <https://doi.org/10.1016/B978-012373654-3.50013-4>.
- [80] Uçkun Kiran E, Stamatelatos K, Antonopoulou G, Lyberatos G. Production of biogas via anaerobic digestion. *Handbook of Biofuels Production: Processes and Technologies: Second Edition* 2016:259–301. <https://doi.org/10.1016/B978-0-08-100455-5.00010-2>.
- [81] Angelidaki I, Xie L, Luo G, Zhang Y, Oechsner H, Lemmer A, et al. Biogas Upgrading: Current and Emerging Technologies. *Biomass, Biofuels, Biochemicals: Biofuels: Alternative Feedstocks and Conversion Processes for the Production of Liquid and Gaseous Biofuels* 2019:817–43. <https://doi.org/10.1016/B978-0-12-816856-1.00033-6>.
- [82] Vilniškis R, Baltrėnas P, Vasarevičius S, Baltrėnaitė E, Warunkach Beztlenowych W. Research and Assessment of Biogas Evolved during Anaerobic Digestion of Biodegradable Agricultural Waste. *Ecological Chemistry and Engineering* 2011;18.
- [83] Kristoferson LA, Bokalders V. Biogas. *Renewable Energy Technologies*, 1986, p. 100–13. <https://doi.org/10.1016/B978-0-08-034061-6.50015-9>.
- [84] Ruan R, Zhang Y, Chen P, Liu S, Fan L, Zhou N, et al. Biofuels: Introduction. *Biomass, Biofuels, Biochemicals: Biofuels: Alternative Feedstocks and Conversion Processes for the Production of Liquid and Gaseous Biofuels* 2019:3–43. <https://doi.org/10.1016/B978-0-12-816856-1.00001-4>.

- [85] Si Y, Desai D, Bozhilova D, Puffer S, Stephens JC. Fossil fuel companies' climate communication strategies: Industry messaging on renewables and natural gas. *Energy Res Soc Sci* 2023;98:103028. <https://doi.org/10.1016/J.ERSS.2023.103028>.
- [86] Wilkie AC. Biogas a Renewable Biofuel 2019. <https://biogas.ifas.ufl.edu/biogas/biogasdefs.asp> (accessed August 9, 2023).
- [87] Amani T, Nosrati M, Sreekrishnan TR. Anaerobic digestion from the viewpoint of microbiological, chemical, and operational aspects — a review. *Environmental Reviews* 2010;18:255–78. <https://doi.org/10.1139/A10-011>.
- [88] Menzel T, Neubauer P, Junne S. Role of Microbial Hydrolysis in Anaerobic Digestion. *Energies (Basel)* 2020;13:5555. <https://doi.org/10.3390/EN13215555>.
- [89] Nguyen D, Nitayavardhana S, Sawatdeenarunat C, Surendra KC, Khanal SK. Biogas Production by Anaerobic Digestion: Status and Perspectives. *Biomass, Biofuels, Biochemicals: Biofuels: Alternative Feedstocks and Conversion Processes for the Production of Liquid and Gaseous Biofuels* 2019:763–78. <https://doi.org/10.1016/B978-0-12-816856-1.00031-2>.
- [90] Abbassi-Guendouz A, Trably E, Hamelin J, Dumas C, Steyer JP, Delgenès JP, et al. Microbial community signature of high-solid content methanogenic ecosystems. *Bioresour Technol* 2013;133:256–62. <https://doi.org/10.1016/J.BIORTECH.2013.01.121>.
- [91] Dasappa S. Thermochemical Conversion of Biomass. *Transformation of Biomass: Theory to Practice* 2014;9781119973270:133–57. <https://doi.org/10.1002/9781118693643.CH6>.
- [92] Nges IA, Liu J. Effects of solid retention time on anaerobic digestion of dewatered-sewage sludge in mesophilic and thermophilic conditions. *Renew Energy* 2010;35:2200–6. <https://doi.org/10.1016/J.RENENE.2010.02.022>.
- [93] Bolzonella D, Pavan P, Battistoni P, Cecchi F. Mesophilic anaerobic digestion of waste activated sludge: influence of the solid retention time in the wastewater treatment process. *Process Biochemistry* 2005;40:1453–60. <https://doi.org/10.1016/J.PROCBIO.2004.06.036>.
- [94] Rizvi H, Ahmad N, Abbas F, Bukhari IH, Yasar A, Ali S, et al. Start-up of UASB reactors treating municipal wastewater and effect of temperature/sludge age and hydraulic retention time (HRT) on its performance. *Arabian Journal of Chemistry* 2015;8:780–6. <https://doi.org/10.1016/J.ARABJC.2013.12.016>.
- [95] Lindmark J, Thorin E, Bel Fdhila R, Dahlquist E. Effects of mixing on the result of anaerobic digestion: Review. *Renewable and Sustainable Energy Reviews* 2014;40:1030–47. <https://doi.org/10.1016/J.RSER.2014.07.182>.
- [96] Singh B, Szamosi Z, Siménfalvi Z. Impact of mixing intensity and duration on biogas production in an anaerobic digester: a review. *Crit Rev Biotechnol* 2020;40:508–21. <https://doi.org/10.1080/07388551.2020.1731413>.
- [97] Drosig B, Braun R, Bochmann G, Al Saedi T. Analysis and characterisation of biogas feedstocks. *The Biogas Handbook: Science, Production and Applications* 2013:52–84. <https://doi.org/10.1533/9780857097415.1.52>.
- [98] Filer J, Ding HH, Chang S. Biochemical Methane Potential (BMP) Assay Method for Anaerobic Digestion Research. *Water (Basel)* 2019;11:921. <https://doi.org/10.3390/W11050921>.

- [99] Ramachandran A, Rustum R, Adeloye AJ. Anaerobic digestion process modeling using Kohonen self-organising maps. *Heliyon* 2019;5:e01511. <https://doi.org/10.1016/J.HELIYON.2019.E01511>.
- [100] Johnson DK, Elander RT. Pretreatments for Enhanced Digestibility of Feedstocks. *Biomass Recalcitrance: Deconstructing the Plant Cell Wall for Bioenergy* 2009:436–53. <https://doi.org/10.1002/9781444305418.CH14>.
- [101] Montgomery LFR, Bochmann G. Pretreatment of feedstock for enhanced biogas production Pretreatment of feedstock for enhanced biogas production (electronic version) 2014.
- [102] Khadaroo SNBA, Poh PE, Gouwanda D, Grassia P. Applicability of various pretreatment techniques to enhance the anaerobic digestion of Palm oil Mill effluent (POME): A review. *J Environ Chem Eng* 2019;7:103310. <https://doi.org/10.1016/J.JECE.2019.103310>.
- [103] Khadaroo SNBA, Grassia P, Gouwanda D, He J, Poh PE. Enhancing the biogas production and the treated effluent quality via an alternative Palm Oil Mill Effluent (POME) treatment process: Integration of thermal pretreatment and dewatering. *Biomass Bioenergy* 2021;151:106167. <https://doi.org/10.1016/J.BIOMBIOE.2021.106167>.
- [104] Machnicka A, Grübel K. The effect of pre-treatment and anaerobic digestion for pathogens reduction in agricultural utilization of sewage sludge. *Environmental Science and Pollution Research* 2023;30:13801–10. <https://doi.org/10.1007/S11356-022-23164-9>.
- [105] Tsigkou K, Zagklis D, Tsafrakidou P, Zapanti P, Manthos G, Karamitou K, et al. Expired food products and used disposable adult nappies mesophilic anaerobic co-digestion: Biochemical methane potential, feedstock pretreatment and two-stage system performance. *Renew Energy* 2021;168:309–18. <https://doi.org/10.1016/J.RENENE.2020.12.062>.
- [106] Lin CSK, Pfaltzgraff LA, Herrero-Davila L, Mubofu EB, Abderrahim S, Clark JH, et al. Food waste as a valuable resource for the production of chemicals, materials and fuels. Current situation and global perspective. *Energy Environ Sci* 2013;6:426–64. <https://doi.org/10.1039/C2EE23440H>.
- [107] Sun H, Wu S, Dong R. Monitoring Volatile Fatty Acids and Carbonate Alkalinity in Anaerobic Digestion: Titration Methodologies. *Chem Eng Technol* 2016;39:599–610. <https://doi.org/10.1002/CEAT.201500293>.
- [108] Karthikeyan OP, Visvanathan C. Bio-energy recovery from high-solid organic substrates by dry anaerobic bio-conversion processes: a review. *Reviews in Environmental Science and Bio/Technology* 2012 12:3 2012;12:257–84. <https://doi.org/10.1007/S11157-012-9304-9>.
- [109] Gerber M, Span R. An Analysis of Available Mathematical Models for Anaerobic Digestion of Organic Substances for Production of Biogas. *International gas union research conference*, 2008.
- [110] Mazzucotelli CA, Ponce AG, Kotlar CE, Moreira M del R. Isolation and characterization of bacterial strains with a hydrolytic profile with potential use in bioconversion of agroindustrial by-products and waste. *Food Science and Technology* 2013;33:295–303. <https://doi.org/10.1590/S0101-20612013005000038>.
- [111] Raveendran S, Parameswaran B, Ummalyma SB, Abraham A, Mathew AK, Madhavan A, et al. Applications of Microbial Enzymes in Food Industry. *Food Technol Biotechnol* 2018;56:16–30. <https://doi.org/10.17113/FTB.56.01.18.5491>.
- [112] Shin J Du, Xu C, Kim SH, Kim H, Mahmood N, Kim M. Biomass Conversion of Plant Residues. *Food Bioconversion* 2017;2:351–83. <https://doi.org/10.1016/B978-0-12-811413-1.00010-3>.

- [113] Gerardi MH. The Microbiology of Anaerobic Digesters. The Microbiology of Anaerobic Digesters 2003. <https://doi.org/10.1002/0471468967>.
- [114] Shah YT. Chemical energy from natural and synthetic gas. Chemical Energy from Natural and Synthetic Gas 2017;1–688. <https://doi.org/10.1201/9781315302355>.
- [115] Dareioti MA, Vavouraki AI, Kornaros M. Effect of pH on the anaerobic acidogenesis of agroindustrial wastewaters for maximization of bio-hydrogen production: A lab-scale evaluation using batch tests. Bioresour Technol 2014;162:218–27. <https://doi.org/10.1016/J.BIORTECH.2014.03.149>.
- [116] Van DP, Fujiwara T, Tho BL, Toan PPS, Minh GH. A review of anaerobic digestion systems for biodegradable waste: Configurations, operating parameters, and current trends. Environmental Engineering Research 2020;25:1–17. <https://doi.org/10.4491/EER.2018.334>.
- [117] Zhang J, Wang S, Wang Y. Biobutanol Production From Renewable Resources: Recent Advances. Advances in Bioenergy 2016;1:1–68. <https://doi.org/10.1016/BS.AIBE.2016.09.001>.
- [118] Shin HS, Youn JH. Conversion of food waste into hydrogen by thermophilic acidogenesis. Biodegradation 2005;16:33–44. <https://doi.org/10.1007/S10531-004-0377-9>.
- [119] Shin HS, Youn JH, Kim SH. Hydrogen production from food waste in anaerobic mesophilic and thermophilic acidogenesis. Int J Hydrogen Energy 2004;29:1355–63. <https://doi.org/10.1016/J.IJHYDENE.2003.09.011>.
- [120] Ali Shah F, Mahmood Q, Maroof Shah M, Pervez A, Ahmad Asad S. Microbial ecology of anaerobic digesters: The key players of anaerobiosis. The Scientific World Journal 2014;2014. <https://doi.org/10.1155/2014/183752>.
- [121] Manyi-Loh CE, Mamphweli SN, Meyer EL, Okoh AI, Makaka G, Simon M. Microbial Anaerobic Digestion (Bio-Digesters) as an Approach to the Decontamination of Animal Wastes in Pollution Control and the Generation of Renewable Energy. International Journal of Environmental Research and Public Health 2013, Vol 10, Pages 4390-4417 2013;10:4390–417. <https://doi.org/10.3390/IJERPH10094390>.
- [122] Ahmad A, Ghufuran R, Wahid ZA. Bioenergy from anaerobic degradation of lipids in palm oil mill effluent. Reviews in Environmental Science and Bio/Technology 2011 10:4 2011;10:353–76. <https://doi.org/10.1007/S11157-011-9253-8>.
- [123] Katsyv A, Müller V. Overcoming Energetic Barriers in Acetogenic C1 Conversion. Front Bioeng Biotechnol 2020;8. <https://doi.org/10.3389/FBIOE.2020.621166>.
- [124] Wang Z, Yang ST. Propionic acid production in glycerol/glucose co-fermentation by *Propionibacterium freudenreichii* subsp. *shermanii*. Bioresour Technol 2013;137:116–23. <https://doi.org/10.1016/J.BIORTECH.2013.03.012>.
- [125] Agnihotri S, Yin DM, Mahboubi A, Sapmaz T, Varjani S, Qiao W, et al. A Glimpse of the World of Volatile Fatty Acids Production and Application: A review. Bioengineered 2022;13:1249–75. <https://doi.org/10.1080/21655979.2021.1996044>.
- [126] Cazier EA, Trably E, Steyer JP, Escudie R. Biomass hydrolysis inhibition at high hydrogen partial pressure in solid-state anaerobic digestion. Bioresour Technol 2015;190:106–13. <https://doi.org/10.1016/J.BIORTECH.2015.04.055>.

- [127] Silva OB da, Carvalho LS, de Almeida GC, Oliveira JD de, Carmo TS, Parachin NS, et al. Biogas - Turning Waste into Clean Energy. *Fermentation Processes* 2017. <https://doi.org/10.5772/64262>.
- [128] Birkett J, Lester J. *Microbiology and Chemistry for Environmental Scientists and Engineers*. Microbiology and Chemistry for Environmental Scientists and Engineers 2018. <https://doi.org/10.4324/9780203477397>.
- [129] Sheehan JD, Jiang J, Savage PE. *Algae and Environmental Sustainability*. Johnson Matthey Technology Review 2017;61:133–7. <https://doi.org/10.1595/205651317X695109>.
- [130] Anaerobic treatment processes. *Handbook of Water and Wastewater Microbiology*, 2003, p. 391–426. <https://doi.org/10.1016/b978-012470100-7/50025-x>.
- [131] D. S. EM, N. N. A, S.M EM, A. M. A. Improvement of Anaerobic Digesters using Pre-Selected Micro-Organisms. *International Water Technology Journal*, 2013;3.
- [132] Sbizris I. Start-Up of a Laboratory-Scale Anaerobic Sequencing Batch Reactor Treating Glucose. University of Toronto, 2000.
- [133] Wesley Awe O, Lu J, Wu S, Zhao Y, Nzihou A, Lyczko N, et al. Waste and Biomass Valorization. *Waste Biomass Valorization* 2018;9. <https://doi.org/10.1007/s12649-017-0179-4>.
- [134] Das A, Mondal C. Comparative Kinetic Study of Anaerobic Treatment of Thermally Pretreated Source-Sorted Organic Market Refuse. *Journal of Engineering (United Kingdom)* 2015;2015. <https://doi.org/10.1155/2015/684749>.
- [135] Barampouti EMP, Mai ST, Vlyssides AG. Dynamic modeling of biogas production in an UASB reactor for potato processing wastewater treatment. *Chemical Engineering Journal* 2005;106:53–8. <https://doi.org/10.1016/J.CEJ.2004.06.010>.
- [136] Lo HM, Kurniawan TA, Sillanpää MET, Pai TY, Chiang CF, Chao KP, et al. Modeling biogas production from organic fraction of MSW co-digested with MSWI ashes in anaerobic bioreactors. *Bioresour Technol* 2010;101:6329–35. <https://doi.org/10.1016/J.BIORTECH.2010.03.048>.
- [137] Yang B, Wang C, Zhao X, - al, Soliu G, Onunka C, et al. Comparison of kinetic model for biogas production from corn cob. *IOP Conf Ser Mater Sci Eng* 2018;345:012004. <https://doi.org/10.1088/1757-899X/345/1/012004>.
- [138] Ahmed S, Kazda M. Characteristics of on-demand biogas production by using sugar beet silage. *Anaerobe* 2017;46:114–21. <https://doi.org/10.1016/J.ANAEROBE.2017.04.016>.
- [139] Motte JC, Escudié R, Bernet N, Delgenes JP, Steyer JP, Dumas C. Dynamic effect of total solid content, low substrate/inoculum ratio and particle size on solid-state anaerobic digestion. *Bioresour Technol* 2013;144:141–8. <https://doi.org/10.1016/J.BIORTECH.2013.06.057>.
- [140] Abu-Reesh IM. Kinetics of anaerobic digestion of labaneh whey in a batch reactor. *African Journal of Biotechnology* 2014;13:1745–55. <https://doi.org/10.5897/AJB2013.13310>.
- [141] Howell G, Bennett C, Materić D. A comparison of methods for early prediction of anaerobic biogas potential on biologically treated municipal solid waste. *J Environ Manage* 2019;232:887–94. <https://doi.org/10.1016/J.JENVMAN.2018.11.137>.
- [142] Shitophyta LM, Maryudi M, Budiyo B. Comparison of kinetic models for biogas production from rice straw. *Jurnal Bahan Alam Terbarukan* 2017;6:107–11. <https://doi.org/10.15294/JBAT.V6I2.9325>.

- [143] Zuru AA, Dangoggo SM, Birnin-Yauri UA, Tambuwal AD. Adoption of thermogravimetric kinetic models for kinetic analysis of biogas production. *Renew Energy* 2004;29:97–107. [https://doi.org/10.1016/S0960-1481\(03\)00074-0](https://doi.org/10.1016/S0960-1481(03)00074-0).
- [144] Bilgili MS, Demir A, Varank G. Evaluation and modeling of biochemical methane potential (BMP) of landfilled solid waste: A pilot scale study. *Bioresour Technol* 2009;100:4976–80. <https://doi.org/10.1016/J.BIORTECH.2009.05.012>.
- [145] Schofield P, Pitt RE, Pell AN. Kinetics of fiber digestion from in vitro gas production. *J Anim Sci* 1994;72:2980–91. <https://doi.org/10.2527/1994.72112980X>.
- [146] Lay J-J, Li Y-Y, Noike T. Effect of moisture content and chemical nature on methane fermentation characteristics of municipal solid wastes. *Doboku Gakkai Ronbunshu* 1996;1996:101–8. https://doi.org/10.2208/JSCEJ.1996.552_101.
- [147] Zwietering MH, Jongenburger I, Rombouts FM, Van't Riet K. Modeling of the Bacterial Growth Curve. *Appl Environ Microbiol* 1990;56:1875–81. <https://doi.org/10.1128/AEM.56.6.1875-1881.1990>.
- [148] Alizadeh HHA, Seifi R, Radmard SA. Evaluation of the anaerobic digestion of kitchen waste by thermal pretreatment in a batch leach bed reactor with down flow and the kinetics of methane yields. *Biofuels* 2016;9:315–23. <https://doi.org/10.1080/17597269.2016.1266235>.
- [149] Ware A, Power N. Modelling methane production kinetics of complex poultry slaughterhouse wastes using sigmoidal growth functions. *Renew Energy* 2017;104:50–9. <https://doi.org/10.1016/J.RENENE.2016.11.045>.
- [150] Zhang H, An D, Cao Y, Tian Y, He J. Modeling the Methane Production Kinetics of Anaerobic Co-Digestion of Agricultural Wastes Using Sigmoidal Functions. *Energies (Basel)* 2021;14:258. <https://doi.org/10.3390/EN14020258>.
- [151] Pererva Y, Miller CD, Sims RC. Existing Empirical Kinetic Models in Biochemical Methane Potential (BMP) Testing, Their Selection and Numerical Solution. *Water (Basel)* 2020;12:1831. <https://doi.org/10.3390/W12061831>.
- [152] Li L, Kong X, Yang F, Li D, Yuan Z, Sun Y. Biogas production potential and kinetics of microwave and conventional thermal pretreatment of grass. *Appl Biochem Biotechnol* 2012;166:1183–91. <https://doi.org/10.1007/S12010-011-9503-9>.
- [153] Pitt RE, Cross TL, Pell AN, Schofield P, Doane PH. Use of in vitro gas production models in ruminal kinetics. *Math Biosci* 1999;159:145–63. [https://doi.org/10.1016/S0025-5564\(99\)00020-6](https://doi.org/10.1016/S0025-5564(99)00020-6).
- [154] Shen J, Yan H, Zhang R, Liu G, Chen C. Characterization and methane production of different nut residue wastes in anaerobic digestion. *Renew Energy* 2018;116:835–41. <https://doi.org/10.1016/J.RENENE.2017.09.018>.
- [155] Weinrich S, Nelles M. Systematic simplification of the Anaerobic Digestion Model No. 1 (ADM1) – Model development and stoichiometric analysis. *Bioresour Technol* 2021;333:125124. <https://doi.org/10.1016/J.BIORTECH.2021.125124>.
- [156] Simeonov I, Stoyanov S. Modelling and Dynamic Compensator Control of the Anaerobic Digestion of Organic Wastes. *Chemical and Biochemical Engineering* 2003;17:285–92.

- [157] Kiely G, Tayfur G, Dolan C, Tanji K. Physical and mathematical modelling of anaerobic digestion of organic wastes. *Water Res* 1997;31:534–40. [https://doi.org/10.1016/S0043-1354\(96\)00175-3](https://doi.org/10.1016/S0043-1354(96)00175-3).
- [158] Bornhöft A, Hanke-Rauschenbach R, Sundmacher K. Steady-state analysis of the Anaerobic Digestion Model No. 1 (ADM1). *Nonlinear Dyn* 2013;73:535–49. <https://doi.org/10.1007/S11071-013-0807-X>.
- [159] Boubaker F, Ridha BC. Modelling of the mesophilic anaerobic co-digestion of olive mill wastewater with olive mill solid waste using anaerobic digestion model No. 1 (ADM1). *Bioresour Technol* 2008;99:6565–77. <https://doi.org/10.1016/J.BIORTECH.2007.11.035>.
- [160] Roati C, Fiore S, Ruffino B, Marchese F, Novarino D, Zanetti MC. Preliminary Evaluation of the Potential Biogas Production of Food-Processing Industrial Wastes. *Am J Environ Sci* 2012;8:291–6. <https://doi.org/10.3844/AJESSP.2012.291.296>.
- [161] Moletta R, Verrier D, Albagnac G. Dynamic modelling of anaerobic digestion. *Water Res* 1986;20:427–34. [https://doi.org/10.1016/0043-1354\(86\)90189-2](https://doi.org/10.1016/0043-1354(86)90189-2).
- [162] Manchala KR, Sun Y, Zhang D, Wang ZW. Anaerobic Digestion Modelling. *Advances in Bioenergy* 2017;2:69–141. <https://doi.org/10.1016/BS.AIBE.2017.01.001>.
- [163] Buswell AM, Mueller HF. Mechanism of Methane Fermentation. *Ind Eng Chem* 2002;44:550–2. <https://doi.org/10.1021/IE50507A033>.
- [164] Gallert C, Winter J. Bacterial Metabolism in Wastewater Treatment Systems. *Environmental Biotechnology: Concepts and Applications* 2005:1–48. <https://doi.org/10.1002/3527604286.CH1>.
- [165] Balmant W, Oliveira BH, Mitchell DA, Vargas JVC, Ordonez JC. Optimal operating conditions for maximum biogas production in anaerobic bioreactors. *Appl Therm Eng* 2014;62:197–206. <https://doi.org/10.1016/J.APPLTHERMALENG.2013.09.033>.
- [166] Beschkov V, Sapundzhiev T, Angelov I. Modelling of Biogas Production from Glycerol by Anaerobic Process in a Baffled Multi-Stage Digester. *Biotechnology & Biotechnological Equipment* 2014;26:3244–8. <https://doi.org/10.5504/BBEQ.2012.0061>.
- [167] Yoon H, Klinzing G, Blanch HW. Competition for mixed substrates by microbial populations. *Biotechnol Bioeng* 1977;19:1193–210. <https://doi.org/10.1002/BIT.260190809>.
- [168] Zwietering MH, De Koos JT, Hasenack BE, De Wit JC, Van 'T Riet K. Modeling of bacterial growth as a function of temperature. *Appl Environ Microbiol* 1991;57:1094–101. <https://doi.org/10.1128/AEM.57.4.1094-1101.1991>.
- [169] Alzate-Ibañez AM, Ocampo-Martinez C, Alzate CAC, Montoya VMT. Risk index to monitor an anaerobic digester using a dynamic model based on dilution rate, temperature, and pH. *Nonlinear Engineering* 2020;9:35–50. <https://doi.org/10.1515/NLENG-2018-0055>.
- [170] Angelidaki I, Ellegaard L, Ahring BK. A mathematical model for dynamic simulation of anaerobic digestion of complex substrates: Focusing on ammonia inhibition. *Biotechnol Bioeng* 1993;42:159–66. <https://doi.org/10.1002/BIT.260420203>.
- [171] Lin Z, Junming F, Jia Z, Li Q, Luling L. Formula calculation methods of water content in sweet natural gas and their adaptability analysis. *Natural Gas Industry B* 2014;1:144–9. <https://doi.org/10.1016/J.NGIB.2014.11.004>.

- [172] Moisture in biogas. Inoplex 2022. <https://inoplex.com.au/information/moisture-in-biogas/> (accessed August 9, 2023).
- [173] Hernández JR. Water vapor removal from biogas. 2021.
- [174] Oh ST, Martin AD. Thermodynamic equilibrium model in anaerobic digestion process. *Biochem Eng J* 2007;34:256–66. <https://doi.org/10.1016/J.BEJ.2006.12.011>.
- [175] Dasgupta PK, Dong S. Solubility of ammonia in liquid water and generation of trace levels of standard gaseous ammonia. *Atmospheric Environment* (1967) 1986;20:565–70. [https://doi.org/10.1016/0004-6981\(86\)90099-5](https://doi.org/10.1016/0004-6981(86)90099-5).
- [176] Pauss A, Andre G, Perrier M, Guiot SR. Liquid-to-Gas Mass Transfer in Anaerobic Processes: Inevitable Transfer Limitations of Methane and Hydrogen in the Biomethanation Process. *Appl Environ Microbiol* 1990;56:1636–44. <https://doi.org/10.1128/AEM.56.6.1636-1644.1990>.
- [177] Merchuk JC. Further considerations on the enhancement factor for oxygen absorption into fermentation broth. *Biotechnol Bioeng* 1977;19:1885–9. <https://doi.org/10.1002/BIT.260191211>.
- [178] Weichgrebe D, Nelting K, Rosenwinkel K-H. Determination of wastewater specific mass transfer coefficients for methane in a Gas/Liquid-Batch reactor. IWA, 14th World Congress on Anaerobic Digestion, Viña Del Mar: 2015.
- [179] Puiman L, Elisiário MP, Crasborn LML, Wagenaar LECH, Straathof AJJ, Haringa C. Gas mass transfer in syngas fermentation broths is enhanced by ethanol. *Biochem Eng J* 2022;185:108505. <https://doi.org/10.1016/J.BEJ.2022.108505>.
- [180] Yao K, Chi Y, Wang F, Yan J, Ni M, Cen K. The effect of microbubbles on gas-liquid mass transfer coefficient and degradation rate of COD in wastewater treatment. *Water Science and Technology* 2016;73:1969–77. <https://doi.org/10.2166/WST.2016.018>.
- [181] Kodama T, Goto E, Minoda Y. Determination of Dissolved Hydrogen Concentration and in Submerged Culture Vessels. *Agric Biol Chem* 2014;40:2373–7. <https://doi.org/10.1080/00021369.1976.10862424>.
- [182] Liu Y, Wang Y, Wen X, Shimizu K, Lei Z, Kobayashi M, et al. Enhanced bioconversion of hydrogen and carbon dioxide to methane using a micro-nano sparger system: mass balance and energy consumption. *RSC Adv* 2018;8:26488–96. <https://doi.org/10.1039/C8RA02924E>.
- [183] Chezeau B, Fontaine JP, Vial C. Analysis of liquid-to-gas mass transfer, mixing and hydrogen production in dark fermentation process. *Chemical Engineering Journal* 2019;372:715–27. <https://doi.org/10.1016/J.CEJ.2019.04.191>.
- [184] Yang J, Williams CL, Ramasubramaniam A, Dauenhauer PJ. Aqueous-phase hydrodeoxygenation of highly oxygenated aromatics on platinum. *Green Chemistry* 2014;16:675–82. <https://doi.org/10.1039/C3GC41138A>.
- [185] Dutraive O, Benito S, Fritsch S, Beisert B, Patz CD, Rauhut D. Effect of Sequential Inoculation with Non-Saccharomyces and Saccharomyces Yeasts on Riesling Wine Chemical Composition. *Fermentation* 2019;5:79. <https://doi.org/10.3390/FERMENTATION5030079>.
- [186] Diaz M, Vega A, Coca J. Correlation for the estimation of gas-liquid diffusivity. *Chem Eng Commun* 2007;52:271–81. <https://doi.org/10.1080/00986448708911872>.

- [187] Treybal RE. Mass-transfer operations. vol. 2. John Wiley & Sons, Ltd; 1956. <https://doi.org/10.1002/AIC.690020430>.
- [188] Hikita H, Konishi Y. Desorption of carbon dioxide from supersaturated water in an agitated vessel. *AIChE Journal* 1984;30:945–51. <https://doi.org/10.1002/AIC.690300609>.
- [189] Hikita H, Asai S, Ishikawa H, Saito Y. Kinetics of absorption of chlorine in aqueous acidic solutions of ferrous chloride. *Chem Eng Sci* 1975;30:607–16. [https://doi.org/10.1016/0009-2509\(75\)80033-9](https://doi.org/10.1016/0009-2509(75)80033-9).
- [190] Moo-Young M, Blanch HW. Design of biochemical reactors mass transfer criteria for simple and complex systems. *Advances in Biochemical Engineering* 1981;19:1–69. https://doi.org/10.1007/3-540-10464-X_16.
- [191] Solsvik J. Lagrangian modeling of mass transfer from a single bubble rising in stagnant liquid. 370-383 2018;190:370–83. <https://doi.org/10.1016/J.CES.2018.06.002>.
- [192] Makkonen L, Vehmas T. Comment on “On the thermodynamic stability of bubbles, immiscible droplets, and cavities” by G. S. Manning, *Phys. Chem. Chem. Phys.*, 2020, 22, 17523. *Physical Chemistry Chemical Physics* 2021;23:12490–2. <https://doi.org/10.1039/D1CP01122G>.
- [193] Smirnov BM, Stephen Berry R. Growth of bubbles in liquid. *Chem Cent J* 2015;9:1–8. <https://doi.org/10.1186/S13065-015-0127-Y>.
- [194] Bahramian A, Danesh A, Gozalpour F, Tohidi B, Todd AC. Vapour–liquid interfacial tension of water and hydrocarbon mixture at high pressure and high temperature conditions. *Fluid Phase Equilib* 2007;252:66–73. <https://doi.org/10.1016/J.FLUID.2006.12.013>.
- [195] Espinoza DN, Santamarina JC. Water-CO₂-mineral systems: Interfacial tension, contact angle, and diffusion—Implications to CO₂ geological storage. *Water Resour Res* 2010;46:7537. <https://doi.org/10.1029/2009WR008634>.
- [196] Chow YTF, Maitland GC, Trusler JPM. Interfacial tensions of the (CO₂ + N₂ + H₂O) system at temperatures of (298 to 448) K and pressures up to 40 MPa. *J Chem Thermodyn* 2016;93:392–403. <https://doi.org/10.1016/J.JCT.2015.08.006>.
- [197] Hosseini M, Fahimpour J, Ali M, Keshavarz A, Iglauer S. H₂–brine interfacial tension as a function of salinity, temperature, and pressure; implications for hydrogen geo-storage. *J Pet Sci Eng* 2022;213:110441. <https://doi.org/10.1016/J.PETROL.2022.110441>.
- [198] Chow YTF, Maitland GC, Trusler JPM. Interfacial tensions of (H₂O + H₂) and (H₂O + CO₂ + H₂) systems at temperatures of (298–448) K and pressures up to 45 MPa. *Fluid Phase Equilib* 2018;475:37–44. <https://doi.org/10.1016/J.FLUID.2018.07.022>.
- [199] El-Banbi A, Alzahabi A, El-Maraghi A. Dry Gases. *PVT Property Correlations* 2018:29–63. <https://doi.org/10.1016/B978-0-12-812572-4.00003-5>.
- [200] Kulkarni AA, Joshi JB. Bubble Formation and Bubble Rise Velocity in Gas–Liquid Systems: A Review. *Ind Eng Chem Res* 2005;44:5873–931. <https://doi.org/10.1021/IE049131P>.
- [201] Thanh BT, Duc LA, Thanh BT, Duc LA. Determination on Fluidization Velocity Types of the Continuous Refined Salt Fluidized Bed Drying. *Current Drying Processes* 2020. <https://doi.org/10.5772/INTECHOPEN.92077>.

- [202] Kelsall GH, Tang S, Smith AL, Yurdakul S. Measurement of rise and electrophoretic velocities of gas bubbles. *Journal of the Chemical Society, Faraday Transactions* 1996;92:3879–85. <https://doi.org/10.1039/FT9969203879>.
- [203] Zheng L, Yapa PD. Buoyant Velocity of Spherical and Nonspherical Bubbles/Droplets. *Journal of Hydraulic Engineering* 2000;126:852–4. [https://doi.org/10.1061/\(ASCE\)0733-9429\(2000\)126:11\(852\)](https://doi.org/10.1061/(ASCE)0733-9429(2000)126:11(852)).
- [204] Engelking PC. Lifetimes of metastable microbubbles. *Journal of Physical Chemistry* 1985;89:1520–3. <https://doi.org/10.1021/J100254A042>.
- [205] Moshtari B, Ganji Babakhani E, Moghaddas JS. Experimental study of gas hold-up and bubble behavior in gas-liquid bubble column. *Petroleum & Coal* 2009;51:27–32.
- [206] Filippa L, Trento A, Álvarez AM. Sauter mean diameter determination for the fine fraction of suspended sediments using a LISST-25X diffractometer. *Measurement* 2012;45:364–8. <https://doi.org/10.1016/J.MEASUREMENT.2011.11.009>.
- [207] Kowalczyk PB, Drzymala J. Physical meaning of the Sauter mean diameter of spherical particulate matter. *Particulate Science and Technology* 2016;34:645–7. <https://doi.org/10.1080/02726351.2015.1099582>.
- [208] Mugele RA, Evans HD. Droplet Size Distribution in Sprays. *Ind Eng Chem* 2002;43:1317–24. <https://doi.org/10.1021/IE50498A023>.
- [209] Azzopardi BJ. Sauter mean diameter. *A-to-Z Guide to Thermodynamics, Heat and Mass Transfer, and Fluids Engineering* 2011. https://doi.org/10.1615/ATOZ.S.SAUTER_MEAN_DIAMETER.
- [210] Malvern. Application note: Basic principles of particle size analysis. 2017.
- [211] Zhao L, Sun L, Mo Z, Du M, Xie G, Tang J. An investigation on the effect of divergent angle on performance of Venturi-type bubble generators. *Deep Rock Mechanics: From Research to Engineering* 2018:137–46. <https://doi.org/10.1201/9781351042666-14>.
- [212] Mairet F, Bernard O, Ras M, Lardon L, Steyer JP. Modeling anaerobic digestion of microalgae using ADM1. *Bioresour Technol* 2011;102:6823–9. <https://doi.org/10.1016/J.BIORTECH.2011.04.015>.
- [213] Campos E, Flotats X. Dynamic simulation of pH in anaerobic processes. *Applied Biochemistry and Biotechnology - Part A Enzyme Engineering and Biotechnology* 2003;109:63–76. <https://doi.org/10.1385/ABAB:109:1-3:63>.
- [214] Sharma K, Ganigue R, Yuan Z. pH dynamics in sewers and its modeling. *Water Res* 2013;47:6086–96. <https://doi.org/10.1016/J.WATRES.2013.07.027>.
- [215] Bernard O. Mass Balance Modelling of Bioprocesses. Comore, Inria: 2001.
- [216] Bates RG, Pinching GD. Acidic Dissociation Constant of Ammonium Ion at 0 ° to 50 ° C, and the Base Strength of Ammonia. *J Res Natl Bur Stand (1934)* 1949;42.
- [217] Flores-Estrella RA, Estrada-Baltazar A, Femat R, Flores-Estrella RA, Estrada-Baltazar A, Femat R. A mathematical model and dynamic analysis of anaerobic digestion of soluble organic fraction of municipal solid waste towards control design. *Rev Mex Ing Quim* 2016;15:243–58.

- [218] Lindberg A, Rasmuson ÅC. Selective desorption of carbon dioxide from sewage sludge for in situ methane enrichment—Part II: modelling and evaluation of experiments. *Biotechnol Bioeng* 2007;97:1039–52. <https://doi.org/10.1002/BIT.21328>.
- [219] Lindorfer H, Braun R, Kirchayr R. Self-heating of anaerobic digesters using energy crops. *Water Science and Technology* 2006;53:159–66. <https://doi.org/10.2166/WST.2006.246>.
- [220] Holland FA, Bragg R. Mixing of liquids in tanks. *Fluid Flow for Chemical Engineers* 1995:164–88. <https://doi.org/10.1016/B978-034061058-9.50007-4>.
- [221] Hall S. Blending and Agitation. *Branan’s Rules of Thumb for Chemical Engineers* 2012:257–79. <https://doi.org/10.1016/B978-0-12-387785-7.00016-5>.
- [222] Sánchez Pérez JA, Rodríguez Porcel EM, Casas López JL, Fernández Sevilla JM, Chisti Y. Shear rate in stirred tank and bubble column bioreactors. *Chemical Engineering Journal* 2006;124:1–5. <https://doi.org/10.1016/J.CEJ.2006.07.002>.
- [223] Smith JM. Agitation devices. *A-to-Z Guide to Thermodynamics, Heat and Mass Transfer, and Fluids Engineering* 2011. https://doi.org/10.1615/ATOZ.A.AGITATION_DEVICES.
- [224] Green DW, Southard MZ. *Mixing and processing of liquids and solids*. McGraw-Hill Education; 2019.
- [225] Cadafalch J, Carbonell D, Consul R, Ruiz R. Modelling of storage tanks with immersed heat exchangers. *Solar Energy* 2015;112:154–62. <https://doi.org/10.1016/J.SOLENER.2014.11.032>.
- [226] Boetcher SKS. Natural convection transfer from vertical cylinders. *SpringerBriefs in Applied Sciences and Technology* 2014:23–42. https://doi.org/10.1007/978-3-319-08132-8_3.
- [227] Popiel CO. Free Convection Heat Transfer from Vertical Slender Cylinders: A Review. *Heat Transfer Engineering* 2011;29:521–36. <https://doi.org/10.1080/01457630801891557>.
- [228] Churchill SW, Chu HHS. Correlating equations for laminar and turbulent free convection from a vertical plate. *Int J Heat Mass Transf* 1975;18:1323–9. [https://doi.org/10.1016/0017-9310\(75\)90243-4](https://doi.org/10.1016/0017-9310(75)90243-4).
- [229] Zhou X, Zhang QM, Liu Q, Zhang ZY, Ding YY, Zhou L, et al. Densities, isobaric thermal expansion coefficients and isothermal compressibilities of linear alkylbenzene. *Phys Scr* 2015;90:055701. <https://doi.org/10.1088/0031-8949/90/5/055701>.
- [230] Teymourtash AR, Rezaei Khonakdar D, Raveshi MR. Natural convection on a vertical plate with variable heat flux in supercritical fluids. *J Supercrit Fluids* 2013;74:115–27. <https://doi.org/10.1016/J.SUPFLU.2012.12.010>.
- [231] Rosa V da S, Júnior D de M, Rosa V da S, Júnior D de M. Design of Heat Transfer Surfaces in Agitated Vessels. *Heat Exchangers - Design, Experiment and Simulation* 2017. <https://doi.org/10.5772/66729>.
- [232] Pietranski JF. *Overall Heat Transfer Coefficients in Agitated Vessels*. 2020.
- [233] Chilton TH, Drew TB, Jebens RH. Heat Transfer Coefficients in Agitated Vessels. *Ind Eng Chem* 2002;36:510–6. <https://doi.org/10.1021/IE50414A006>.

- [234] Farahbod F. Experimental investigation of thermo-physical properties of drilling fluid integrated with nanoparticles: Improvement of drilling operation performance. *Powder Technol* 2021;384:125–31. <https://doi.org/10.1016/J.POWTEC.2021.02.002>.
- [235] Jacimovic B, Genic S, Lelea D. Calculation of the Heat Transfer Coefficient for Laminar Flow in Pipes in Practical Engineering Applications. *Heat Transfer Engineering* 2017;39:1794–800. <https://doi.org/10.1080/01457632.2017.1388949>.
- [236] Kuchibhotla A, Banerjee D, Dhir V. Forced convection heat transfer of molten Salts: A review. *Nuclear Engineering and Design* 2020;362:110591. <https://doi.org/10.1016/J.NUCENGDDES.2020.110591>.
- [237] Moate PJ, Boston RC, Jenkins TC, Lean IJ. Kinetics of Ruminant Lipolysis of Triacylglycerol and Biohydrogenation of Long-Chain Fatty Acids: New Insights from Old Data. *J Dairy Sci* 2008;91:731–42. <https://doi.org/10.3168/JDS.2007-0398>.
- [238] Astals S, Koch K, Weinrich S, Hafner SD, Tait S, Peces M. Impact of Storage Conditions on the Methanogenic Activity of Anaerobic Digestion Inocula. *Water (Basel)* 2020;12:1321. <https://doi.org/10.3390/W12051321>.
- [239] Hwang S, Hansen CL. Evaluating a correlation between volatile suspended solid and adenosine 5'-triphosphate levels in anaerobic treatment of high organic suspended solids wastewater. *Bioresour Technol* 1998;63:243–50. [https://doi.org/10.1016/S0960-8524\(97\)00131-4](https://doi.org/10.1016/S0960-8524(97)00131-4).
- [240] Tang Y, Yang YL, Li XM, Yang Q, Wang DB, Zeng GM. The isolation, identification of sludge-lysing thermophilic bacteria and its utilization in solubilization for excess sludge. *Environ Technol* 2011;33:961–6. <https://doi.org/10.1080/09593330.2011.603754>.
- [241] 2540 SOLIDS - Standard Methods For the Examination of Water and Wastewater. American Public Health Association 2023. <https://www.standardmethods.org/doi/10.2105/SMWW.2882.030> (accessed August 9, 2023).
- [242] Dusci JC, Hager J, Coyle S, Tidwell J. Evaluation of freshwater prawn, *Macrobrachium rosenbergii*, for biological solids control in raft aquaponic systems and the protective effectiveness of root guards. *J World Aquac Soc* 2022;53:290–308. <https://doi.org/10.1111/JWAS.12856>.
- [243] Liu C, Morrison C, Jia J, Xu X, Liu M, Zhang S. Does the Nitrification-Suppressed BOD5 Test Make Sense? *Environ Sci Technol* 2020;54:5323–4. <https://doi.org/10.1021/ACS.EST.0C00997>.
- [244] Jouanneau S, Recoules L, Durand MJ, Boukabache A, Picot V, Primault Y, et al. Methods for assessing biochemical oxygen demand (BOD): A review. *Water Res* 2014;49:62–82. <https://doi.org/10.1016/J.WATRES.2013.10.066>.
- [245] Dedkov YM, Elizarova O V., Kel'ina SY. Dichromate method for the determination of chemical oxygen demand. *Journal of Analytical Chemistry* 2000;55:777–81. <https://doi.org/10.1007/BF02757915>.
- [246] Bertrand-Krajewski JL, Winkler S, Saracevic E, Torres A, Schaar H. Comparison of and uncertainties in raw sewage COD measurements by laboratory techniques and field UV-visible spectrometry. *Water Science and Technology* 2007;56:17–25. <https://doi.org/10.2166/WST.2007.759>.

- [247] Putra AM, Syarifuddin A, Dirpan A. Characterization pH, stability of emulsion, and viscosity canola oil (*Brassicca napus L.*) emulsion (O/W). *IOP Conf Ser Earth Environ Sci* 2020;575:012007. <https://doi.org/10.1088/1755-1315/575/1/012007>.
- [248] Šánek L, Pecha J, Kolomazník K. Simultaneous determination of main reaction components in the reaction mixture during biodiesel production. *J Sep Sci* 2013;36:1029–36. <https://doi.org/10.1002/JSSC.201200967>.
- [249] Kim MJ, Yun JP, Yang JBR, Choi SJ, Kim D. Prediction of the Temperature of Liquid Aluminum and the Dissolved Hydrogen Content in Liquid Aluminum with a Machine Learning Approach. *Metals (Basel)* 2020;10:330. <https://doi.org/10.3390/MET10030330>.
- [250] Emebu S, Martinez CM, Mankonen A, Ogunleye RO, Kubalčík M, Janáčková D, et al. Guide to adequate curve-fitting of models | Comparison between multi-step, and single-step curve-fitting techniques based on anaerobic hydrolysis of lipid. 2023.
- [251] Langtangen HP. Generalizations. *Lecture Notes in Computational Science and Engineering* 2016;110:67–89. https://doi.org/10.1007/978-3-319-29439-1_3.
- [252] Zayen A, Ksibi H. Numerical Optimization of Biogas Production through a 3-Steps Model of Anaerobic Digestion: Sensitivity of Biokinetic Constants Values. *Journal of Bioremediation & Biodegradation* 2015 6:4 2015;6:1–10. <https://doi.org/10.4172/2155-6199.1000302>.
- [253] Mazzeo L, Signorini A, Lembo G, Bavasso I, Di Palma L, Piemonte V. In Situ Bio-Methanation Modelling of a Randomly Packed Gas Stirred Tank Reactor (GSTR). *Processes* 2021;9:846. <https://doi.org/10.3390/PR9050846>.
- [254] Labatut RA, Angenent LT, Scott NR. Conventional mesophilic vs. thermophilic anaerobic digestion: A trade-off between performance and stability? *Water Res* 2014;53:249–58. <https://doi.org/10.1016/J.WATRES.2014.01.035>.
- [255] Ge H, Jensen PD, Batstone DJ. Temperature phased anaerobic digestion increases apparent hydrolysis rate for waste activated sludge. *Water Res* 2011;45:1597–606. <https://doi.org/10.1016/J.WATRES.2010.11.042>.
- [256] Elias M, Wieczorek G, Rosenne S, Tawfik DS. The universality of enzymatic rate–temperature dependency. *Trends Biochem Sci* 2014;39:1–7. <https://doi.org/10.1016/J.TIBS.2013.11.001>.
- [257] Wu B. Integration of mixing, heat transfer, and biochemical reaction kinetics in anaerobic methane fermentation. *Biotechnol Bioeng* 2012;109:2864–74. <https://doi.org/10.1002/BIT.24551>.
- [258] Ryckebosch E, Drouillon M, Vervaeren H. Techniques for transformation of biogas to biomethane. *Biomass Bioenergy* 2011;35:1633–45. <https://doi.org/10.1016/J.BIOMBIOE.2011.02.033>.
- [259] Scott S, Turra F. Six reasons to dry biogas to a low dewpoint before combustion in a CHP engine. 2013.
- [260] Gao J, Li J, Wachemo AC, Yuan H, Zuo X, Li X. Mass conversion pathway during anaerobic digestion of wheat straw. *RSC Adv* 2020;10:27720–7. <https://doi.org/10.1039/D0RA02441D>.
- [261] Thermophysical Properties: Hydrogen at 1 atm. *Global Digital Centra* 2010. https://www.thermalfluidscentral.org/encyclopedia/index.php/Thermophysical_Properties:_Hydrogen_at_1_atm (accessed August 9, 2023).

- [262] Hydrogen Properties | Hydrogen Tools. Pacific Northwest National Laboratory 2023.
<https://h2tools.org/hyarc/hydrogen-properties> (accessed August 9, 2023).
- [263] Some measured data online. Peace Software 2023.
http://www.peacesoftware.de/einigewerte/einigewerte_e.html (accessed August 9, 2023).
- [264] Thermophysical Properties: Carbon dioxide at 1 atm. Global Digital Central 2010.
https://www.thermalfluidscentral.org/encyclopedia/index.php/Thermophysical_Properties:_Carbon_dioxide_at_1_atm (accessed August 9, 2023).
- [265] Thermophysical Properties: Nitrogen at 1 atm. Global Digital Central 2010.
https://www.thermalfluidscentral.org/encyclopedia/index.php/Thermophysical_Properties:_Nitrogen_at_1_atm (accessed August 10, 2023).
- [266] Thermophysical Properties: Nitrogen at 1 atm. Global Digital Central 2010.
https://www.thermalfluidscentral.org/encyclopedia/index.php/Thermophysical_Properties:_Nitrogen_at_1_atm (accessed August 9, 2023).
- [267] Thermophysical Properties: Air at 1 atm. Global Digital Central 2010.
https://www.thermalfluidscentral.org/encyclopedia/index.php/Thermophysical_Properties:_Air_at_1_atm (accessed August 9, 2023).
- [268] Palm oil properties. Chempro Technovation Pvt Ltd 1999.
<https://www.chempro.in/palmoilproperties.htm> (accessed August 9, 2023).
- [269] Thermophysical Properties: Water. Global Digital Central 2012.
https://www.thermalfluidscentral.org/encyclopedia/index.php/Thermophysical_Properties:_Water (accessed August 9, 2023).
- [270] Thermophysical Properties: Water vapor at 1 atm. Global Digital Central 2010.
https://www.thermalfluidscentral.org/encyclopedia/index.php/Thermophysical_Properties:_Water_vapor_at_1_atm (accessed August 9, 2023).
- [271] Water - Heat of Vaporization vs. Temperature. The Engineering ToolBox 2010.
https://www.engineeringtoolbox.com/water-properties-d_1573.html (accessed August 9, 2023).
- [272] Sutherland's Law 1999.
https://doc.comsol.com/5.5/doc/com.comsol.help.cfd/cfd_ug_fluidflow_high_mach.08.27.html (accessed August 9, 2023).
- [273] Van Der Tempel L, Melis GP, Brandsma TC. Thermal conductivity of a glass: I. Measurement by the glass-metal contact. *Glass Physics and Chemistry* 2000;26:606–11.
<https://doi.org/10.1023/A:1007164501169>.
- [274] DeWitt H, Slattery W. Validity of the linear mixing rule for strongly coupled ionic fluids. *Contributions to Plasma Physics* 2003;43:279–81. <https://doi.org/10.1002/CTPP.200310027>.

Appendix

A.1. Properties of fluids

The following data were curve-fitted in relation to temperature (K) to model the fluid properties (density, (kg.m⁻³), viscosity (Pa.s), thermal conductivity (W.m⁻¹.k⁻¹), specific heat capacity (J.Kg⁻¹.K⁻¹), etc. The curve fitted properties showed adequate fit with R² values > 0.95 as shown in Table (A.1).

Table A.1. Evaluation criteria (R² values) for the curve-fitted models

Species/properties	R ² values			
	Density	Viscosity	Thermal conductivity	Specific heat capacity
Water	0.9993	0.9999	0.9998	0.9990
Lipid (Palm oil)	0.9992	0.9992	0.9994	1.0000
Water vapour	–	–	1.0000	0.9996
Nitrogen gas	0.9999	0.9999	1.0000	0.9999
Ammonia gas	0.9987	0.9991	0.9999	1.0000
Carbon dioxide	0.9998	0.9998	0.9997	0.9995
Hydrogen gas	1.0000	1.0000	0.9998	1.0000
Methane gas	1.0000	0.9999	0.9998	0.9996
Air	–	0.9989	0.9997	0.9998

A.2. Hydrogen gas

The density, ρ_{H₂} (kg.m⁻³), viscosity, η_{H₂} (Pa.s), thermal conductivity, k_{H₂} (W.m⁻¹.k⁻¹), and specific heat capacity, C_{P-H₂} (J.Kg⁻¹.K⁻¹) of hydrogen gas were curve-fitted as given in Equation (A.1) – (A.4) as function of temperature, as well as illustrated in Figure (A.1), and evaluation metrics given in Table (A.1). Applicable within temperature limit, 173 – 398 K, using data from literature [261,262].

$$\rho_{H_2} = 0.4287 \exp(-0.01303T) + 0.1378 \exp(-0.002158T) \quad (A.1)$$

$$\eta_{H_2} = -1.26 * 10^{-11}T^2 + 2.81 * 10^{-8}T + 1.664 * 10^{-6} \quad (A.2)$$

$$k_{H_2} = -3.263 * 10^{-7}T^2 + 7.021 * 10^{-4}T + 0.004938 \quad (A.3)$$

$$C_{P-H_2} = 1.501 * 10^4 \exp(-7.033 * 10^{-5}T) - 1.341 * 10^4 \exp(-0.01183T) \quad (A.4)$$

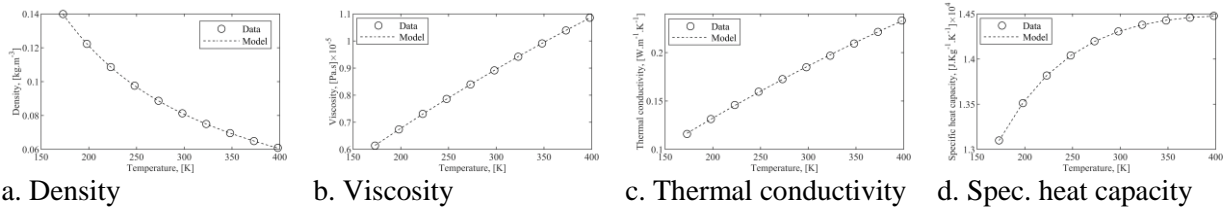


Figure A.1. Properties of hydrogen gas curve fitted as function of temperature

A.3. Methane gas

The density, ρ_{CH₄} (kg.m⁻³), viscosity, η_{CH₄} (Pa.s), thermal conductivity, k_{CH₄} (W.m⁻¹.k⁻¹), and specific heat capacity, C_{P-CH₄} (J.Kg⁻¹.K⁻¹) of methane gas are curve-fitted as given in Equation (A.5) – (A.8) as function of temperature, as well as illustrated in Figure (A.2), and evaluation metrics given in Table (A.1). These models are applicable within temperature limit, 180 – 500 K, using data from literature [263]

$$\rho_{CH_4} = 3.332 \exp(-0.01194T) + 0.9734 \exp(-0.001899T) \quad (A.5)$$

$$\eta_{\text{CH}_4} = -1.994 * 10^{-11}T^2 + 4.505 * 10^{-8}T - 5.255 * 10^{-7} \quad (\text{A.6})$$

$$\kappa_{\text{CH}_4} = 1.772 * 10^{-7}T^2 + 2.812 * 10^{-5}T + 0.01001 \quad (\text{A.7})$$

$$C_{P-\text{CH}_4} = 2185 \exp(-0.0115T) + 1408 \exp(0.001442T) \quad (\text{A.8})$$

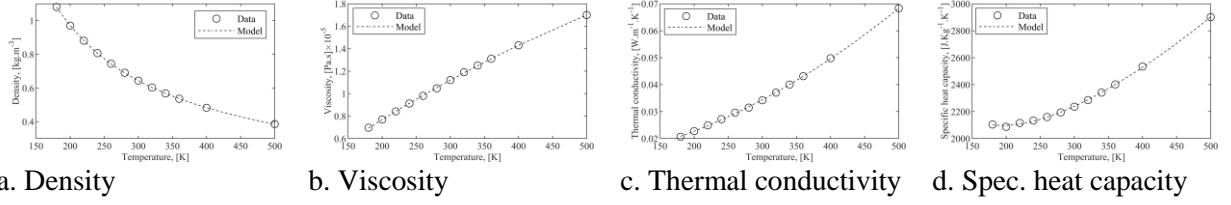


Figure A.2. Properties of methane gas curve fitted as function of temperature

A.4. Carbon dioxide gas

The density, ρ_{CO_2} (kg.m^{-3}), viscosity, η_{CO_2} (Pa.s), thermal conductivity, κ_{CO_2} ($\text{W.m}^{-1}\text{.K}^{-1}$), and specific heat capacity, $C_{P-\text{CO}_2}$ ($\text{J.Kg}^{-1}\text{.K}^{-1}$) of carbon dioxide gas are curve-fitted as given in Equation (A.9) – (A.12) as function of temperature, as well as illustrated in Figure (A.3), and evaluation metrics given in Table (A.1). Applicable within temperature limit, 253 – 393 K, using data from literature [264].

$$\rho_{\text{CO}_2} = 1.744 * 10^{-5}T^2 - 0.01667T + 5.23 \quad (\text{A.9})$$

$$\eta_{\text{CO}_2} = 9.959 * 10^{-6} \exp(0.001867T) - 1.625 * 10^{-5} \exp(-0.00636T) \quad (\text{A.10})$$

$$\kappa_{\text{CO}_2} = 8.183 * 10^{-5}T - 0.007682 \quad (\text{A.11})$$

$$C_{P-\text{CO}_2} = 0.9223T + 575.7 \quad (\text{A.12})$$

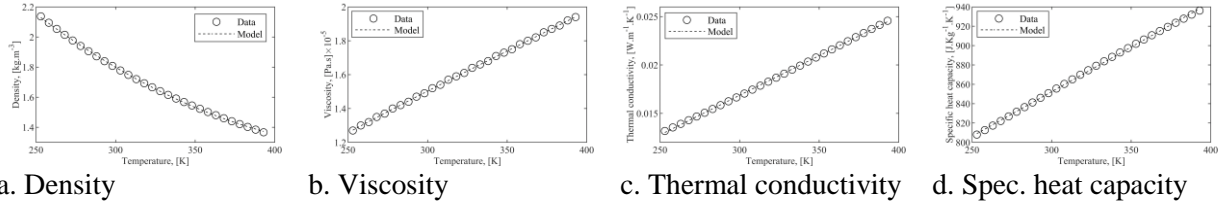


Figure A.3. Properties of carbon dioxide gas curve fitted as function of temperature

A.5. Nitrogen gas

The density, ρ_{N_2} (kg.m^{-3}), viscosity, η_{N_2} (Pa.s), thermal conductivity, κ_{N_2} ($\text{W.m}^{-1}\text{.K}^{-1}$), and specific heat capacity, $C_{P-\text{N}_2}$ ($\text{J.Kg}^{-1}\text{.K}^{-1}$) of nitrogen gas are curve-fitted as given in Equation (A.13) – (A.16) as function of temperature, as well as illustrated in Figure (A.4), and evaluation metrics given in Table (A.1). These models are applicable within temperature limit, 100 – 1300 K, using data from literature [265].

$$\rho_{\text{N}_2} = 363.9T^{-1.013} \quad (\text{A.13})$$

$$\eta_{\text{N}_2} = 1.208 * 10^{-14}T^3 - 3.997 * 10^{-11}T^2 + 6.688 * 10^{-8}T + 8.824 * 10^{-7} \quad (\text{A.14})$$

$$\kappa_{\text{N}_2} = 2.286 * 10^{-11}T^3 - 6.021 * 10^{-8}T^2 + 1.022 * 10^{-4}T - 2.104 * 10^{-5} \quad (\text{A.15})$$

$$C_{P-N_2} = 1248 \exp\left(-\left(\frac{T-1734}{2842}\right)^2\right) + 31.72 \exp\left(-\left(\frac{T-285}{294.8}\right)^2\right) + 3198 \exp\left(-\left(\frac{T+373.1}{240.4}\right)^2\right) + 85.96 \exp\left(-\left(\frac{T-97.31}{236.8}\right)^2\right) \quad (\text{A.16})$$

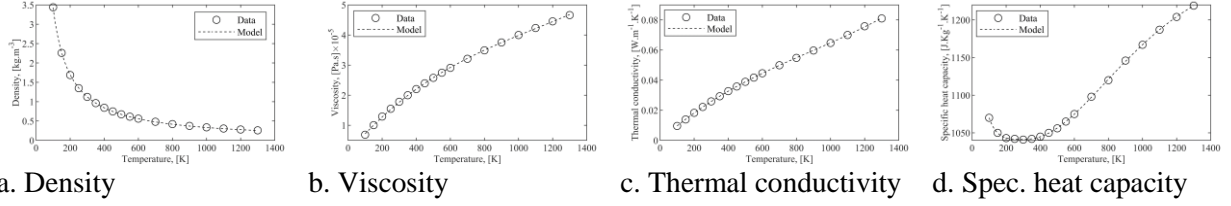


Figure A.4. Properties of nitrogen gas curve fitted as function of temperature

A.6. Ammonia gas

The density, ρ_{H_2} ($\text{kg}\cdot\text{m}^{-3}$), viscosity, η_{H_2} ($\text{Pa}\cdot\text{s}$), thermal conductivity, ℓ_{H_2} ($\text{W}\cdot\text{m}^{-1}\cdot\text{K}^{-1}$), and specific heat capacity, C_{P-H_2} ($\text{J}\cdot\text{Kg}^{-1}\cdot\text{K}^{-1}$) of ammonia gas are curve-fitted as given in Equation (A.17) – (A.20) as function of temperature, as well as illustrated in Figure (A.5), and evaluation metrics given in Table (A.1). These models are applicable within temperature limit, 220 – 390 K, using data from literature [266].

$$\rho_{NH_3} = 3.303 * 10^{-23} T^{9.426} \quad (\text{A.17})$$

$$\eta_{NH_3} = 1.682 * 10^{-12} T^3 - 1.395 * 10^{-9} T^2 + 4.201 * 10^{-7} T - 3.453 * 10^{-5} \quad (\text{A.18})$$

$$\ell_{NH_3} = 0.08199 \exp\left(-\left(\frac{T-435}{61.33}\right)^2\right) - 2.756 * 10^{-4} \exp\left(-\left(\frac{T-253.8}{35.64}\right)^2\right) + 0.004923 \exp\left(-\left(\frac{T-351.8}{38.45}\right)^2\right) + 0.03056 \exp\left(-\left(\frac{T-374.4}{190.8}\right)^2\right) \quad (\text{A.19})$$

$$C_{P-NH_3} = 3.095 * 10^6 \exp\left(-\left(\frac{T-706.6}{128.4}\right)^2\right) + 6.489 * 10^{13} \exp\left(-\left(\frac{T-707}{64.95}\right)^2\right) + 1913 \exp\left(-\left(\frac{T-377.2}{102.9}\right)^2\right) + 1997 \exp\left(-\left(\frac{T-437.7}{941}\right)^2\right) \quad (\text{A.20})$$

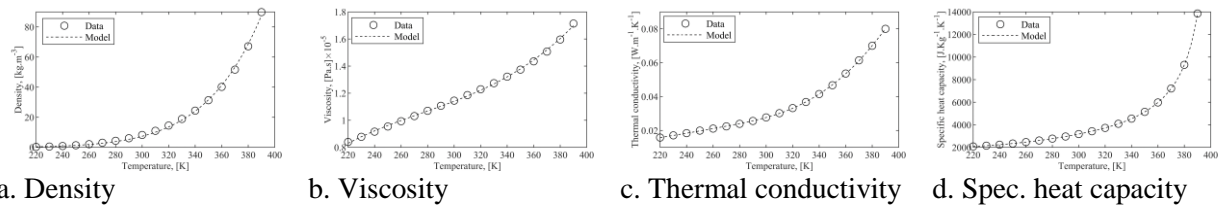


Figure A.5. Properties of ammonia gas curve fitted as function of temperature

A.7. Air

The viscosity, η_{Air} ($\text{Pa}\cdot\text{s}$), thermal conductivity, ℓ_{Air} ($\text{W}\cdot\text{m}^{-1}\cdot\text{K}^{-1}$), and specific heat capacity, C_{P-Air} ($\text{J}\cdot\text{Kg}^{-1}\cdot\text{K}^{-1}$) of air are curve-fitted as given in Equation (A.22) – (A.24) as function of temperature, as well as illustrated in Figure (A.6), and evaluation metrics given in Table (A.1). These models are applicable

within temperature limit, 253 – 398 K, using data from literature[267]. Note that density, ρ_{Air} ($\text{kg}\cdot\text{m}^{-3}$), Equation (A.21), was estimated using the ideal gas law.

$$\rho_{\text{Air}} = \frac{M_{\text{Air}}P_{\text{atm}}}{RT} \quad (\text{A.21})$$

$$\eta_{\text{Air}} = 2.214 * 10^{-7}T^{0.7757} \quad (\text{A.22})$$

$$k_{\text{Air}} = 0.0002199T^{0.8373} \quad (\text{A.23})$$

$$C_{P-\text{Air}} = 0.0004002T^2 - 0.2015T + 1031 \quad (\text{A.24})$$

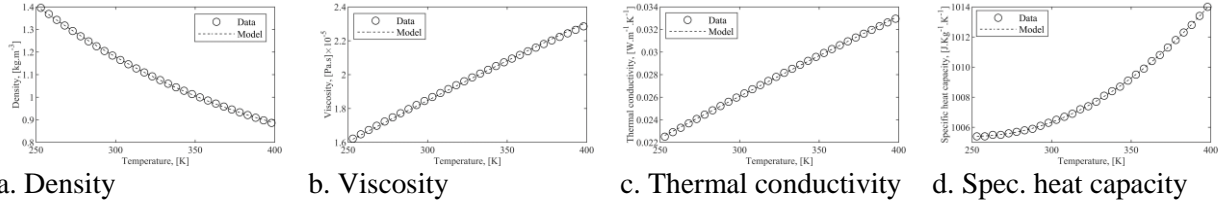


Figure A.6. Properties of air curve fitted as function of temperature

A.8.Lipid (Palm oil)

The density, ρ_{Lip} ($\text{kg}\cdot\text{m}^{-3}$), viscosity, η_{Lip} (Pa.s), thermal conductivity, k_{Lip} ($\text{W}\cdot\text{m}^{-1}\cdot\text{K}^{-1}$), and specific heat capacity, $C_{P-\text{Lip}}$ ($\text{J}\cdot\text{Kg}^{-1}\cdot\text{K}^{-1}$) of lipid are curve-fitted as given in Equation (A.25) – (A.28) as function of temperature, as well as illustrated in Figure (A.7), and evaluation metrics given in Table (A.1). These models are applicable within temperature limit, 293 – 573 K, using data from literature [268].

$$\rho_{\text{lip}} = -249.4T^{0.2023} + 1677 \quad (\text{A.25})$$

$$\eta_{\text{lip}} = 8.971 * 10^7 \exp(-0.07078T) + 0.5186 \exp(-0.01158T) \quad (\text{A.26})$$

$$k_{\text{lip}} = 122.4T^{-1.478} + 0.146 \quad (\text{A.27})$$

$$C_{\text{lip}} = 0.003468T^2 + 0.601T + 1374 \quad (\text{A.28})$$

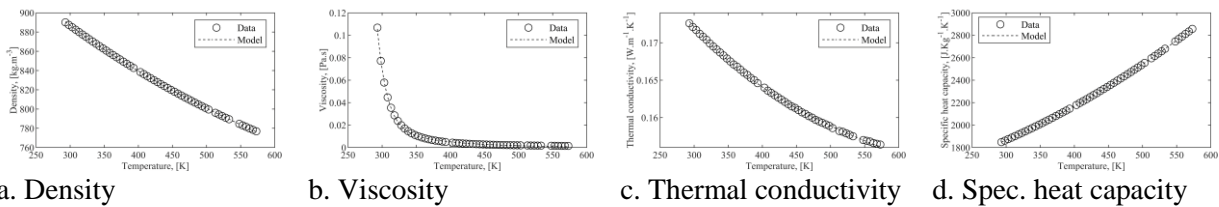


Figure A.7. Properties of lipid curve fitted as function of temperature

A.9.Liquid water

The density, ρ_{W} ($\text{kg}\cdot\text{m}^{-3}$), viscosity, η_{W} (Pa.s), thermal conductivity, k_{W} ($\text{W}\cdot\text{m}^{-1}\cdot\text{K}^{-1}$), and specific heat capacity, $C_{P-\text{W}}$ ($\text{J}\cdot\text{Kg}^{-1}\cdot\text{K}^{-1}$) of liquid water are curve-fitted as given in Equation (A.29) – (A.32) as function of temperature, as well as illustrated in Figure (A.8), and evaluation metrics given in Table (A.1). These models are applicable within temperature limit, 273 – 373 K, using data from literature [269].

$$\rho_{\text{W}} = -0.003547T^2 + 1.863T + 756.4 \quad (\text{A.29})$$

$$\eta_{\text{W}} = 556.6 \exp(-0.04841T) + 0.0132 \exp(-0.01043T) \quad (\text{A.30})$$

$$k_{\text{W}} = -9.518 * 10^{-6}T^2 + 0.007335T - 0.7331 \quad (\text{A.31})$$

$$C_{W} = 6.865 * 10^{16} \exp\left(-\left(\frac{T + 1.587e+04}{2920}\right)^2\right) + 1.132 * 10^4 \exp\left(-\left(\frac{T - 391.6}{91.14}\right)^2\right) - 9447 \exp\left(-\left(\frac{T - 388.1}{85.41}\right)^2\right) + 2.239 \exp\left(-\left(\frac{T - 298}{16.85}\right)^2\right) \quad (\text{A.32})$$

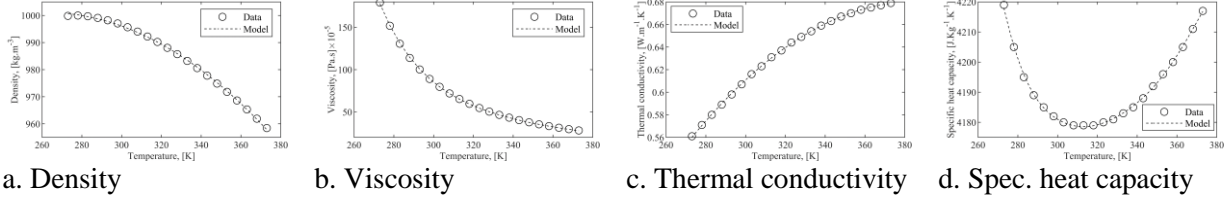


Figure A.8. Properties of liquid water, applicable within temperature limit, 273 – 373 K

A.10. Water vapour

The thermal conductivity, k_{W_v} ($\text{W}\cdot\text{m}^{-1}\cdot\text{K}^{-1}$), and specific heat capacity, C_{P-W_v} ($\text{J}\cdot\text{Kg}^{-1}\cdot\text{K}^{-1}$) of water vapour are curve-fitted as given in Equation (A.35) – (A.36) as function of temperature, as well as illustrated in Figure (A.9), and evaluation metrics given in Table (A.1). These models are applicable within temperature limit, 175 – 500 K, using data from literature [270]. In addition, the heat of vapourisation, $\Delta H_{W_v}^{\text{Evp}}$ ($\text{J}\cdot\text{kg}^{-1}$), was also curved fitted, Equation (A.37) with the limit of 275 – 473 K, as shown in Figure (A.9) [271] with $R^2 = 0.9997$. Furthermore, the density, ρ_{W_v} ($\text{kg}\cdot\text{m}^{-3}$), is estimated from the saturated pressure of water and viscosity, η_{W_v} (pa.s) is as reported in literature [272].

$$\rho_{W_v} = \frac{M_W P_{\text{sat}}}{RT} \quad (\text{A.33})$$

$$\eta_{W_v} = 1.12 * 10^{-5} \left(\frac{T}{350}\right)^{1.5} \left(\frac{1414}{T + 1064}\right) \quad (\text{A.34})$$

$$k_{W_v} = 1.952 * 10^{-5} T^{1.258} + 0.01811 \quad (\text{A.35})$$

$$C_{W_v} = 0.001009T^2 - 0.3576T + 1881 \quad (\text{A.36})$$

$$\Delta H_{W_v}^{\text{Evp}} = -3.42T^2 - 200.9T + 2.806 * 10^6 \quad (\text{A.37})$$

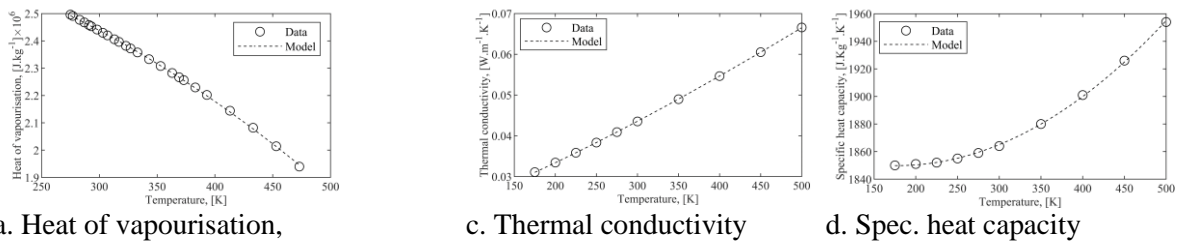


Figure A.9. Properties of water vapour curve fitted as function of temperature

A.11. Properties of solid

Considering that the laboratory scale bioreactor is made of glass, the thermal conductivity of glass, Equation (A.38), as reported in literature [273] was applied.

$$k_{W_v} = -5.268T^{-0.78} + 1.244 \quad (\text{A.38})$$

A.12. Interfacial tension of gases-water

The interfacial tension between carbon dioxide and water, as well as hydrogen gas together with water as respectively given in Equation (5.15h) – (5.15i) were deduced by curve fitting data from literature [195–198]. The curve fitted model as well as the R^2 values are illustrated in Figure (A.10) and since the $R^2 > 0.95$ the model can be considered adequate.

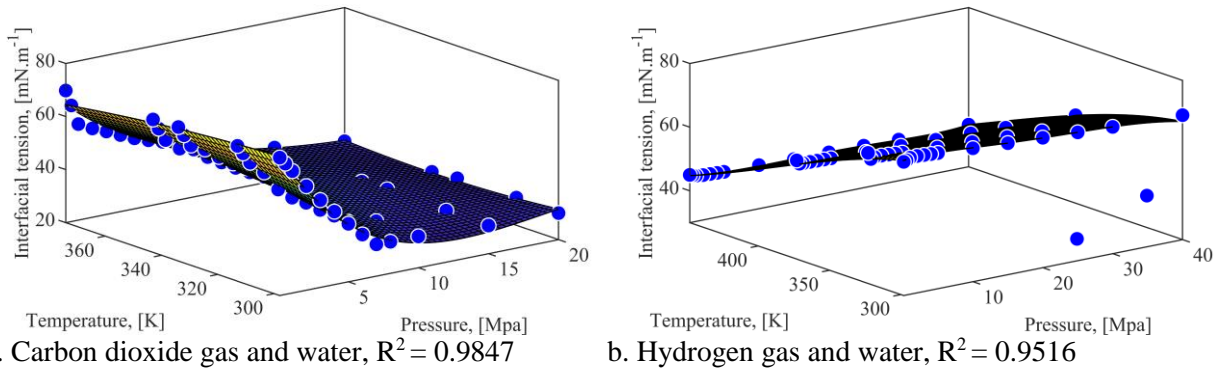


Figure A.10. Interfacial tension of carbon dioxide and hydrogen with water

A.13. Experimental data deduced from the lipid hydrolysis.

The Table (A.3) was the experimentally deduced changes in concentration of lipid into LCFA with time and based on temperature applied to deduce Equation (8.2) – (8.3) with parameter given in Table (9.1).

Table A.3. Experimental data on the effect of temperature on lipid hydrolysis

Time(h)	Temperature(°C)	Concentration(kg.m ⁻³)			
		Triglyceride	Diglyceride	Monoglyceride	LCFA
0.0000	25	2.2974	0.0094	0.1092	0.0840
0.5000		1.4441	0.3949	0.0645	0.5964
1.0000		1.0203	0.4208	0.0762	0.9827
1.5000		0.7098	0.3871	0.0877	1.3154
2.0000		0.4564	0.3215	0.0858	1.6363
3.0000		0.1872	0.1888	0.1043	2.0197
5.0000		0.0811	0.0813	0.0820	2.2556
8.0000		0.0371	0.0269	0.0652	2.3708
24.0000		0.0305	0.0196	0.0629	2.3870
0.0000	30	2.2974	0.0094	0.1092	0.0840
0.5000		1.3997	0.3928	0.0696	0.6379
1.0000		0.8308	0.3971	0.0913	1.1807
1.5000		0.4613	0.3192	0.1171	1.6024
2.0000		0.2467	0.2416	0.1251	1.8866
3.0000		0.1261	0.1132	0.1082	2.1525
5.0000		0.0713	0.0516	0.0816	2.2955
8.0000		0.0450	0.0227	0.0675	2.3648
24.0000		0.0384	0.0193	0.0660	2.3762
0.0000	35	2.2974	0.0094	0.1092	0.0840
0.5000		0.7218	0.3971	0.0890	1.2921
1.0000		0.3028	0.2468	0.1083	1.8421
1.5000		0.0956	0.1300	0.1187	2.1557
2.0000		0.0606	0.0666	0.1221	2.2508

3.0000		0.0466	0.0321	0.0999	2.3215
5.0000		0.0905	0.0213	0.0700	2.3182
8.0000		0.0625	0.0151	0.0644	2.3580
24.0000		0.0380	0.0086	0.0622	2.3912
0.0000		2.2974	0.0094	0.1092	0.0840
0.5000		0.5571	0.3479	0.0858	1.5092
1.0000		0.2918	0.1923	0.0827	1.9332
1.5000		0.1433	0.1031	0.0768	2.1768
2.0000	45	0.0978	0.0707	0.0754	2.2560
3.0000		0.0990	0.0537	0.0779	2.2694
5.0000		0.0596	0.0326	0.0720	2.3358
8.0000		0.0404	0.0190	0.0739	2.3667
24.0000		0.0329	0.0149	0.0813	2.3709
0.0000		2.2974	0.0094	0.1092	0.0840
0.5000		0.5067	0.2873	0.0969	1.6090
1.0000		0.3840	0.1862	0.0853	1.8445
1.5000		0.2468	0.1245	0.0761	2.0526
2.0000	50	0.1788	0.1021	0.0770	2.1421
3.0000		0.1566	0.0839	0.0749	2.1847
5.0000		0.1308	0.0664	0.0930	2.2097
8.0000		0.0818	0.0333	0.1014	2.2835
24.0000		0.0464	0.0182	0.0805	2.3549

A.14.Hypothetical data for maximum specific growth rate of microbes

The Table (A.4) illustrate technically assumed maximum specific growth rate in relation to temperature for microbes responsible for the utilisation of LCFA and glycerol into biogas as given by Equation (7.5e), with parameter in Table (9.2).

Table A.4. Hypothetical data of maximum specific growth rate in relation to temperature

Temperature(°C)	Maximum specific growth rate, μ_{\max}	
	LCFA	Glycerol
0	0.0000	0.0000
4	0.0000	0.0000
10	0.0010	0.0003
20	0.0030	0.0010
25	0.0050	0.0017
27	0.0062	0.0021
29	0.0075	0.0026
31	0.0105	0.0036
33	0.0155	0.0053
35	0.0183	0.0063
37	0.0198	0.0067
39	0.0205	0.0070
41	0.0220	0.0075
43	0.0230	0.0078
45	0.0232	0.0079
47	0.0233	0.0079
49	0.0234	0.0080
51	0.0233	0.0079
53	0.0230	0.0078
55	0.0200	0.0068
57	0.0180	0.0061
59	0.0060	0.0010
61	0.0006	0.0005

63	0.0000	0.0000
65	0.0000	0.0000
67	0.0000	0.0000
69	0.0000	0.0000
71	0.0000	0.0000

A.15. Fluid mixing rule

In simulating the interaction of fluids to estimate the average properties (p) of type (i) of mixed gaseous and liquid phase with different species (i) were estimated based on the linear mixing rule [274] as given in Equation (5.15j) can be generally expressed as given in Equation (A.39). Where x is the fraction of specie (j) in the gaseous or liquid phase being considered with J total number of species in the various phases.

$$p_i = \sum_j^J x_j p_i \quad (\text{A.39})$$

A.16. Auxiliary equations

The mass and volumetric outflow from the gaseous outlet of the bioreactor can be deduced from the integration of Equation (A.41) – (A.42). While the remaining amount in the bioreactor is given by Equation (A.43) – (A.44). This models also apply for the water calculated from the saturated water pressure.

$$\dot{m}_{o-G_{j^*}} = \frac{dm_{o-G_{j^*}}}{dt} = q_{o-G} G_{j^*} \quad (\text{A.41})$$

$$\dot{V}_{o-G_{j^*}} = \frac{dV_{o-G_{j^*}}}{dt} = \frac{\dot{m}_{o-G_{j^*}} RT}{P_G M_{j^*}} \quad (\text{A.42})$$

$$m_{G_{j^*}} = V_G G_{j^*} \quad (\text{A.43})$$

$$V_{G_{j^*}} = \frac{m_{G_{j^*}} RT}{P_G M_{j^*}} \quad (\text{A.44})$$

List of figures

Figure 4.1. Summary of biogas utilisation with treatment level	15
Figure 5.1. Illustrative scheme of anaerobic digestion stages [68].	18
Figure 6.1. Illustration of degradation level considered in the multi-step dynamic models	23
Figure 6.2. Typical growth curve of biomass in a biochemical process	25
Figure 7.1. Description of anaerobic digestion in a continuous stirred tank reactor (CSTR) type bioreactor with material and heat transfer.....	26
Figure 7.2. Schematics of semi-batch anaerobic digestion bioreactor at atmospheric condition.....	27
Figure 7.3. Interfacial mass transfer of biogas from a liquid to gaseous phase	37
Figure 6.4. Cross-sectional area of the bioreactor with material and heat transfer	49
Figure 8.1. Experimental setup utilised for the anaerobic digestion	55
Figure 9.1. Illustration of hydrolysis kinetic, and Gaussian model for lipid degradation	58
Figure 9.2. Biogas production, and maximum microbe specific growth rate	59
Figure 9.3. Changes in liquid level, lipid, and microbes in the liquid phase (1).....	60
Figure 9.4. Concentration dynamics for microbes, biogas formation and water (1).....	60
Figure 9.5. Concentration, mass, and volume of biogas obtainable in headspace (1)	60
Figure 9.6. Pressure in headspace, mass, and volume of biogas from headspace (1)	61
Figure 9.7. pH bioreactor, pressure in bubbles, and diameter of biogas bubbles (1).....	62
Figure 9.8. Biogas bubbles distribution and its rising height in liquid phase (1).....	62
Figure 9.9. Bubbles surface pressure, fluid, and wall temperature of reaction system (1)	63
Figure 9.10. Changes in liquid level, lipid, and microbes in the liquid phase (2).....	63
Figure 9.11. Concentration dynamics for microbes, biogas formation and water (2).....	64
Figure 9.12. Concentration, mass, and volume of biogas obtainable in headspace (2).....	64
Figure 9.13. Pressure in headspace, mass, and volume of biogas from headspace (2)	65
Figure 9.14. pH bioreactor, pressure in bubbles, and diameter of biogas bubbles (2).....	65
Figure 9.15. Biogas bubbles distribution and its rising height in liquid phase (2).....	66
Figure 9.16. Bubbles surface pressure, fluid, and wall temperature of reaction system (2)	66
Figure 9.17. Changes in liquid level, lipid, and microbes in the liquid phase (3).....	67
Figure 9.18. Concentration dynamics for microbes, biogas formation and water (3).....	67
Figure 9.19. Concentration, mass, and volume of biogas obtainable in headspace (3).....	67
Figure 9.20. Pressure in headspace, mass, and volume of biogas from headspace (3)	68
Figure 9.21. pH bioreactor, pressure in bubbles, and diameter of biogas bubbles (3).....	68
Figure 9.22. Biogas bubbles distribution and its rising height in liquid phase (3).....	68
Figure 9.23. Bubbles surface pressure, fluid, and wall temperature of reaction system (3)	69
Figure 9.24. Changes in liquid level, lipid, and microbes in the liquid phase (4).....	69

Figure 9.25. Concentration dynamics for microbes, biogas formation and water (4).....	70
Figure 9.26. Concentration, mass, and volume of biogas obtainable in headspace (4).....	70
Figure 9.27. Pressure in headspace, mass, and volume of biogas from headspace (4)	70
Figure 9.28. pH bioreactor, pressure in bubbles, and diameter of biogas bubbles (4)	71
Figure 9.29. Biogas bubbles distribution and its rising height in liquid phase (4).....	71
Figure 9.30. Bubbles surface pressure, fluid, and wall temperature of reaction system (4)	71
Figure 9.31. Changes in liquid level, lipid, and microbes in the liquid phase (5).....	72
Figure 9.32. Concentration dynamics for microbes, biogas formation and water (5).....	73
Figure 9.33. Concentration, mass, and volume of biogas obtainable in headspace (5).....	73
Figure 9.34. Pressure in headspace, mass, and volume of biogas from headspace (5)	73
Figure 9.35. pH bioreactor, pressure in bubbles, and diameter of biogas bubbles (5)	74
Figure 9.36. Biogas bubbles distribution and its rising height in liquid phase (5).....	74
Figure 9.37. Bubbles surface pressure, fluid, and wall temperature of reaction system (5)	74
Figure 9.38. Changes in liquid level, lipid, and microbes in the liquid phase (6).....	75
Figure 9.39. Concentration dynamics for microbes, biogas formation and water (6).....	75
Figure 9.40. Concentration, mass, and volume of biogas obtainable in headspace (6).....	75
Figure 9.41. Pressure in headspace, mass, and volume of biogas from headspace (6)	76
Figure 9.42. pH bioreactor, pressure in bubbles, and diameter of biogas bubbles (6)	76
Figure 9.43. Biogas bubbles distribution and its rising height in liquid phase (6).....	76
Figure 9.44. Bubbles surface pressure, fluid, and wall temperature of reaction system (6)	77
Figure 9.45. Changes in liquid level, lipid, and microbes in the liquid phase (7).....	77
Figure 9.46. Concentration dynamics for microbes, biogas formation and water (7).....	77
Figure 9.47. Concentration, mass, and volume of biogas obtainable in headspace (7).....	78
Figure 9.48. Pressure in headspace, mass, and volume of biogas from headspace (7)	78
Figure 9.49. pH bioreactor, pressure in bubbles, and diameter of biogas bubbles (7)	78
Figure 9.50. Biogas bubbles distribution and its rising height in liquid phase (7).....	78
Figure 9.51. Bubbles surface pressure, fluid, and wall temperature of reaction system (7)	79
Figure A.1. Properties of hydrogen gas curve fitted as function of temperature	102
Figure A.2. Properties of methane gas curve fitted as function of temperature	103
Figure A.3. Properties of carbon dioxide gas curve fitted as function of temperature.....	103
Figure A.4. Properties of nitrogen gas curve fitted as function of temperature	104
Figure A.5. Properties of ammonia gas curve fitted as function of temperature	104
Figure A.6. Properties of air curve fitted as function of temperature	105
Figure A.7. Properties of lipid curve fitted as function of temperature	105
Figure A.8. Properties of liquid water, applicable within temperature limit, 273 – 373 K.....	106
Figure A.9. Properties of water vapour curve fitted as function of temperature.....	106

Figure A.10. Interfacial tension of carbon dioxide and hydrogen with water..... 107

List of tables

Table 4.1. Biogas utilisation and required composition [80]	15
Table 4.2. Thermophysical properties of biogas [82].....	16
Table 4.3. Comparative Compositions of Natural Gas and Biogas [84]	16
Table 4.4. Energy density of biofuels [86].....	17
Table 6.1. Popularly reported dynamic single–equation model	21
Table 6.2. Popularly reported cumulative single-equation model.....	22
Table 6.3. Theoretical yield estimate of the substrate from feedstock, biogas and microbes from the substrate, ammonia from microbes for lipid (triglyceride with oleic acid).....	25
Table 7.1. Coefficients of polynomial model used for the calculation of the interfacial tension.....	40
Table 7.2. Coefficients for dissociation constants of components in anaerobic digestion [213]	45
Table 8.1. Average physicochemical properties, and composition of sludge sample	54
Table 8.2. Simulation parameters based on laboratory scale, and literature review	57
Table 9.1. Estimated parameters and evaluation metrics of hydrolysis model	58
Table 9.2. Ratkowsky constants for estimation of maximum specific growth rate.....	59
Table 9.3. Iteratively estimated heat transfer properties for the AD process	79
Table A.1. Evaluation criteria (R^2 values) for the curve-fitted models	102
Table A.3. Experimental data on the effect of temperature on lipid hydrolysis.....	107
Table A.4. Hypothetical data of maximum specific growth rate in relation to temperature	108

List of Abbreviations

Abbreviation	Definition
AD	Anaerobic digestion
ADM1	Anaerobic Digestion Model No. 1
AM2	Acidogenesis-methanogenesis-two-steps
ATP	Adenosine triphosphate
BMP	Biochemical Methane Potential
BOD	Biochemical oxygen demand
CFRT	Closed floating roof tank
CSTR	Continuous Stirred Tank Reactor
CNG	Compressed natural gas
COD	Chemical oxygen demand
DAGs	Diacylglycerols
EFRT	External floating roof tank
FA	Fatty acids
FFA	Free fatty acids
FRT	Fixed roof tank
FTIR	Fourier-transform infrared spectroscopy
HRT	Hydraulic retention time
HW	Heating or hot water
HJ	Heating jacket
IFRT	Internal floating roof tank
LC	Level controller
LCFA	Long-chain fatty acid
LNG	Liquefied natural gas
MAGs	Monoacylglycerols
MSDM	Multi-step-degradation model
OLR	Organic loading rate
PC	Pressure controller
pHC	pH controller
rps	Revolution per second
SRT	Solids retention time
SSDM	Single-step-degradation model
TAGs	Triacylglycerols
TC	Temperature controller
TKN	Total kjeldahl nitrogen
TOC	Total organic carbon
TS	Total solid
TSS	Total suspended solids
VS	Volatile solid
VSS	Volatile suspended solids

List of symbols

Symbols (unit)	Definition
a (mg.g ⁻¹ . s ⁻¹); a (s ⁻¹)	Biogas production constant; Rate constants
a^* (mg. g ⁻¹ . time ⁻¹)	Biogas production constant
a_j (m ⁻¹)	Specific interfacial area of gas per unit volume of liquid
A (m ²); A (mg. g ⁻¹)	Area of bioreactor; Biogas production potential
A_a (s ⁻¹)	Preexponential factor
A_H (m ²)	Area of heating jacket
b (mg.g ⁻¹ . s ⁻²); b (s ⁻¹)	Biogas production constant; Rate constants
b^* (s ⁻¹)	Biogas production time constant
b_{ij}	Coefficients of interfacial tension polynomial model
B_j (kg.m ⁻³)	Microbes' concentration
c (s ⁻¹)	Biogas production time or rate constant
C_p (J.kg ⁻¹ .K ⁻¹)	Specific heat capacity
d_j (m)	Biogas bubble diameter
$d_{j,h}$ (m)	Gas bubble diameters at specific height in the liquid
$d_{j,m}$ (m)	Mean diameter of the gas bubble
$d_{j,m\log}$ (m)	Natural logarithm of mean of bubble diameter
d_{S_j} (m)	Sauter mean diameter
d_{st} (m)	Diameter of impeller
D_R (m)	Bioreactor diameter
D_H (m)	Heating jacket hydraulic inner diameter
D_L (m ² .s ⁻¹)	Diffusivity of biogas species in liquid
\bar{D}_R (m)	Logarithmic mean diameter of bioreactor
\bar{D}_H (m)	Logarithmic mean hydraulic diameter of heating jacket
$e = \exp(1)$	Exponential constant
E_a (J.mol ⁻¹)	Activation energy
$f(x)$	Biogas yield
F (kg.m ⁻³)	Feedstock/macronutrients concentration
G (kg.m ⁻³)	General or headspace biogas concentration
G_D (kg.m ⁻³)	Liquid biogas concentration
G_s (m ⁻³ . kg ⁻¹)	Gas production factor
Gr	Grashof number
h_j (m)	Height of the biogas bubble specie in the liquid phase
h_L (m)	Level of the liquid in bioreactor
h_R (m)	Total height of bioreactor
k (s ⁻¹)	Rate constants
$K_{aj\pm}$ (kgmole)	Disassociation constant
K_d (s ⁻¹)	Microbe death rate
k_{hyd} (s ⁻¹)	Rate constants
K_H (kg.m ⁻³ .Pa ⁻¹)	Henry's constant
K_{lipid} (s ⁻¹)	Hydrolysis rate constant
K_La (s ⁻¹)	Mass transfer coefficient
K_{mB} (time ⁻¹)	Maintenance coefficient
k_T (K ⁻¹)	Temperature constant
k_p (Pa.m ³ .s ⁻¹)	Pipe resistance coefficient
k_0 (hr ⁻¹)	Preexponential factor of the reaction
L_c (m)	Characteristic length
\dot{m} (kg.s ⁻¹)	Mass flowrate

$M(\text{kg.kgmole}^{-1})$	Molecular mass
n	Number of process factors; order sequence of the polynomial model
$n_b(\text{kgmoles})$	Biogas compositional term
$\dot{n}(\text{kgmole.s}^{-1})$	Molar flowrate
n_K	Factor for mass transfer coefficient
$n_{st}(\text{rps})$	Impeller speed of bioreactor
$N(\text{kgmoles})$	Compositional term
N_p	Power number of the stirrer
N_{Re}	Reynold number of stirring of bioreactor
$p(\text{pa})$	Partial pressure of biogas bubble
$P(\text{pa})$	Partial pressure in headspace
$P_G(\text{pa})$	Total pressure of biogas species
pH_{ul} and pH_{ll}	Upper and lower pH limits
$P_{Mix}(W)$	Stirring power
$P_{N_2}(\text{pa})$	Pressure of inert gas or nitrogen
$P_R(\text{pa})$	Fixed or desired operating pressure of the bioreactor
$P_{sw}(\text{pa})$	Saturated vapour pressure
$p_T(\text{pa})$	Total pressure on biogas bubble
Pr	Prandtl number
$q_{c-L}(\text{m}^{-3} \cdot \text{s}^{-1})$	Controller volumetric flowrate for pH control
$q_{i-L}(\text{m}^{-3} \cdot \text{s}^{-1})$	Input volumetric flowrate of liquid
$q_{o-G}(\text{m}^{-3} \cdot \text{s}^{-1})$	Output volumetric flowrate of gaseous and vapour outlet of bioreactor
$q_{o-GG}(\text{m}^{-3} \cdot \text{s}^{-1})$	Flowrate of biogas or gaseous component only in q_{o-G}
$q_{o-L}(\text{m}^{-3} \cdot \text{s}^{-1})$	Output volumetric flowrate of liquid
$q_{i-hw} \equiv q_{o-hw} \equiv q_{hw}(\text{m}^{-3} \cdot \text{s}^{-1})$	Flowrate of heating or hot water
$Q_{HE}(W)$	Heating energy from hot water
$Q_{H-En}(W)$	Heat loss from heating jacket to the environment or surrounding
$Q_{R-En}(W)$	Heat loss to environment from bioreactor
$r_{Ri}(m)$	Radius of the liquid in bioreactor, i.e., inner
$R(\text{pa} \cdot \text{kgmol}^{-1} \cdot \text{k}^{-1})$	Ideal gas constant
$R_{AD}(\text{kg} \cdot \text{m}^{-3} \cdot \text{s}^{-1})$	Rate of anaerobic digestion
$R_{Bd}(\text{kg} \cdot \text{m}^{-3} \cdot \text{s}^{-1})$	Death rate of biomass
$R_{Bg}(\text{kg} \cdot \text{m}^{-3} \cdot \text{s}^{-1})$	Growth rate of biomass
$R_{B/A}(\text{kg} \cdot \text{m}^{-3} \cdot \text{s}^{-1})$	Conversion rate of acetic acid to biomass
$R_{B/S}(\text{kg} \cdot \text{m}^{-3} \cdot \text{s}^{-1})$	Conversion rate of substrate to biomass
$R_{B/\gamma}(\text{kg} \cdot \text{m}^{-3} \cdot \text{s}^{-1})$	Conversion rate of intermediates acid to biomass
$R_e(\text{kg} \cdot \text{m}^{-3} \cdot \text{s}^{-1})$	Evolution of biogas bubble from liquid to gas headspace
$R_E(\text{kg} \cdot \text{m}^{-3} \cdot \text{s}^{-1})$	Evolution of biogas from liquid to gas headspace
$R_{Evap}(\text{kg} \cdot \text{s}^{-1})$	Rate of evaporation of water
Re	Reynold number due to fluid flow
$R_F(\text{kg} \cdot \text{m}^{-3} \cdot \text{s}^{-1})$	Consumption rate of feedstock
$R_{G/A}(\text{kg} \cdot \text{m}^{-3} \cdot \text{s}^{-1})$	Conversion rate of acetic acid to biogas
$R_{G/\gamma}(\text{kg} \cdot \text{m}^{-3} \cdot \text{s}^{-1})$	Conversion rate of intermediates to biogas
$R_{max}(\text{mg} \cdot \text{g}^{-1} \cdot \text{s}^{-1})$	Maximal biogas production rate
$R_S(\text{kg} \cdot \text{m}^{-3} \cdot \text{s}^{-1})$	Formation rate of substrate
$R_{A/S}(\text{kg} \cdot \text{m}^{-3} \cdot \text{s}^{-1})$	Conversion rate of substrate to acetic acid
$R_{A/\gamma}(\text{kg} \cdot \text{m}^{-3} \cdot \text{s}^{-1})$	Consumption rate of intermediates to acetic acid
$R_{\gamma/S}(\text{kg} \cdot \text{m}^{-3} \cdot \text{s}^{-1})$	Conversion rate of substrate to intermediates
$S(\text{kg} \cdot \text{m}^{-3})$	Substrates concentration
$S_0(\text{kg} \cdot \text{m}^{-3})$	Initial substrate concentration

Sc	Schmidt number
t(s)	Digestion time
t_0 (s)	Time when the maximal biogas production rate occurs
T(K)	AD temperature
T_C (K)	Critical temperature
T_f (K)	Film temperature
T_{hw} (K)	Temperature heating water
T_H (K)	Heating jacket wall temperature
T_{min} and T_{max} (K)	Minimum and maximum temperature tolerance of microbes
T_O (K)	Reference temperature of hydrolysis reaction
T_{wc} (K)	Cold side wall temperature of bioreactor
T_{wh} (K)	Hot side wall temperature of bioreactor
u (m.s ⁻¹)	Velocity of fluid
u_b (m.s ⁻¹)	Terminal or rising velocity of the bubble
U_{HE} (W.m ⁻² .K ⁻¹)	Overall heat coefficient of bioreactor with heating jacket
U_{H-En} (W.m ⁻² .K ⁻¹)	Overall heat coefficient of heating jacket with environment
v (m ³)	Volume of biogas bubble
V_G (m ³)	Gas headspace volume
V_{hw} (m ³)	Volume of heating jacket or heating water
v_{H_2O} (m ³ .kgmol ⁻¹)	Average molecular volume of water
V_L (m ³)	Liquid volume
V_R (m ³)	Constant control volume
V_t (m ³)	Volume of biogas generated over a time, t
V_∞ (m ³)	Total volume of biogas produced
W_{H_2O} (kg H ₂ O per m ³ gas)	Inherent moisture accompanying biogas output from the bioreactor
w_v	Water vapour concentration
x_i and x_j	Represent the process factors (pH, temperature, etc.)
x_{j^*} and y_{j^*}	Liquid and gaseous fraction of specie, j^* , in liquid and gaseous phase
y (mg.g ⁻¹ . s ⁻¹); y	Biogas production rate; Generic output of data
$Y_{B/S}$ (kg.kg ⁻¹)	Microbe yield from substrate
Y_{cat}	Cation yield from microbes
$Y_{G_D/S}$ (kg.kg ⁻¹)	Biogas yield from substrate
$Y_{S/F}$ (kg.kg ⁻¹)	Substrate yield from feedstock
\bar{y}	Mean output of data
\hat{y}	Model output
[Z](kgmoles.m ⁻³)	Ionic molar concentration
ΔH_{AD} (J.kgmoles ⁻¹)	Heat of reaction of the anaerobic reaction
ΔH_{Evap} (J.kg ⁻¹)	Latent heat of vapourisation of water
$\Delta\rho$	Change in density
ΔT (K)	Temperature difference between fluid and wall
a, b, c, d, and e	Elemental stoichiometric ratio of generic substrate
α_{j^*} (m ⁻¹)	Specific interfacial area of gas bubble per unit volume of liquid
α (s ⁻¹)	Rate constants
σ , β & δ	Dimensionless shape factors
\mathcal{A} (kg.m ⁻³)	Acetic acid concentration
\mathcal{B} (K ⁻¹)	Exponential constant
β	Fluid thermal expansion coefficient
β_o	Model constant
β_i	Coefficient for linear term
β_{ii}	Coefficient for quadratic term

β_{ij}	Coefficient for interactive term
\mathcal{D} (s^{-1})	Bioreactor dilution rate
\dot{h}_{Air} ($W.m^{-2}.K^{-1}$)	Heat transfer coefficient of air
\dot{h}_H ($W.m^{-2}.K^{-1}$)	Heat transfer coefficient of fluid in heating jacket
\dot{h}_L and \dot{h}_G ($W.m^{-2}.K^{-1}$)	Represent the liquid and gas portion of \dot{h}_R
\dot{h}_R ($W.m^{-2}.K^{-1}$)	Heat transfer coefficient of fluid in bioreactor
\dot{i}	Inhibition of various biogas species
I	Inhibitory concentration, e.g., S , \mathcal{P} and pH
J ($kg.m^{-3}$)	Intermediates concentration
\mathcal{K}_b ($kg.m^{-3}$)	Kinetic parameter
\mathcal{K}_{CH}	Kinetic parameter
\mathcal{K}_{i-i} ($kg.m^{-3}$)	Inhibition parameter
\mathcal{K}_s ($kg.m^{-3}$)	Half-saturation coefficient
\mathcal{K}_1 & \mathcal{K}_2 ($kg.m^{-3}$)	Kinetic parameters
k ($W.m^{-1}.K^{-1}$)	Thermal conductivity
ζ_*	Standard deviation of the bubble diameter
ζ_{*log}	Natural logarithm standard deviation of bubble diameter
n	Number of substrate-binding sites per enzyme molecules
n_o	Fitting constant unique to the system
η_L (Pa.s)	Viscosity of liquid
Θ	Stirrer characteristic constant
Φ_B	Fraction of substrate converted to microbe biomass
Φ_G	Fraction of substrate converted to biogas
Φ_{H_2O}	Fugacity coefficient of water
Φ_v	Volatile fraction of the feedstock
\mathcal{P} ($kg.m^{-3}$)	Product concentration
ρ_L ($kg.m^{-3}$)	Density of liquid
ρ_* ($kg.m^{-3}$)	Density of biogas species
q ($m^3.kmole^{-1}$)	Molar volume
τ (N.m)	Torque of stirrer
μ (s^{-1})	Specific microbe growth rate
μ_{max} (s^{-1})	Maximum microbe growth rate
$\mu_{max,a}$ and $\mu_{max,m}$ (s^{-1})	Maximum microbe growth rate for acidogenes and methanogens
ψ^o	Chemical potential
$\omega_{F_{j_o}}$	Mass fraction of the specific molecule in feedstock
δ_G (kg^{-1})	Ideal gas conversion factor
λ (s)	Lag time
χ	Volumetric fraction of biogas produced
x	Thickness of bioreactor or heating jacket
Υ	pH inhibitory constant
$\gamma_{Lj,*}$ ($N.m^{-1}$)	Interfacial tension between the biogas bubble species and liquid
γ ($N.m^{-1}$)	Average interfacial tension of the biogas with the liquid phase

* Note that more clarity on symbols can be deduced in appropriate sections of this work

List of subscripts

Subscript	Definition
c	Controller (specifically pH controller)
G	Gaseous
Gw	Gaseous water content
H	Heating jacket
i	Input, inner/internal
<i>i</i>	Inhibitory species e.g., S, [H ⁺] and pH
$j = 1, 2, \dots, n$	Indicates the number of species or order being considered
$j_* = \text{CH}_4, \text{CO}_2, \text{H}_2, \text{etc.}$	Represents the various biogas species
$j_o = \text{Lipid, protein, etc.}$	Specific molecule in feedstock
L	Liquid
o	Output, outer
R	Bioreactor
w	Water or wall
w_v	Water vapour

List of publications

Journal Articles	<p>Samuel Emebu, Clara Mendoza Martinez, Osaze Omoregbe, Aleksi Mankonen, Ebuka A. Ogbuoji, Ibrahim Shaikh, Even Pettersen, Marek Kubalčík, & Charity Okieimen. Design, techno-economic evaluation, and optimisation of renewable methanol plant model: Finland case study. Chemical Engineering Science, Vol. 278, 2023, 118888</p> <hr/> <p>Samuel Emebu, Jiří Pecha, Dagmar Janáčová. Review on anaerobic digestion models: Model classification & elaboration of process. Renewable and Sustainable Energy Reviews, Vol. 160, 2022, 112288.</p> <hr/> <p>Samuel Emebu, Marek Kubalčík, Christoph Josef Backi & Dagmar Janáčová. A comparative study of linear and nonlinear optimal control of a three-tank system. ISA Transactions, Vol. 132, 2023, Pp. 419-427.</p> <hr/> <p>Christoph Josef Backi, Samuel Emebu, Sigurd Skogestad & Brian Arthur Grimes. A simple modeling approach to control emulsion layers in gravity separators. Computer Aided Chemical Engineering, Vol. 46, 2019, Pp. 1159-1164.</p> <hr/> <p>S. Emebu, O. Osaikhuiwuomwan, A. Mankonen, C. Udoe, C. O. Okieimen & D. Janáčová. Influence of moisture content, temperature, and time on free fatty acid in stored crude. Scientific Reports, Vol. 12(1), 2022.</p> <hr/> <p>Alves Elem Patricia Rocha, Orlando Salcedo-Puerto, Jesús Nuncira, Samuel Emebu, & Clara Mendoza-Martinez. Renewable Energy Potential and CO2 Performance of Main Biomasses Used in Brazil. Energies, Vol.16(9), 2023, 3959.</p> <hr/> <p>Ogunleye, Raphael Olabanji, Sona Rusnakova, Milan Zaludek, and Samuel Emebu. The Influence of Ply Stacking Sequence on Mechanical Properties of Carbon/Epoxy Composite Laminates. Polymers, Vol. 14(24), 2022, 5566.</p> <hr/> <p>Oghenekohwiroro Edjere, Justina E. Ukpebor, Samuel Emebu & Felix E. Okieimen. Preliminary studies of Organochlorine Pesticides (OCPs) in sediment, water and fish samples from Ethiope river, Abraka axis, southern Nigeria. International Letters of Natural Sciences, Vol. 80, 2020, pp. 1-12.</p> <hr/> <p>E. A. Elimian, S. Emebu, C. O. Okieimen, G. O. Madojemu & G. E. Eluro. Optimization of Non-Competitive Adsorption of Benzene, Toluene and Xylene (BTX) from Aqueous Solutions using Activated Orange Peels. Technical Transactions of Materials Science and Technology Society of Nigeria, Vol. 2, 2019, pp 209-214</p> <hr/>
Manuscript for submission	<p>Samuel Emebu, Lubomír Šánek, Jakub Husár, Jiří Pecha, & Dagmar Janáčová. Modelling the kinetics of anaerobic hydrolysis of lipid-rich-waste: Elucidation of the effect of temperature. Manuscript has been invited for submission to BIORESTEC-2023 special issue to the journal of Bioresource Technology.</p> <hr/> <p>Samuel Emebu, Clara Mendoza Martinez, Aleksi Mankonen, Raphael Olabanji Ogunleye, Ojeaga Evans Imanah, Marek Kubalčík, Dagmar Janáčová & Felix Ebhodaghe Okieimen. Guide to adequate curve-fitting of models Comparison between multi-step, and single-step curve-fitting techniques. Manuscript has been submitted to the journal of Scientific Reports</p> <hr/>

Samuel Emebu, Raphael Olabanji Ogunleye, Eva Achbergerová, Lenka Vítková, Petr Ponížil, Clara Mendoza Martinez. Review and proposition for model-based multivariable-multiobjective optimisation of extrusion-based bioprinting. Manuscript has been prepared for submission to the journal of **Applied Materials today**

Sohaibullah Zarghoon, Samuel Emebu, Radek Matušů, Cyril Belavý, Lukáš Bartalský, Clara Mendoza Martinez. Modelling, simulation, and control of induction heating of steel billet based on full-state feedback LQR controllers. Manuscript has been prepared for submission to the **Journal of Process Control**

Conference

Samuel Emebu, Lubomír Šánek, Jakub Husár, Jirí Pecha, & Dagmar Janáčková. Modelling the kinetics of anaerobic hydrolysis of lipid-rich-waste: Elucidation of the effect of temperature. BIORESTEC-2023 conference, Lake Garda Italy, 14–17, May 2023. Manuscript has been invited for submission to the journal of **Bioresource Technology**.

Curriculum vitae

Personal information

Name Samuel Emebu
Address Budovatelska, 4810, 760 05, Zlin, Czechia
Telephone +420733458998
Email emebu@utb.cz
Date of birth 19-09-1988
Gender Male
Nationality Nigerian (Nigeria)

Education and training

2020 – 2023 Engineering informatics (Doctoral studies)
Tomas Bata University, Zlin, Czech Republic
2016 – 2018 Chemical Engineering-Process Systems (master's degree Programme)
Norwegian University of Science and Technology, Trondheim, Norway
2007 – 2012 Chemical Engineering (bachelor's degree Programme)
The University of Benin, Benin City, Nigeria. Department of Chemical Engineering

Digital skills MATLAB & Simulink, Python for statistics, Overleaf/Latex, Aspen HYSYS, Aspen PLUS, SOLIDWORKS, Microsoft Office.

Project-Grant

2021 – 2023 Hydrolysis of lipid-rich waste within the scope of anaerobic digestion
Funded by the Internal Grant Agency (IGA/CebiaTech/2021/002, IGA/CebiaTech/2022/002, IGA/CebiaTech/2023/004) of Tomas Bata University

2021 – 2023 Development of biopolymer-based hydrogel for micro-extrusion
(Modelling and optimisation)
Funded by the Junior Grant Program, through the Ministry of Education, Youth & Sport (Czech Republic) and the European Union
